Tailoring Molecular Weight of the Conjugated Model Polymer MEH-PPV and its Structure-Property Relations

Dissertation
zur Erlangung des Grades
"Doktor der Naturwissenschaften"

Am Fachbereich Chemie, Pharmazie und Geowissenschaften
der Johannes Gutenberg-Universität Mainz

vorgelegt von
Mardiyati
geboren in Jambi, Indonesien

Mainz, 2011

Contents

1. Introduction……..... 1

1.1 Scientific and Technological Background……..... 1

1.2 Major Steps of the Work……..... 3

2. Theoretical Background……..... 5

2.1 Fractionation…… 5

2.1.1 Precipitation Fractionation…….. 5

2.1.2 Solubility Parameters..... 7

2.2 Spin Coating Theory…… 8

2.3 Planar Waveguides and Prism Coupling……... 10

2.3.1 Waveguide Modes……..... 12

2.3.2 Basic Principles of Prism Coupling……. 16

3. Experimental Methods……..... 19

3.1 Precipitation Fractionation..... 19

3.2 Gel Permeation Chromatography..... 20

3.3 Spin Coating..... 21

3.4 Thickness Measurement..... 22

3.5 UV-Vis-NIR Transmission and Reflection Spectroscopy..... 22

3.6 FTIR Spectroscopy..... 23

3.7 Wide Angle X-Ray Scattering..... 24

3.8 Prism Coupling..... 24

3.9 Attenuation Loss of Slab Waveguides..... 25

3.10 UV- Irradiation……. 26

3.11 NMR Spectroscopy……... 26

3.12 Dip Coating……... 26

4. Tailoring Molecular Weight and Solution Studies..... 28

4.1 Precipitation Fractionation..... 28

4.1.1 Gel Permeation Chromatography…… 33

4.1.2 UV-Vis Absorption Spectroscopy……... 37

4.1.3 Summary and Conclusions..... 40
4.2 Chain Scission by UV- Irradiation…….. 40
4.2.1 Gel Permeation Chromatography…… 41
4.2.2 UV-Vis Absorption Spectroscopy…….. 42
4.2.3 NMR Spectroscopy..... 43
4.2.4 Infrared Spectroscopy..... 49
4.3 Summary and Conclusions ……. 54

5. Thin Films Prepared by Spin Coating..... 56
5.1 Influence of Molecular Weight..... 56
5.1.1 Film Preparation..... 56
5.1.2 Reflectometry..... 57
5.1.3 Prism Coupling..... 59
5.1.4 Wide Angle X-Ray Scattering..... 62
5.1.5 Summary and Conclusions..... 64
5.2 Influence of Film Casting Conditions..... 64
5.2.1 Solvent effects..... 64
5.2.2 Influences of Film Casting Temperature..... 75
5.3 Summary and Conclusions..... 77

6. Dip Coating Experiments..... 79
6.1 Planar Substrates..... 79
6.2 Fibers……..... 81
6.3 Summary of Fiber Resonator Studies..... 83

7. Influence of Side-Chain Substitution on Film Morphology Investigated by FTIR Spectroscopy..... 84
7.1 Materials……. 84
7.2 FTIR Spectroscopy……. 84
7.2.1 Results……. 84
7.2.2 Discussion……... 86

8. Summary……. 87

9. Zusammenfassung…….. 88

10. References……... 90

Appendix A: GPC Results of Fractionations..... 99
Appendix B: Full Chemical Names and Properties of PPV Derivatives..... 106
Appendix C: UV-Vis Spectra of MEH-PPV in Mixed Solutions..... 107
Appendix D: Calculation of Solubility Parameter of MEH-PPV……... 108
Appendix E: ^{1}H NMR of MEH-PPV..... 109
Appendix F: Studies of Dip Coating on Fibers..... 111
List of Publications..... 112
Acknowledgements..... 113
Curriculum Vitae..... 114

1 Introduction

1.1 Scientific and Technological Background

Conjugated polymers are attractive materials for several applications such as light emitting diodes, plastic lasers, photovoltaic devices, nonlinear optical devices and integrated optical components and circuits [Braun'91, Scott'96, Friend'99, McGehee'00, Turnbull'03, Gaal'03, Sariciftci'93, Yu'95, Petrisch'99, Koynov'02, Stegeman'89, Hornak'92, Ma'02]. For application as integrated optical waveguide devices, for instance optical switches, prerequisites are good quality of thin polymer films and detailed knowledge of specific basic optical properties such as refractive index, birefringence, absorption coefficient and propagation loss of optical slab waveguides. High reproducibility of their optical properties, in particular the optical constants is also mandatory for applications. However, there are several reports of basic optical properties of thin film of conjugated polymers such as their refractive index and absorption coefficient which show significant disagreements [Fitrilawati'02, Boudrioua'00, Bader'02, Wasey'01, Tammer'02, Kranzelbinder'02, Campoy'05]. Therefore, it is important to investigate parameters that determine the morphology because it influences optical properties of thin polymers films considerably.

The control of morphology of thin films is a crucial step in the development of polymeric materials for devices. Improved knowledge of structure-property relations is beneficial for waveguide applications and other disciplines as well. The morphology of thin films of conjugated polymers depends on many parameters and has strong impact on applications [Nguyen'00, Nguyen'02, Ruini'04, Tsao'10]. The ways the films are cast and the processing conditions determine their morphology [Shi'00, Nguyen'01, Liu'01, Schwartz'03, Yang'98, Jeng'05]. As an example, films produced by spin coating have conjugated segments mainly oriented parallel to the substrate and on the contrary, films produced by ink jet printing can have conjugated segments perpendicular to the substrate [Barbosa'09].

In this work we use poly[2-methoxy-5-(2-ethylhexyloxy)-1,4-phenylene-vinylene] (MEH-PPV, see Fig 1.1 for its chemical structure) as model material to gain basic understanding of structure-optical properties relationship of a typical conjugated polymer [McGehee'00, Scott'96, Scwartz'03]. MEH-PPV has some advantages such as outstanding semiconducting, luminescent, nonlinear optical properties, solubility in common organic solvent and relatively easy processing properties to thin films.

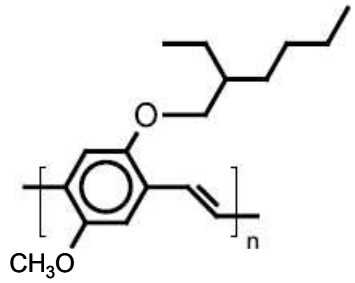

Fig.1.1: Chemical structure of MEH-PPV

In previous studies it turned out that molecular weight of MEH-PPV has crucial impact on most properties [Koynov'04, Koynov'06]. MEH-PPV with low molecular weight ($M_w \approx 4.03 \times 10^4$ g/mol) is optimally suited for the realization of all-optical switching application because of the ease of thin film preparation, and good combination of high nonlinearity and ultimately low waveguide propagation losses [Bahtiar'08, Bahtiar'09]. However, MEH-PPV with certain M_w, especially with low M_w and small polydispersity index (PDI), is not commercially available. In general, commercial synthetic polymers have a broad distribution of molecular weight. However, we can obtain polymer with low M_w and small PDI by fractionation of these polymers. Fractionation is a technique to separate polymer chains for getting a polymer which has a narrower molecular weight distribution. On a laboratory scale, we can use the so-called precipitation fractionation [Cantow'67, Koningsveld'70]. Fig. 1.2 displays curves of successive fractionations for seven precipitates [Schulz'40].

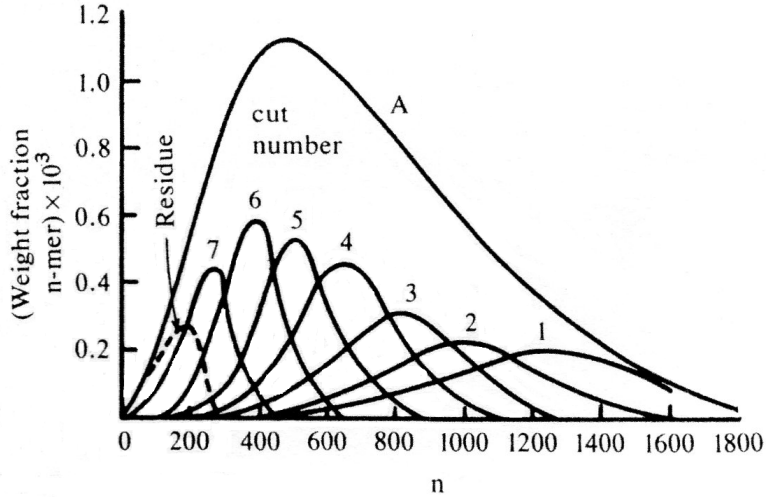

Fig. 1.2: Molecular weight distribution of fractionation steps 1 - 7, compared with the starting material A [Schulz'40].

Another way to obtain narrower molecular weight is cleavage of polymer chains by using UV-irradiation [Müller'84, Rau'84]. It was reported by Müller et al. that molecular weight and PDI of the polymer are reduced by chain scission after UV-irradiation. Therefore, the starting point of our work will be tailoring of molecular weight of MEH-PPV by performing precipitation fractionation and chain cleavage by UV-irradiation to obtain MEH-PPV with lower molecular weight and small PDI.

1.2 Major Steps of the Work

The general aim of this work is tailoring the molecular weight of the model conjugated polymer MEH-PPV and to investigate influences of preparation conditions of thin polymer films on morphology and optical properties of thin films. Improved understanding of such structure-property relations is also beneficial for device applications. Following are major steps that had to be executed to accomplish these goals.

We started this work by doing precipitation fractionation [Kotera'67] and chain cleavage by UV-irradiation [Müller'84] to obtain several different molecular weights which have narrow molecular weight distribution. We measured molecular weight distribution by means of gel permeation chromatography. We studied the absorption spectra of the solutions of different molecular weights of polymers obtained by fractionation and UV-irradiation and observed the relation between chain length and absorption maximum. It turned out that UV-irradiation produce polymer with chain defects which interrupt the π-electron conjugation along polymer backbone. We have performed ^{1}H NMR and FTIR spectroscopy to characterize the chain defects.

Spin coating is the most commonly used technique to produce uniform and homogeneous thin films [Weil'88, Norman'05]. Earlier work shows that the morphology of thin films can be controlled by variation of the spin coating conditions such as solvent, concentration of solution, spinning speed, and casting temperature [Schwartz'03, Jaczewska'08]. In this work, we prepared thin films and planar waveguides using spin coating technique. We have performed spin casting at different temperature and used solvents with different boiling points to investigate effects of processing conditions of spin casting on morphology and optical properties.

As an alternate approach, we also used dip-coating to prepare thin films of MEH-PPV using two types of substrates: planar glass slides and thin fibers of fused silica. We have prepared dip-coated films of MEH-PPV as cladding of bottle microresonators for the

realization of optical switching applications. This part of the work was performed in collaboration with the Applied Quantum Physics group at Department of Physics, Mainz University.

Optical properties of thin films such as absorption coefficient, refractive index, birefringence and waveguide loss are very important for optoelectronics applications. We have used transmission and reflection spectroscopy [Mathy'96, Penzkofer'98] to measure the dispersion of optical constants in thin films. For measuring refractive index of planar waveguides, we used the prism coupler technique [Tien'77].

Some optical properties are influenced by physical conformation of polymer chains and the ways chains pack together in films [McGehee'00]. We have used wide angle X-ray diffraction (WAXS) to characterize crystallinity in films [Yang'98] and have also characterized chain conformation and chain orientation with respect to the layer plane by using Fourier-Transform Infrared (FTIR) spectroscopy.

2 Theoretical Background

2.1 Fractionation

Polymers are usually polydisperse and have a molecular weight distribution. There are several average values used to represent the molecular weight distribution. The two most important molecular weight averages are the number-average molecular weight, M_n, and weight-average molecular weight, M_w [Sperling'01].

$$M_n = \frac{\sum_i N_i M_i}{\sum_i N_i} \tag{2.1}$$

$$M_w = \frac{\sum_i N_i M_i^2}{\sum_i N_i M_i} \tag{2.2}$$

where N_i is the number of molecules of molecular weight M_i.

The ratio M_w/M_n is called the polydispersity index (PDI) and provides a simple definition of molecular weight distribution. The quantities M_n and M_w are equal only if all polymer chains have the same length, which means they are mono-disperse. Polymers with large PDI have a broad molecular weight distribution.

Fractionation is a separation of a polydispersive polymer into fractions of narrower molecular mass distribution. Fractionation is performed to reduce the polydispersity of polymers. The usual procedures for polymer fractionation involve the distribution of the polymer molecules between two phases [Huggins'67].

2.1.1 Precipitation Fractionation

The objective of fractionation could be for analytical or preparative purposes. The aim of preparative fractionation is to obtain an amount of fractionated material on which further investigations can be carried out [Koningsveld'70]. For this purpose, we can use the classical precipitation and extraction procedure. The basic principle of fractionation technique is subdivision of the polymer sample into fractions due to the different solubility of the species or one can perform a fractionation by changing the dissolution power [Francuskiewicz'94]. The precipitation in fractional precipitation is carried out by stepwise decrease in the solvent power of the system. There are three methods to achieve

this condition; addition of poor solvent (or precipitant), elimination of solvent by evaporation and lowering the temperature of system. In our study, we used addition of poor solvent to perform fractional precipitation as well as temperature reduction.

The principles of fractionation by precipitation dealing with experimental and theoretical work are described in several reviews [Cragg'46, Desreux'52, Guzmán'61, Cantow'67 and Koningsveld'70]. Following is the general procedure of precipitation fractionation by adding precipitant described by Kotera [Kotera'67].

The polymer sample is dissolved in a suitable solvent and an appropriate poor solvent is added gradually to this solution at constant temperature and continuously stirred. After a certain amount of poor solvent has been added, the addition of more drops of poor solvent starts to cause turbidity, which is not disappearing quickly during stirring. At this stage, the dropwise addition of poor solvent is continued more carefully until the system reaches a point just short of the turbidity end point. The slow drop wise addition of a further small amount of poor solvent is continued until the solution turns milky. The precipitated phase is separated from the supernatant phase by centrifugation and washed by poor solvent. The precipitate contains the highest molecular weight fraction dried at an appropriate temperature in vacuum. The supernatant liquid is treated with a further volume of poor solvent, using the same procedure described above, to obtain the next fraction. The procedure is repeated as many times as necessary until a fairly large proportion of poor solvent would be necessary to obtain the desired fraction. The final fraction is obtained by evaporating the supernatant liquid to dryness in a vacuum.

Theoretically, the solvent power is expressed in terms of the "Flory-Huggins polymer-solvent interaction constant, χ." A solvent for a given polymer with $\chi < ½$ is called a good solvent. A solvent with $\chi > ½$ is called a poor solvent. As χ increases, the solvent becomes unable to dissolve the polymer and then it is called a nonsolvent.

Gradual addition of a poor solvent will cause the χ value of the system to successively exceed the χ_c value for each component. In this way, phase separation will occur when the χ value of the system is somewhat in excess of 0.5. The component will then be precipitated in the order of decreasing value of the segment number N. The critical value χ_c will depend upon the molecular weight of the dissolved polymer molecules [Kotera'67, Teraoka'02].

$$\chi_c = \frac{(1+N^{1/2})^2}{2N} \cong \frac{1}{2} + \frac{1}{\sqrt{N}} \qquad (2.3)$$

where N is number of segments per polymer chain.

Fig. 2.1 displays a phase diagram of the solution in the Flory-Huggins mean-field theory. The concept of this theory can be found in literature [Huggins'67, Teraoka'02].

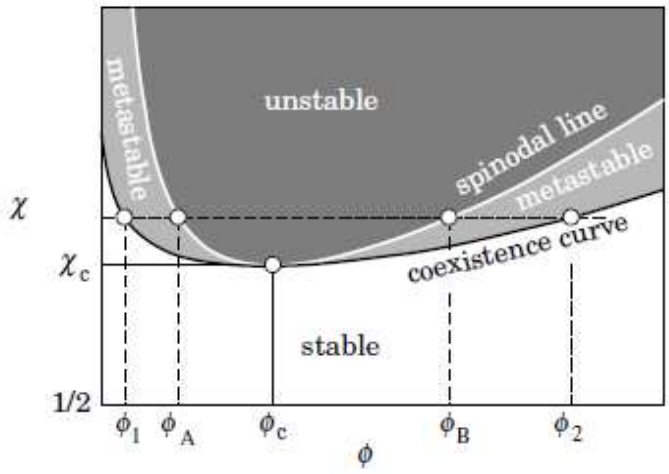

Fig. 2.1: Spinodal line and the coexistence curve in the mean-field theory. The solution is unstable in the darkly shaded region, metastable in lightly shaded region, and stable in the other region [Teraoka'02].

Spinodal line is the line that separates the stable region from the unstable region and minimized to χ_c at $\phi = \phi_c$, where ϕ is the volume fraction of the polymer. This point is called the critical point. As shown in Fig.2.1, the system is unstable and spontaneously separates into two phases at $\phi < \phi_c$ or $\phi > \phi_c$. The lower curve is called coexistence curve (or a binodal line), the curve that demarcates the single-phase regime from the two-phase regime. Solutions in the two regions between the two curves are metastable.

2.1.2 Solubility Parameters

Hansen developed solubility parameters based on three specific molecular interactions: dispersive forces, polar cohesive forces and Hydrogen bonding [Hansen'00, Miller-Chou'03]. Therefore, the cohesive energy has three components corresponding to the three types of interactions:

$$E = E_D + E_P + E_H \tag{2.4}$$

Dividing the cohesive energy by the molar volume gives the square of the Hildebrand solubility parameters as the sum of the squares of the Hansen dispersion (D), polar (P) and hydrogen bonding (H) components:

$$E/V = E_D/V + E_P/V + E_H/V \tag{2.5}$$

$$\delta = \delta_D^2 + \delta_P^2 + \delta_H^2 \tag{2.6}$$

The solubility parameters of a given material can be calculated either from the cohesive energy, or from the molar attractive constant, *F*. Van Krevelen and Hoftzyer [Krevelen'08] compiled a set of group contribution values based on atomic contributions to calculated *F* derived by Van Krevelen and *E* calculations based on Small's method. Their method estimates the individual solubility parameter components from group contributions using the following equations:

$$\delta_D = \frac{\sum F_{Di}}{V} \tag{2.7}$$

$$\delta_P = \frac{\sqrt{\sum F_{Pi}^{\,2}}}{V} \tag{2.8}$$

$$\delta_H = \sqrt{\frac{\sum E_{Hi}}{V}} \tag{2.9}$$

Eq. (2.8) is chosen to correct the interaction of polar groups. The polar component is further reduced, if two identical polar groups are present in a symmetrical position. To take this effect into account, the value of δ_P, calculated with Eq. (2.8) must be multiplied by a symmetry factor of 0.5 for one plane of symmetry, 0.25 for two planes of symmetry, 0 for more planes of symmetry. The *F*-method is not applicable to the calculation of δ_H. Hansen stated that the hydrogen bonding energy E_{Hi} per structural group is approximately constant, which leads to the form of Eq. (2.9). For molecules with several planes of symmetry, $\delta_H = 0$.

2.2 Spin Coating Theory

There are several factors involved in the spin coating process such as hydrodynamics, rheology of the polymer solution, heat transfer, solvent mass transfer, momentum transfer (fluid flow) and the interplay of these processes [Washo'77, Meyerhofer'78, Lai'79, Chen'86, Weil'88]. In general, higher spinning speed and lower concentration (or viscosity) will create thinner films as defined by Eqs. 2.10 and 2.11, respectively [Bornside'87, Lawrence'88],

$$d = k_1 \omega^{\alpha} \tag{2.10}$$

where d is film thickness, ω is spinning speed, while k_1 and α are empirically determined constants. Frequently, it is reported that the exponent α is -0.5 [Meyerhofer'78, Lai'79, Givens'79, Daughton'82, Chen'83, Spangler'90]. The molar mass of polymer as measured by intrinsic viscosity η, has an effect on the film thickness at constant rotation speed through the Eq. (2.11) with a constant γ.

$$d = \eta^{\gamma} \tag{2.11}$$

The intrinsic viscosity (η) is related to the viscosity-average molecular weight M_v through the Mark-Houwink Sakurada equation

$$\eta = K(M_v)^{\sigma}, \tag{2.12}$$

where σ is the Mark-Houwink-Sakurada exponent.

Spangler et al. [Spangler'90] studied the effect of molecular weight and polydispersity of the polymer on the film thickness in which polydispersity of polymer is defined as the M_w/M_n ratio. M_v is related to the type of solvent (through the parameter σ) and to the molecular weight distribution. They expressed the viscosity average molecular weight M_v through Eq. (2.13) controlling this way the molecular weight parameter for the film thickness

$$M_v = (\sum w_i M_i^{\sigma})^{1/\sigma}, \tag{2.13}$$

where w_i is the weight fraction of the ith component and M_i is the molecular weight of the ith component. Therefore, the final thickness of spin coated film eventually becomes a function of the spinning speed, concentration and viscosity through Eq. (2.14).

$$d = \omega^{\alpha} (C_w)^{\beta} (M_w)^{\gamma} \tag{2.14}$$

Thus, we can prepare films with required thicknesses by using Eq. (2.15).

$$d_1 = d_0 \left(\frac{\omega_1}{\omega_0} \right)^{\alpha} \left(\frac{C_{w_1}}{C_{w_0}} \right)^{\beta} \tag{2.15}$$

In order to get a desired film thickness, we can use Eq. (2.15) first by determining α, β and d_0 experimentally at particular spin speed ω_0 and concentration C_{w0} for samples with a specific molecular weight.

2.3 Planar Waveguides and Prism Coupling

Dielectric waveguides are structures that are used to confine and guide the light in guided-wave devices and integrated optical circuits [Kogelnik'79]. A planar waveguide is characterized by parallel planar boundaries with respect to one (x) direction, but is treated as infinite in extent in the lateral directions (y and z) as shown in Fig. 2.2 [Hunsperger'84]. A planar film of refractive index n_2 and thickness d is sandwiched between a substrate and a cover material with lower refractive indices n_3 and n_1 ($n_2 > n_3 \geq n_1$) and often the cover material is air, in which $n_1 = 1$. There are two types of planar waveguide; symmetric and asymmetric. We have a symmetric waveguide if $n_1 = n_3$. In this thesis, we study the asymmetric planar waveguide where $n_1 \neq n_3$.

The fundamental theory of planar waveguides has been described by many authors [McWhorter'63, McKenna'67, Tien'71, Marcuse'74, Taylor'74 and Kogelnik'79]. Following is the approach developed by Taylor and Yariv and the description is taken from Hunsperger [Taylor'74, Hunsperger'84].

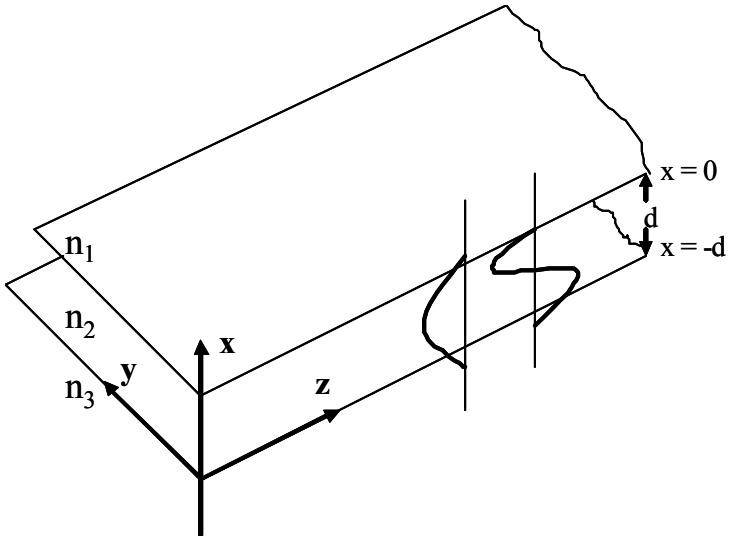

Fig. 2.2: Diagram of the basic three-layer planar waveguide structure. Two modes are shown, representing distributions of electric field in the x direction [Hunsperger'84].

As shown in Fig. 2.2, light waves are assumed to be propagating in the z direction. A mode is a spatial distribution of optical energy in one or more dimensions. An equivalent mathematical definition of a mode is that it is an electromagnetic field which is a solution of Maxwell's wave equation [Hunsperger'84]

$$\nabla^2 E(r,t) = \left[\frac{n^2(r)}{c^2}\right]\frac{\partial^2 E(r,t)}{\partial t^2}, \qquad (2.16)$$

where E is the electric field vector, r is the radius vector, $n(r)$ is the index of refraction, and c is the speed of light in vacuum. For monochromatic waves, the solutions of (2.16) have the form

$$E(r,t) = E(r)e^{i\omega t} \tag{2.17}$$

where ω is the radian frequency. Substituting (2.17) into (2.16) we obtain

$$\nabla^2 E(r) + k^2 n^2(r) E(r) = 0\,, \tag{2.18}$$

where $k = \omega/c = (2\pi/\lambda)$. If we assume a harmonic wave traveling in positive z direction with propagation constant $\beta, E(r) = E(x,y)\exp(-i\beta z)$ then (2.18) becomes

$$\frac{\partial^2 E(x,y)}{\partial x^2} + \frac{\partial^2 E(x,y)}{\partial y^2} + \left[k^2 n^2(r) - \beta^2\right] E(x,y) = 0\,. \tag{2.19}$$

We can write (2.19) separately for three regions in x, by assuming waveguide infinite in the y direction

$$\begin{aligned}
&\text{Region 1} \quad \partial^2 E(x,y)/\partial x^2 + (k^2 n_1^2 - \beta^2) E(x,y) = 0\,,\\
&\text{Region 2} \quad \partial^2 E(x,y)/\partial x^2 + (k^2 n_2^2 - \beta^2) E(x,y) = 0\,,\\
&\text{Region 3} \quad \partial^2 E(x,y)/\partial x^2 + (k^2 n_3^2 - \beta^2) E(x,y) = 0\,,
\end{aligned} \tag{2.20}$$

where $E(x,y)$ is one of the Cartesian components of $E(x,y)$. The solutions of (2.20) are either sinusoidal or exponential function of x in each of the regions, depending on whether $(k^2 n_i^2 - \beta^2)$, where i = 1, 2, 3, is greater than or less than zero which $E(x,y)$ and $\partial E(x,y)/\partial x$ continuous at the interface between layers. Hence the possible modes are limited to those shown in Fig. 2.3.

For the case $n_2 > n_3 > n_1$ at constant frequency ω, the mode shape changes as function of β. When $\beta > kn_2$, the function $E(x)$ must be exponential in all three regions and only the mode shape shown as (a) in Fig. 2.3 could satisfy the boundary condition. This mode is not physically viable because the field increases unboundedly in layers 1 and 3, implying infinite energy.

For $kn_3 < \beta < kn_2$, modes (b) and (c) are well confined guided modes, generally referred to as the zeroth order and first order transverse electric modes, TE_0 and TE_1 [Yariv'76].

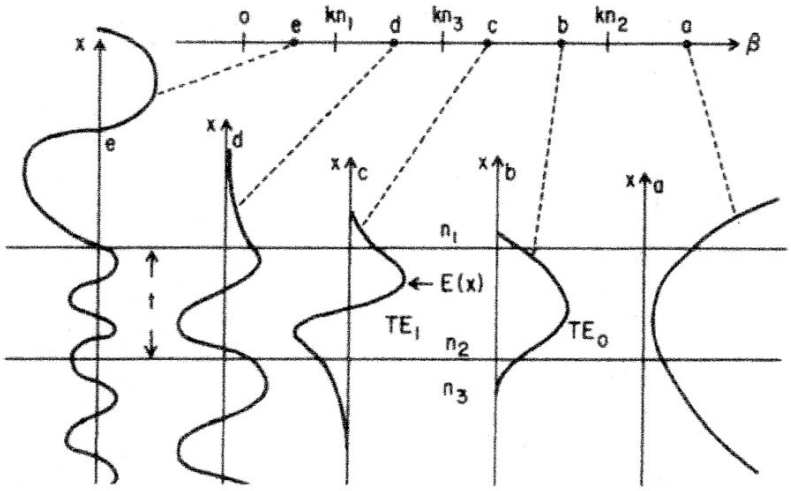

Fig 2.3: Diagram of the possible modes in a planar waveguide [Taylor'74, Hunsperger'84].

If $kn_1 < \beta < kn_3$, a mode (d) will result. This type of mode, which is confined at the air interface but sinusoidally varying at the substrate, is often called a substrate radiation mode. Finally, if $0 < \beta < kn_1$, the solution for $E(x)$ is sinusoidal in all three regions of the waveguide structure (e). These modes are not guided modes because the energy is free to spread out of the waveguiding region 2 and are called as air radiation modes of the waveguide.

2.3.1 Waveguide Modes

The ray optics approach can be used to solve the eigenvalue equation for both TE- and TM-modes. This is possible because the waveguide consists of layers of homogeneous dielectric materials. Wave propagation in each region can be represented by the superposition of two plane waves. One of the plane waves may be considered as the incident wave, while the other is viewed as reflected one. The total internal reflection is sufficient to assure the confinement of energy in the guiding layer. The phenomenon of total internal reflection can be found in literature [Hecht'87, Möller'88, Yeh'88].

Consider a ray of light A propagates in the film toward the film-substrate interface (x = -d) with an incident angle θ, as displayed in Fig. 2.4.

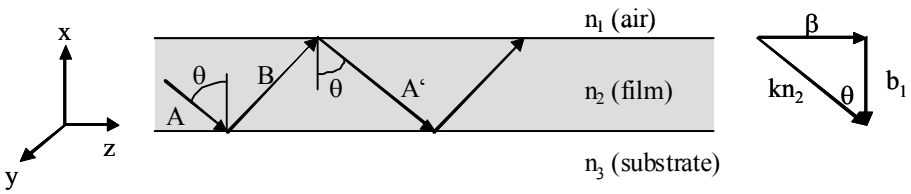

Fig. 2.4: Ray trajectory of a guided wave in a thin film waveguide. The coordinate system and wave vector are also given [Bahtiar'04].

If θ is larger than the critical angle $\sin^{-1}(n_3/n_2)$, the ray *A* will be totally reflected into ray *B* at film-substrate interface. The phase of *B* at this interface is

$$\Phi_{23} = \tan^{-1}\left(\frac{p}{h}\right) \tag{2.21}$$

for the TE modes and

$$\Phi_{23} = \tan^{-1}\left(\frac{n_2}{n_3}\right)^2\left(\frac{p}{h}\right) \tag{2.22}$$

for the TM modes.

Similarly, the *B* is reflected into *A'* at film-air interface (x = 0). In this case the phase changes are

$$\Phi_{12} = \tan^{-1}\left(\frac{q}{h}\right) \tag{2.23}$$

for TE modes, and

$$\Phi_{12} = \tan^{-1}\left(\frac{n_2}{n_1}\right)^2\left(\frac{q}{h}\right) \tag{2.24}$$

for TM modes, respectively. Here, $0 < \Phi_{ij} < \pi/2$, the constants p and h are given by Eq. (2.33).

We will use the ray model ("zigzag model") to derive the mode equation. As shown in Fig. 2.4, the ray *A'* follows the ray *A* after one zigzag path. Because the total reflection at both film-substrate and film-air interfaces, the amplitude of rays *A* and *A*' differs only by a phase Δ. After subsequent zigzags, the ray has phase differences 2Δ, 3Δ …relative to

A. The superposition of such of rays is zero, except when $\Delta = 2m\pi$ with integer m. The total phase difference between A and A' is [Tien'70, Tien'77, Kogelnik'79]

$$2b_1 d - 2\Phi_{23} - 2\Phi_{12} = 2m\pi \qquad m = 0, 1, 2, ... \qquad (2.25)$$

This equation is called as mode equation, where m represents the number of the mode. Equation (2.25) is valid for both TE and TM modes, but Φ_{ij} differ. According to the vector diagram in Fig. 2.4, we have

$$\begin{aligned} b_1 &= kn_2 \cos\theta \\ \beta &= kn_2 \sin\theta \end{aligned} \qquad (2.26)$$

For each allowed mode, there is a corresponding propagation constant β_m and velocity given by

$$\beta_m = kn_2 \sin\theta_m \qquad (2.27)$$

$$v = c(k/\beta_m)$$

Effective refractive index can be defined as

$$n_{eff} = c/v = \beta_m / k \qquad (2.28)$$

which is bounded by $n_3 < n_{\text{eff}} < n_2$.

Transverse Electric Modes

TE modes have their electric field perpendicular to the plane of incidence. Figure 2.2 shows a three-layer waveguide structure. For the case of TE plane waves traveling in z direction, with propagation constant β, Maxwell's wave equation (2.16) reduces to [Hunsperger'84]

$$\nabla^2 E_y = \frac{n_i^2}{c^2}\frac{\partial^2 E_y}{\partial t^2} \quad i = 1, 2, 3,\ldots \qquad (2.29)$$

with solutions of the form

$$E_y(x,z,t) = \varepsilon_y(x) e^{i(\omega t - \beta z)}. \qquad (2.30)$$

The subscript i in Eq. (2.29) corresponds to a particular one of the three layers of the waveguide structure. The solution for ε_y can be expressed in terms of a single constant C′.

$$\varepsilon_y(x) = \begin{cases} C'\exp(-qx), & x > 0 \\ C'[\cos(hx) - (q/h)\sin(hx)], & -d < x < 0 \\ C'[\cos(hd) + (q/h)\sin(hd)]\exp[p(x+d)], & x < -d \end{cases} \qquad (2.31)$$

To determine q, h, and p substitute (2.31) Into (2.30) using the resulting expression for $E_y(x,z,t)$ in (2.29) for each or the three regions obtaining

$$\begin{aligned} q &= (\beta^2 - n_1^2 k^2)^{1/2} \\ h &= (n_2^2 k^2 - \beta^2)^{1/2} \\ p &= (\beta^2 - n_3^2 k^2)^{1/2} \\ k &= \omega / c \end{aligned} \qquad (2.32)$$

In Eq. (2.32) q, h and p are all given in terms of the single unknown β. By making $\partial E_y / \partial_x$ continuous at the interface x = 0 and x = -d, a condition on β is derived. By applying these requirements into Eq. (2.31), we obtain

$$\tan(hd) = \frac{p+q}{h(1 - pq/h^2)} \qquad (2.33)$$

This transcendental equation can be solved either graphically or numerically. The result is a set of discrete allowed values of β, corresponding to the allowed modes. For each β_m, the corresponding values of q_m, h_m and p_m can be determined from Eq. (2.32).

Transverse Magnetic Modes

For transverse magnetic or TM modes, the magnetic field vector is perpendicular to the plane of incidence. The development of TM modes is similar to that of TE modes, except that the non-zero components are H_y, E_x, and E_z rather than E_y, H_x, and H_z. The resulting field components are [Taylor'74, Marcus'74 and Hunsperger'84]

$$H_y = (x,z,t) = H_m(x) e^{i(\omega t - \beta z)}, \qquad (2.34)$$

$$E_x(x,z,t) = \frac{i}{\omega\varepsilon}\frac{\partial H_y}{\partial z} = \frac{\beta}{\omega\varepsilon} H_m(x) e^{i(\omega t - \beta z)}, \qquad (2.35)$$

$$E_z(x,z,t) = -\frac{i}{\omega\varepsilon}\frac{\partial H_y}{\partial x}. \qquad (2.36)$$

The transverse magnetic component $H_m(x)$ is given by

$$H_m(x) = \begin{cases} -C'\left[(h/\bar{q})\cos(hd) + \sin(hd)\right]\exp[p(x+d)], & x < -d \\ C'[-(h/\bar{q})\cos(hx) + \sin(hx)], & -d < x < 0 \\ -C'(h/\bar{q})\exp(-qx), & x > 0 \end{cases} \quad (2.37)$$

where h, q, and p are defined by Eq. (2.32) and C′ is normalization constant. When boundary conditions are matched in a manner that is analogous to the TE case, it is found that only those values of β are allowed for which

$$\tan(hd) = \frac{h(\bar{p} + \bar{q})}{(h^2 - \bar{p}\bar{q})} \quad (2.38)$$

where

$$\bar{p} = \left(\frac{n_2}{n_3}\right)^2 p, \quad \bar{q} = \left(\frac{n_2}{n_1}\right)^2 q \quad (2.39)$$

Similar to that of TE, this eigenvalue equation can be solved either graphically or numerically.

2.3.2 Basic Principles of Prism Coupling

The first theoretical treatment of the prism coupler was published in 1962 [Iogansen'62] and the first laboratory experiments were reported in 1964 by Osterberg and Smith [Osterberg'64]. After demonstrating that prism couplers have high efficiencies and can be built for optical surface waves [Tien'69 and Harris'69], many investigations developed. Several experimental works have shown that prism couplers can be constructed for highly efficient broad-band operation [Midwinter'70, Harris'70, Tien'70, Ulrich'70, Tamir'71, Bell'73 and Ulrich'74].

The principle of prism coupling is illustrated in Fig. 2.5 [Hunsperger'84]. A monocromatic beam of light of width W propagates in a high index of refraction medium (n_p) with $n_p > n_1$, which n_1 is assumed to be air. The n_p must be not only larger than n_1 but also larger than n_2.

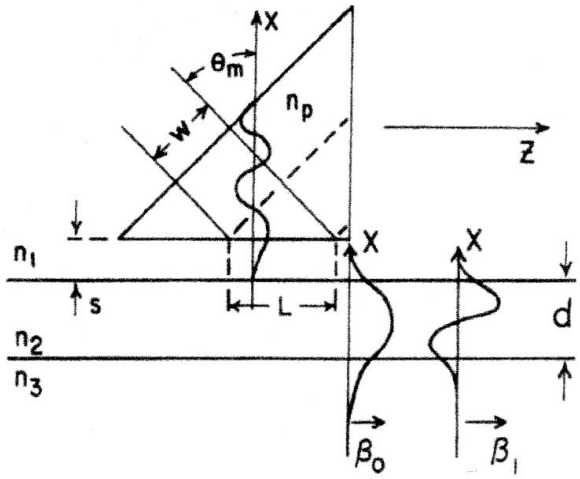

Fig. 2.5: Diagram of prism coupler [Hunsperger'84]

The beam is totally internally reflected at the $n_p - n_1$ interface setting up a standing wave mode along the vertical x direction in the prism, but moves in the z direction with a phase constant β_p. Meanwhile, in the waveguide various guided modes can exist and moving in the z direction with phase constants β_m. All of these guided modes have an evanescent tail extending slightly beyond the $n_1 - n_2$ interface. The tails of waveguide modes overlap the tail of the prism mode if the prism spacing s is small enough. There is coherent coupling of energy from the prism mode to the m waveguide mode when θ_m is chosen so that $\beta_p = \beta_m$. The condition for matching of the β terms is given by

$$\frac{2\pi n_p}{\lambda_0}\sin\theta_m = \beta_m \tag{2.40}$$

In order to couple to a given mode we can change θ_m by changing the angle of incidence of the optical beam. The interaction between prism and waveguide modes can occur only over the length L. A complete interchange of energy between phase-matched modes occurs if the interaction length in the z direction satisfies the relation

$$\kappa L = \pi/2 \tag{2.41}$$

where κ is the coupling coefficient and depends on n_p, n_1 and n_2. The coefficient κ also determines the shape of the mode tails and on the prism spacing s. From (2.41), the length required for complete coupling is given by

$$L = \frac{W}{\cos\theta_m} = \frac{\pi}{2\kappa} \tag{2.42}$$

For a given L, the coupling coefficient required for complete coupling is given by

$$\kappa = \frac{\pi \cos \theta_m}{2W} \tag{2.43}$$

This condition for complete coupling assumes that the amplitude of the electric field is uniform over the entire width W of the beam.

3 Experimental Methods

3.1 Precipitation Fractionation

Poly (2-methoxy-5(2′-ethyl-hexyloxy)-1,4-phenylenevinylene) (MEH-PPV) was commercially available from American Dye Source (ADS), Canada. Several batches were bought, see Chapter 4.1 for details. The fractionation of MEH-PPV was performed as follows. 1 gram of MEH-PPV was dissolved in 100 ml of toluene at 55 °C. It was stirred over night to get a homogeneous solution. Experimental setup of fractionation is shown in Fig.3.1. The solution of the starting polymer (P0) was heated by means of a water bath. We used a hot plate which has digital thermometer to control the temperature of water. The solution of P0 was continuously stirred at the temperature T ≅ 55 °C and at the same time a poor solvent (methanol) was slowly added to the solution until precipitation occurred.

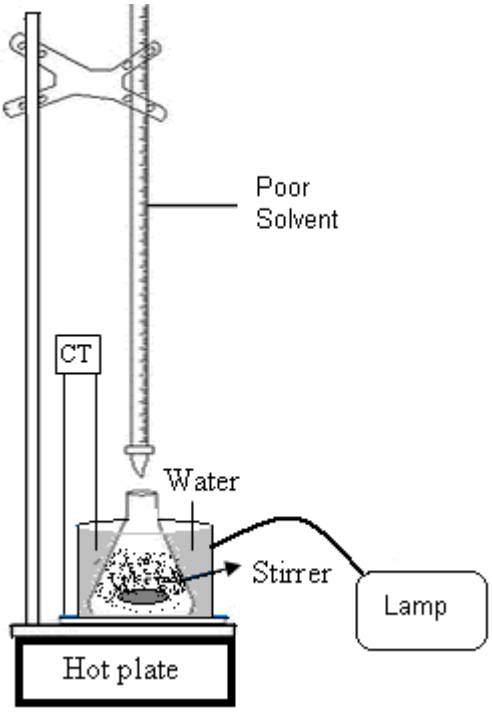

Fig. 3.1: Experimental setup of fractionation, CT: Control of temperature

We stop adding the poor solvent as soon as the solution becomes cloudy, which can be detected by visual inspection of the solution by means of the lamp and the optical fiber. We used Zeiss KL 1500 electronic lamp, Schott Germany equipped with an optical

fibre to detect the cloudy state. It is a condition when the solution becomes opaque and some polymer flakes or fibres appear and precipitate. Before cloudy state, some polymer flakes also will be visible but after stirring they vanish. We stop adding the poor solvent when the flakes still occur after stirring. It needs careful observing to decide when we have to stop adding the poor solvent because it will affect the polydispersity of the resulting precipitate polymer called P1.

This precipitate (first fraction, P1) contains the highest molecular weight. It was separated by centrifugation at room temperature, washed with methanol and dried in vacuum oven at T ≅ 50 °C. The remaining solution (S1) was stirred at lower temperature (for this work, the best temperature was 45 °C) and the above procedure was repeated (see Scheme 3.1, in which T1 > T2 > T3).

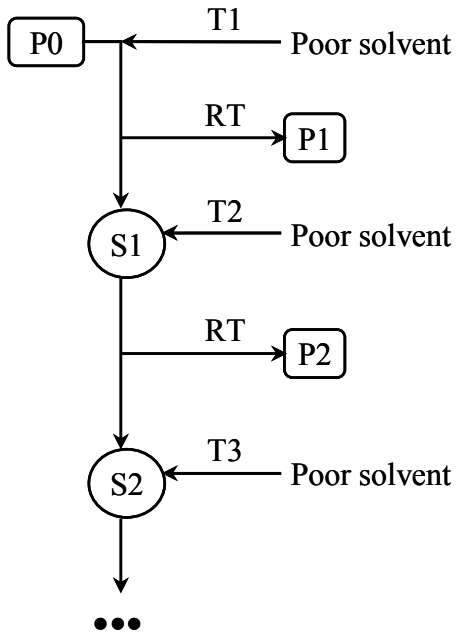

Scheme 3.1: Fractionation procedure. P0: Starting material (MEH-PPV in toluene). T: Temperature of solution. P1, P2: Precipitates 1 and 2. S1, S2: Remaining solutions 1 and 2.

3.2 Gel-Permeation Chromatography (GPC)

Molecular weight of polymer was determined by Gel-Permeation Chromatography (GPC). This technique is widely used as a fast and simple method to determine molecular weights of polymers as well as molecular weight distributions. All molecular weight determinations were performed by the Polymer Analytics group at MPI-P Mainz. They were measured by using UV detector, polystyrene as standard and THF as eluent.

3.3 Spin Coating

Spin coating is a well-known procedure to produce thin (0.2 - 2 μm) and homogeneous films on various substrates. It was performed by flooding the substrate with a polymer solution and rotating at a constant speed on a commercial spin coater (Headway model Pm 101). All films were prepared by spin coating on fused silica substrates (Spectrosil 2000 Präzision Glas & Optik GmbH, Germany) or silicon wafers (Si-Mat Silicon Materials, Germany) which had a thickness of 1 mm. The following cleaning procedure of glass substrates was used:

- 10 times rinsing in purified water (Milli-Q, Millipore) and washing with liquid soap
- 10 times rinsing in purified water
- 15 minutes cleaning in an ultrasonic bath with a solution of 2% detergent (Hellmanex, Hellma) in milli-Q water
- 10 x rinsing in purified water
- Rinsing with ethanol and subsequently drying the substrate in a flow of nitrogen

The polymers were dissolved in suitable organic solvents until they were completely dissolved. The solutions were filtered by means of micro-syringe filters (0.5-5 μm). Thin films were deposited on freshly prepared substrates. Filtered solutions were deposited under a laminar flow hood to minimise dust particles. The rotation speed was varied from 500 to 9000 rpm (rounds per minute). The rotation time was set at 60 s. In general, higher spinning speeds and longer spinning times create thinner films. We can vary the film thickness d by adjusting of concentration of the solution C_w and spinning speed ω, according to the empirical relation [Ziegler'00, Fitrilawati'02]

$$d_1 = d_0 \left(\frac{\omega_1}{\omega_0} \right)^{\alpha} \left(\frac{C_{w_1}}{C_{w_0}} \right)^{\beta} \qquad (3.1)$$

The coefficients d_0, α and β were obtained experimentally. The exponent α was -0.5, which is typical for the spin coating process.

The films were annealed in a vacuum oven about 12 hours at the elevated temperature T_a to remove residual solvent. T_a was set below the glass transition

temperature T_g of polymers, frequently at 50 °C. The cooling process was done slowly (about 20 °C/h) to avoid stress of the polymer films.

3.4 Thickness Measurement

The film thickness d and the average surface roughness R_a of the polymer films was characterized using a step-profilometer (KLA Tencor Coorporation Model P 10) by scanning the surface profile with a diamond tip (radius = 2 μm, force = 2 mg and sampling rate = 50 Hz). The film thickness was measured at a scratch on the film which was made with a sharp needle. The film thickness was evaluated as the height difference between film surface and substrate surface at the scratch. The resolution of the thickness measurement was about 2 nm. The film roughness R_a is quantitatively determined from the average of absolute values of the profile height deviations. The average roughness R_a is defined as:

$$R_a = \frac{1}{n}\sum_{i=1}^{n}|yi| \tag{3.2}$$

The root mean square roughness R_q is:

$$R_q = \sqrt{\frac{1}{n}\sum_{i=1}^{n} y_i^2} \tag{3.3}$$

3.5 UV-Vis-NIR Transmission and Reflection Spectroscopy

The dispersions of intrinsic absorption coefficient $\alpha(\lambda)$ and refractive index $n(\lambda)$ of thin polymer films were determined from the transmission spectra and reflection spectra measured by using a UV-Vis-NIR spectrophotometer (Perkin Elmer model Lambda 900). Samples were prepared onto fused silica substrate with thickness $d \approx 50 - 70$ nm. The configurations for transmission and reflection measurements are shown in Fig. 3.2. The light was s-polarized which means that the electrical field vector was parallel to the film plane. Transmission spectra of thin films were measured at normal incidence [see Fig. 3.2(a)]. Part of light is reflected at air-film-, film-substrate- and substrate-air-interfaces, respectively. The reflection R was measured using a reflection unit [Fig 3.2(b)] at an incidence angle of 15°.

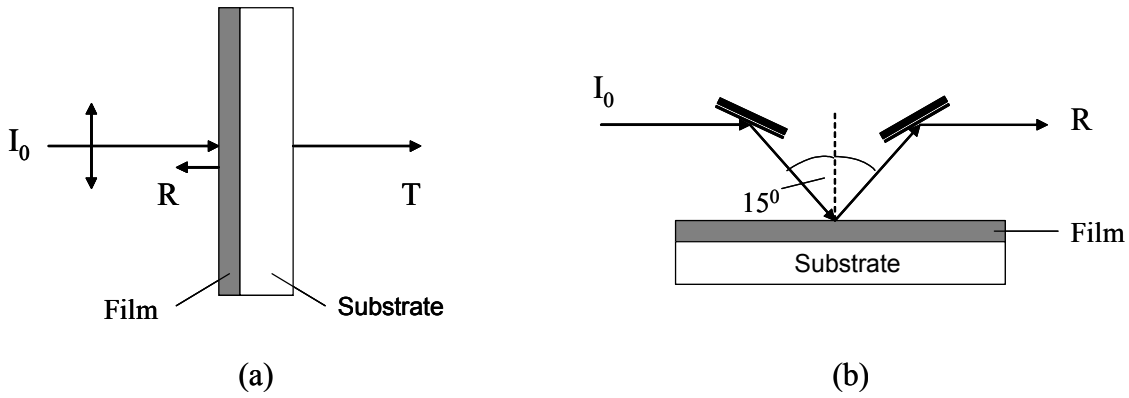

(a) (b)

Fig. 3.2: The configuration for measurement of (a) Transmission and (b) Reflection of thin films on fused silica substrates [Bahtiar'04].

All measurements were performed using a bare fused silica substrate as reference. The dispersions of refractive index n (λ) and absorption coefficient $\alpha(\lambda)$ are calculated by means of the available computer program (Bitrab Version 2.0, 2007) based on the Fresnel equations and Lavenberg-Marquardt Algorithm. This program was developed by W. Scholdei from earlier versions written by K. Ueberhofen [Ueberhofen'96].

3.6 FTIR Spectroscopy

Infrared spectra were recorded with a Nicolet Model Magna 850 FTIR spectrometer at two configurations: Transmission and Grazing Incidence Reflection (GIR). Transmission spectra of thin films ($d \approx 70$ nm, spin coated onto silicon wafers) were measured at normal incidence (the electrical field vector oriented parallel to the plane of film, $E_{\parallel}$). Reflection spectra at grazing incidence (electrical field vector perpendicular to the film plane, $E_{\perp}$) were measured with thin films ($d \approx 70$ nm) that were spin-cast on top of 50 nm thick gold layers prepared before by thermal evaporation onto glass slides. Fig. 3.3 shows the configurations of FTIR measurements at transmission and grazing incidence reflection conditions.

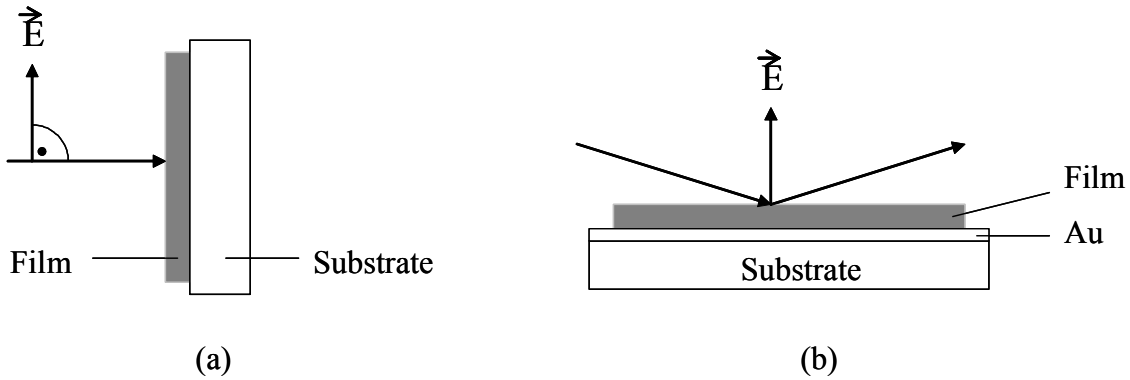

Fig. 3.3: FTIR spectroscopy at (a) Transmission and (b) Grazing incidence reflection (GIR) geometries [Bahtiar'04].

3.7 Wide Angle X-Ray Scattering

Wide Angle X-Ray Scattering (WAXS) was performed by Michael Steiert from X-Ray structure analysis group at MPI-P Mainz by using the Philips goniometer PW 1820 system with Cu Kα line (λ = 0.15418 nm). Thin film polymer was made by spin coating on glass substrates and the X-Ray profile was measured at room temperature under step-scan rate of 0,05° in the scattering angle range of $2\theta = 1^{o} - 45^{o}$.

3.8 Prism Coupling

The refractive indices of waveguides (with thickness in the range of 400 nm – 2 μm) for both TE and TM polarization were measured by using prism coupling, in particular the m-line technique. This technique is well-known to measure refractive index and thickness as well as the anisotropy of waveguides with high accuracy [Tien'69, Ulrich'70 and Ulrich'73]. The experimental setup of prism coupler is shown in Fig. 3.4.

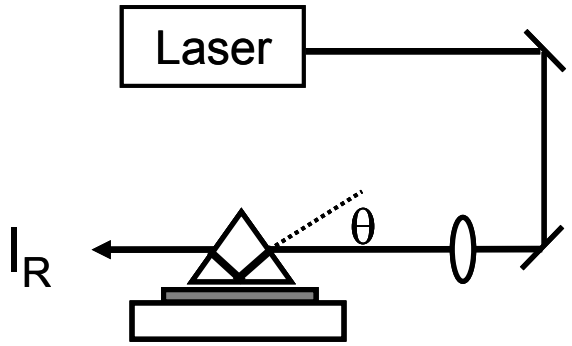

Fig. 3.4: Experimental setup of prism coupling.

We used a HeNe laser (λ = 633nm) and a continuous-wave cw-Nd:YAG laser at 1064 nm. The equilateral triangular prisms consisted of N-LaSF9, SF59 or SF66. The prism is mounted on a rotation stage controlled by computer. The focused incident beam propagating inside the prism reaches the base and suffers total internal reflection. Under total internal reflection condition at the base, coupling of light into the waveguide can occur through evanescent waves in the air gap. The coupling of incident laser beam by a prism into the film is arranged at the incidence angle θ_m of the beam. The coupling occurs only when resonant conditions inside the waveguide are fulfilled. Waveguide modes are excited in the film only at discrete incidences angles θ_m, where m = 0, 1, 2,.. describes the mode number for which the light can be coupled into the waveguide. We can observe the resonant coupling through the appearance of dark and bright lines in the reflected beam. A photo detector converts the intensity of the light to electric output signal measured by a Voltmeter (PREMA 5000) and is recorded by computer. Refractive index and thickness of the film can be determined from θ_m by using the available computer program developed by M. Jahja based on theory of earlier reports [Ulrich'73], [Marcuse'74] and [Yeh'88].

3.9 Attenuation Loss of Slab Waveguides

Waveguide loss experiments were performed by using a HeNe laser (λ = 633 nm) and cw-Nd:YAG laser (λ = 1064 nm). The measurement was executed by the prism coupling technique described above. The experimental setup is shown in Fig. 3.5

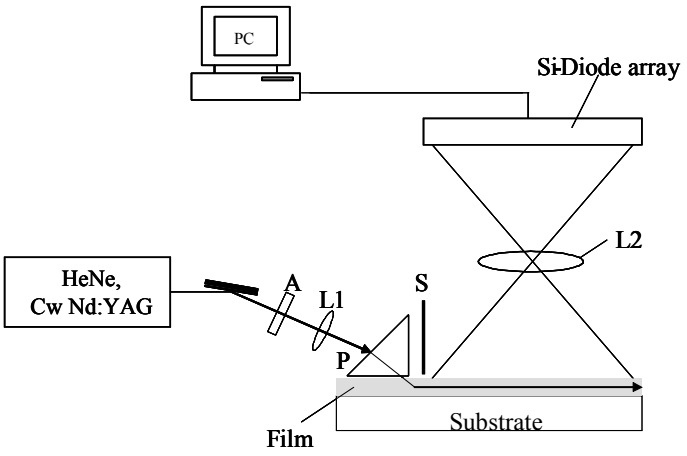

Fig. 3.5: Experimental setup for waveguide attenuation loss measurement. A: polarizer, L1, L2: lenses, P: prism, S: shield, PC: computer.

We used a half-cut glass prism (LaSF18) to couple laser beams into the waveguide. The scattered light from the waveguide was imaged by a lens onto a diode array. The black paper S was used as shield to suppress stray light from the coupling prism. Attenuation loss coefficients α_{gw} were determined from the scattered light intensity as a function of distance from the coupling prism as expressed by

$$\alpha_{gw}[d\mathrm{B}/cm] = \frac{10}{x}\log\left[\frac{I_0}{I_x}\right] \tag{3.4}$$

I_0 and I_x are scattered light intensity at 0 position and after propagation along distance of x, respectively. The distance calibration was performed with a sheet of millimetre paper at the sample position imaged on the diode array. At wavelength 1064 nm, the propagation of light in the waveguide can be observed by using an IR-camera (Microviewer, Polytech model 7290). The detection limit of this method is on the order of $\alpha_{gw} \approx 0.5$ dB/cm.

3.10 UV-Irradiation

The aim of this experiment is to cut the polymer chains by using UV-light. The UV-irradiation experiment was performed in the following way: The solution of polymer with concentration 1 mg /mL was irradiated in a 1 cm quartz-cuvette by using a high pressure 100 Watt mercury lamp (OSRAM Model HBO 100 W/2) combined with water filter and UG-11 filter (Schott Glass, 50mm x 50mm x 2 mm). During irradiation the solution was continuously stirred.

3.11 NMR Spectroscopy

^{1}H-NMR spectra of all samples were obtained by NMR spectroscopy group at MPI-P Mainz and they were recorded on Bruker Avance spectrometer working at basic frequency of 300 MHz. All spectra were obtained in $CDCl_3$ at room temperature and chemical shifts were referred to tetramethylsilane.

3.12 Dip Coating

Dip coating was used to prepare thin films on planar substrates and fibers. The coating was performed by dipping a substrate into the solution at a constant speed by

means of Mgw Lauda Filmlift FL-1 with dipping velocity in the range of 1 – 10 mm/s. The thin film adsorbs on the substrate during the immersion time. The immersion time and withdrawal speed determines the film thickness, which increases with increasing viscosity, immersion time and withdrawal speed [Groenveld´71, Pontin'05]. Schematic diagram of dip coating process is shown in Fig 3.6.

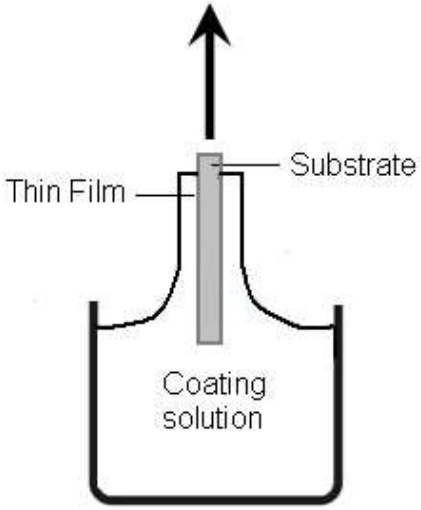

Fig. 3.6: Schematic diagram of the dip coating process.

4 Tailoring Molecular Weight and Solution Studies

In this chapter we present studies of tailoring molecular weight of MEH-PPV in two ways: precipitation fractionation and chain scission by UV-irradiation. Aim is to prepare samples with specified molecular weight and sufficient amount for investigations of their solutions and film forming properties, respectively.

4.1 Precipitation Fractionation

MEH-PPV with different chain lengths and small polydispersity index (PDI) are not commercially available, in particular MEH-PPV with low molecular weight. In order to get MEH-PPV which has different length chains, we carried out fractionation. Goal of the preparative scale is to obtain fractionated polymers that can be used for further investigations [Koningsveld'70]. We performed the so-called precipitation fractionation [Kotera'67, Francuskiewicz'94].

Choice of solvents and precipitants for precipitation fractionation should be according to several factors such as solubility strength of solvent, precipitation strength of precipitant, miscibility, physical and chemical characteristics [Francuskiewicz'94]. Based on these considerations, we have chosen toluene as solvent and methanol as poor solvent (precipitant) for doing fractionation of MEH-PPV. The concentration of starting polymer solution influences the fractionation efficiency strongly. Normal fractionation should start with polymer concentrations of 0.5 – 1 %, in which 100 mL solvent for 1 gram polymer [Francuskiewicz'94]. Thus, we dissolve the starting material (P0) in toluene with a typical concentration corresponding to 1 g (MEH-PPV) per 100 mL (toluene). The polymer must be completely soluble to obtain a good fractionation. Therefore, we dissolved MEH-PPV in toluene over night with continuously stirring at 55 °C. Subsequently, the first amount precipitant (methanol) is added somewhat fast and when the turbidity appears the precipitant is added very slowly and is continued until strong turbidity is reached, which does not disappear anymore by stirring. The addition of methanol is stopped when the cloud point is reached. Then, the solution is slowly cooled with continuously stirring. Precipitate is separated by centrifugation and dried in vacuum at 50 °C. The next fraction is obtained by repeating the procedure with modified fractionation parameters to the residual solution phase.

As starting materials, we purchased MEH-PPV from American Dye Source, Inc (ADS). Information about these materials is listed in Table 4.1. Before carrying out fractionation, the molecular weight distribution of starting materials is crucial knowledge. The weight-average molecular weight (M_w) and number-average molecular weight (M_n) were determined by polymer analytic group at MPI-P Mainz. They were measured by gel permeation chromatography (GPC) using polystyrene as standards and tetrahydrofuran (THF) as eluent. The large experimental errors specified for the M_w data of MPI-P result from large sample inhomogenieties of the batches. The average values are taken from the individual P0 data shown later in Table 4.3.

Table 4.1: Survey of MEH-PPV samples obtained from American Dye Source (ADS).

Catalog #	Amount (g)	Supplier info		MPI-P	
		M_w [kg/mol]	PDI	M_w [kg/mol]	PDI
ADS100RE Lot #V06E013A	5	468	9.5	385 ± 101	8.8
ADS100RE Lot # 07H058V	8	167	6.0	216 ± 29	9.5
ADS100RE Lot # 09C044V	10	410	6.4	605 ± 132	16

We have varied the following fractionation parameters:

P0: Amount of MEH-PPV (starting material)

V0: Volume of toluene to dissolve P0

T1: Temperature of the solution of P0 in toluene, where methanol is added to obtain P1

V1: Volume of methanol added at T1 to get P1

P1: Amount of first fraction of MEH-PPV

T2: Temperature of S1, where methanol is added to get P2

V2: Volume of methanol added at T2 to get P2

P2: Amount of second fraction of MEH-PPV

T3: Temperature of S2, where methanol is added to get P3

V3: Volume of methanol added at T3 to get P3

P3: Amount of third fraction of MEH-PPV

T4: Temperature of S3, where methanol is added to get P4

V4: Volume of methanol added at T4 to get P4

P4: Amount of fourth fraction of MEH-PPV

Table 4.2 shows a list of parameters used for fractionation experiments, which are labeled A – Q in chronological order. The polymer fractions are labeled accordingly, see Table 4.3 as shown later.

Table 4.2: Parameters of fractionation experiments A – Q. Starting materials were MEH-PPV ADS100RE Lot # V06E013A (fractionation numbers No. A - E), MEH-PPV ADS100RE Lot # 07H058V (No. F - M), MEH-PPV ADS100RE Lot # 09C044V (No. N - Q). Fractionation experiments N-Q were performed by Charlotte Degünther under my supervision.

No.	P0 [mg]	V0 [mL]	T1 [°C]	V1 [mL]	P1 [mg]	T2 [°C]	V2 [mL]	P2 [mg]	T3 [°C]	V3 [mL]	P3 [mg]	T4 [°C]	V4 [ml]	P4 [mg]
A	200	20	50	14	176	RT	6	15	RT	6	5	-	-	-
B	1000	110	RT	36	566	RT	28	375	RT	20	36	-	-	-
C	200	13	RT	14	70	RT	3	66	RT	3	50	-	-	-
D	1000	100	50	33	438	30	20	235	RT	40	251	-	-	-
E	970	100	50	32	362	38	10	180	RT	50	146	-	-	-
F	317	31	55	7	66	RT	11	147	-	-	-	-	-	-
G	321	32	45	8	168	RT	11	84	-	-	-	-	-	-
H	470	47	55	11	212	30	15	168	-	-	-	-	-	-
I	307	30	50	8	195	RT	15	60	-	-	-	-	-	-
J	970	99	55	29	504	35	10	195	RT	75	211	-	-	-
K	1067	106	55	32	468	35	9	230	RT	82	242	-	-	-
L	2072	207	55	62	897	35	18	339	RT	160	497	-	-	-
M	2318	230	55	69	910	35	20	488	23	177	600	-	-	-
MM	350	35	RT	20	49	RT	50	225	-	-	-	-	-	-
N	1004	100	55	27	297	45	6.5	347	35	11	94.4	RT	93	58
O	3003	300	55	66	107	46	17	935	36	13.4	781	RT	276	690
P	3003	300	55	75	165	45	33	2174	35	22.5	149	RT	300	183
Q	300	300	55	84	322	45	25	1748	35	109	302	-	-	-

The quality of the solvent for a given polymer can be changed either by changing the temperature or by changing the mixing ratio of a good solvent to a poor solvent [Kotera'02, Mencer'88]. Thus, there are two parameters we had to optimize: the ratio of good solvent to poor solvent V_0/V_1 and the temperature T_1 when the precipitant was added. In a system consisting of two solvents and a polydisperse polymer, the solvent composition is significant because it determines the critical concentration at the critical point (χ_c at $\phi = \phi_c$), where the phase separation occurs [Huggins and Okamoto'67]. Addition of poor solvent increases the χ parameter and leads to phase separation into the sol and gel phases. When $\chi > \chi$ critical (χ_c), precipitation occurs. Adding more poor solvent will produce more precipitate and influence molecular weight distribution of the fractions. Different fractions can be separated by changing the proportions of the solvent [Huggins and Okamoto'67]. For a polydisperse polymer solution, when the quality of solvent becomes poorer, at first the highest molecular fraction precipitates. The next fractions are polymers with lower molecular weights, because they require a more significant increase in χ to precipitate. For different values of N (number of repeat units in each chain), the bimodal curves (boundaries of the phase separation region) have the form as described in Fig 4.1. Meanwhile, Eq. 4.1 and 4.2 show that χ_c and ϕ_c change with N [Kotera'02].

$$\chi_c = \frac{(1+N^{1/2})^2}{2N} \tag{4.1}$$

$$\phi_c = \frac{1}{1+N^{1/2}} \tag{4.2}$$

In our fractionation experiments, we were able to obtain a MEH-PPV with M_w around 40 kg/mol, usually in the so-called P3 fraction, by controlling the ratio of good solvent to poor solvent of the first fraction (P1) and the second fraction (P2).

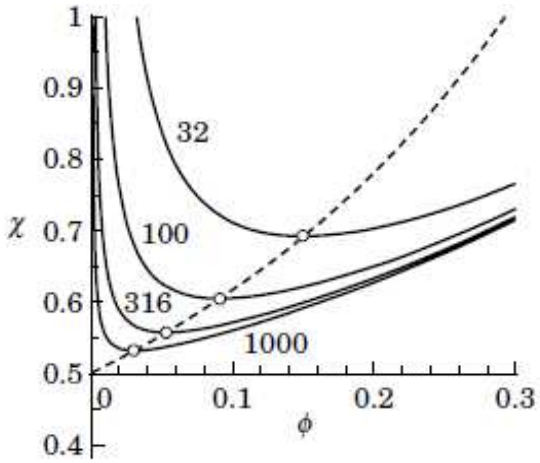

Fig.4.1: Spinodal lines for N = 32, 100, 316 and 1,000. The open circles indicate the critical point for each N [Kotera'02].

By controlling the proportions of solvents, we have obtained the desired fraction (P3) but we did not obtain it with sufficient amount. To achieve a larger amount of fraction P3, we apply different temperatures when the precipitant was added. The Flory-Huggins constant χ can be related to the solubility parameters [Francuskiewicz'94]

$$\chi = (V_s / RT)(\delta_s - \delta_p)^2, \tag{4.3}$$

where V_s is molar volume of the solvent, δ_s and δ_p are solubility parameters of solvent and polymer, respectively. The value χ_c is attained for a certain difference in solubility parameters dependent on temperature T and solvent (V_s). For a given system, χ decreases with increasing temperature, i.e., a system unstable at low temperatures can become stable upon heating. Due to this effect, we have tried to make the desired chains (P3 fraction) more stable during isolation of the longer chains, by heating the solution when the precipitant was added. We expect that this condition can avoid that chain lengths typical of the P3 fraction precipitate together with the longer chains of fractions P1 and P2. The weakest point of the fractional precipitation method is that every fraction contains an appreciable amount of the lower molecular components [Kotera'67]. This is called the tail effect and is usually wrongly attributed to the inclusion of small molecules with larger ones during precipitation of the latter. This results in an incomplete separation of the gel phase. However, this problem is really an inherent characteristic feature of fractional precipitation [Matsumoto'54, Scott'53, Kotera'67].

Therefore, in later experiments we added the precipitant for the P1 fraction at $T_1 \approx$ 55 °C, for P2 fraction at $T_2 \approx$ 35 °C and for P3 fraction at room temperature (T_3 = RT). By combining two crucial parameters of fractionation (proportions of the good and poor

solvents and temperature, respectively) we have succeeded to obtain the desired P3 fraction with optimum amount.

One of difficulty in this experiment is to determine when a meager permanent turbidity occurs after a certain amount of poor solvent has been added. This state is crucial because when this point is achieved adding of one more drop of poor solvent will reduce the sharpness of molecular weight distribution (MWD) of fractionated polymer and will reduce mass of the short chains in the next fraction as well. To overcome this problem we used lamp equipped with an optical fiber to detect cloud point visually. By using this lamp we can detect precipitate more easy due to the light scattering effects. We present results of these effects in section 4.1.2.

4.1.1 Gel Permeation Chromatography

All M_w and M_n of fractionated polymers were measured using gel permeation chromatography (GPC) with polystyrene as standard and THF as eluent by the polymer analytic group at MPI-P Mainz. The GPC curves are normalized with respect to the total weight fractions and each individual GPC curve shows the percentage of yield of fractions obtained from fractionation. As an example, Fig. 4.2 shows molecular weight distributions of fractionations from experiments A and M (for other fractionation results see Appendix A). Table 4.3 lists M_w, M_n, PDI and resulting amounts obtained for the fractionation experiments A - Q. The resulting precipitates are labeled according to the fractionation experiments.

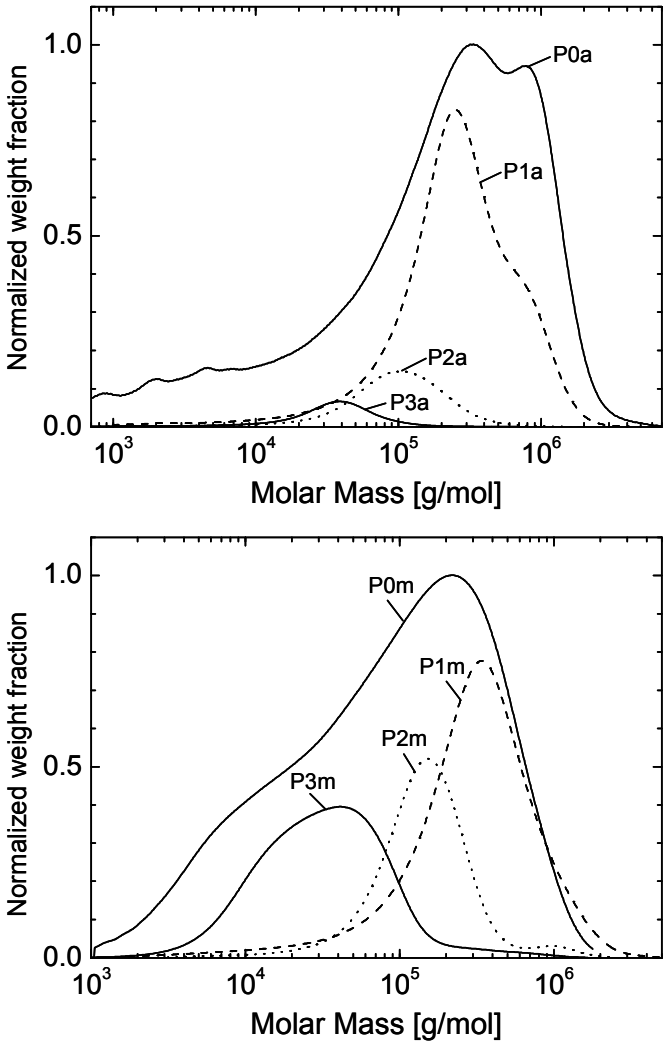

Fig. 4.2: GPC results of fractionation experiments A (above) and M (below).

As shown in Fig. 4.2, we have succeeded to obtain fractions which have PDI much less than the parent polymer (P0). In most cases, we had three fractions in every fractionation cycle. In order to obtain desired fraction with M_w in the order of 4 10^4 g/mol, we did not prepare more than four fractions because by increasing the number of fractions the quantity of each fraction decreases [Kotera'67]. The first fraction contains the polymer with the highest molecular weights and the next fraction contains the polymers with shorter chains.

Fractionation A was carried out before optimizing the parameters of experiment and fractionation M was performed after optimizing the parameters. On fractionation A, because of difficulty to detect turbidity of solution, we added too much of poor solvent so that we precipitated the first fraction (P1a) in excessive amount. As consequence, we got the second fraction (P2a) and the third fraction (P3a) with very low yield only. On the

other hand, on fractionation M, after optimizing preparation parameters and setup of experiment we succeed to improve the fractionation and obtain desired P3 fraction (M_w around 40 kg/mol) in sufficient amount.

Table 4.3 (a): GPC results of fractionations performed with the following MEH-PPV batches: ADS100RE Lot # V06E013A (A – E), ADS100RE Lot # 07H058V (F – M), ADS100RE Lot # 09C044V (N – Q). Fractionation experiments N-Q were performed by Charlotte Degünther under my supervision. (-) could not be measured due to solvent and filtering problems in GPC setup.

No	Polymer	M_w [kg/mol]	M_n [kg/mol]	PDI [M_w/M_n]	Amount [mg]
A	P0a	470	97	4.85	200
	P1a	371	91	4.09	176
	P2a	128	45	2.85	15
	P3a	47	29	1.63	5
B	P0b	440	52	8.31	1,000
	P1b	470	130	3.68	565
	P2b	240	86	2.83	375
	P3b	260	14	1.84	35
	P4b	24,5	11	2.23	5
C	P0c	465	61	7.62	200
	P1c	360	50	7.45	70
	P2c	300	85	3.70	65
	P3c	200	50	3.25	50
D	P0d	292	26	10.9	1,000
	P1d	271	55	4.93	438
	P2d	135	34	3.95	235
	P3d	78	14	5.44	251
E	P0e	260	21	12.4	970
	P1e	240	55	4.42	362
	P2e	190	100	1.80	180
	P3e	77	27	2.79	146
F	P0f	280	23	12.2	317
	P1f	520	91	5.67	66
	P2f	180	55	3.34	147
G	P0g	200	20	10.0	321
	P1g	330	54	6.11	168
	P2g	75	30	2.54	84
H	P0h	214	27	7.88	470
	P1h	480	115	4.15	212
	P2h	83	33	2.52	168
I	P0i	186	23	7.98	307
	P1i	320	60	5.36	195
	P2i	47	18	2.55	60
J	P0j	220	20	10.67	970
	P1j	360	140	2.66	503

	P2j	180	78	2.34	195
	P3j	45	17	2.69	210
K	P0k	220	22	9.93	1067
	P1k	400	140	2.96	468
	P2k	170	79	2.13	230
	P3k	52	17	2.95	242
L	P0l	220	24	9.18	2,072
	P1l	320	150	2.16	897
	P2l	170	84	2.00	339
	P3l	55	19	2.84	497
M	P0m	190	23	8.45	2,318
	P1m	420	120	3.53	910
	P2m	190	96	1.97	488
	P3m	54	20	2.68	600
MM	P0mm	60	19	3.15	350
	P1mm	13	5,8	2.33	49
	P2mm	6,6	4,3	1.53	225
N	P0n	591	203	2.91	1,004
	P1n	600	166	3.62	297
	P2n	378	169	2.24	347
	P3n	114	59	1.94	94
	P4n	30,5	16	1.90	58
O	P0o	-	-	-	3,002
	P1o	422	18	23.4	107
	P2o	700	224	3.12	935
	P3o	370	201	1.84	781
	P4o	107	34	3.15	690
P	P0p	699	33	21.2	3,003
	P1p	193	19	10.1	165
	P2p	678	218	3.11	2174
	P3p	98	71	1.38	148
	P4p	44	19	2.31	183
Q	P0q	708	39	18.2	3,000
	P1q	933	99	9.38	322
	P2q	619	136	4.57	1,748
	P3q	59	34	1.74	301

Table 4.3 (b): (*) MEH-PPV mixture of results of experiments J, K, L, and M.

No	Polymer	M_w [kg/mol]	M_n [kg/mol]	PDI [M_w/M_n]	Amount [mg]
*	P1*	420	99	4.26	2,778
	P2*	180	89	2.08	1,187
	P3*	53	19	2.86	1,550

It is difficult to handle the polymer solution if we have large amount of starting materials. To avoid this problem, we have performed fractionation several times. We are able to reproduce the required results by doing fractionation with similar preparation conditions (fractionation J, K, L and M). Then, we mix the same fractions of fractionated polymer and characterize their molecular weights by GPC. Table 4.3 (b) presents the results of the mixture of fractionated polymers of experiments J, K, L, and M.

We also combine the remaining solutions S3 (after the P3 fractionations) from the experiments J, K, L and M and the fractionation of this solution is the so-called fractionation MM.

We used the precipitates of the fractionations shown in Table 4.3 (a) to investigate the influence of molecular weight on the solution properties of MEH-PPV and polymers shown in Table 4.3 (b) for thin films studies of MEH-PPV, because the latter need a large amount of polymer.

4.1.2 UV-Vis Absorption Spectroscopy

We have performed UV-Vis absorption spectroscopy to observe the cloud point of fractionation. We varied the ratio of good solvent (toluene) to poor solvent (methanol) until precipitation occurs. Fig. 4.3 shows UV-Vis spectra of mixed solutions (see Appendix C for other spectra). If we add more than 23% methanol, for instance 28.5% or 33%, the absorption spectra show an apparent tail towards longer wavelengths (λ > 600 nm).

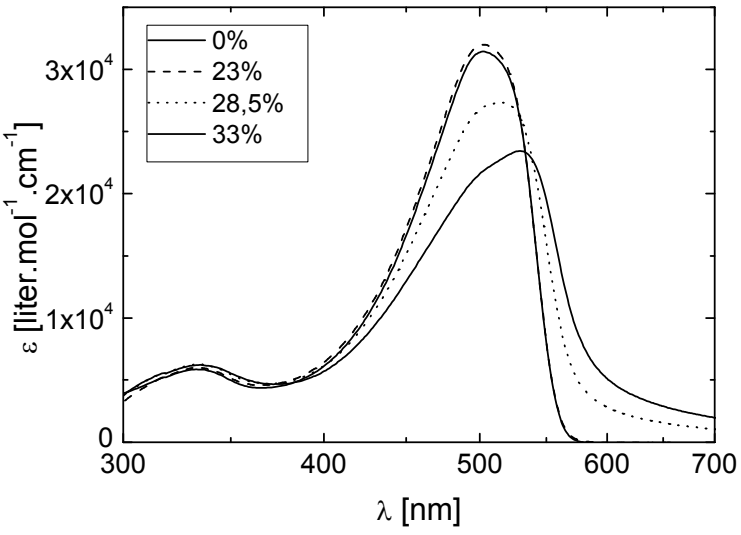

Fig. 4.3: UV-Vis spectra of P2* fraction in mixed solutions of methanol and toluene. The inset shows the relative volume content of methanol.

We explain this apparent absorption tail at $\lambda > 600$ nm with light scattering by larger particles, caused by Rayleigh scattering and may be also by Mie scattering. These particles may be precursors for the precipitate. In these experiments we observe that for different chain lengths it needs different ratios of good solvent to poor solvent to achieve the cloud point. The shorter the polymer chains of starting materials are, the more poor solvent is needed to precipitate the first fraction.

We also used MEH-PPV fractions to study the influence of M_w on solution properties by means of UV-Vis spectroscopy, in particular on the wavelength of the absorption maximum λ_{max}. Table 4.4 provides a list of fractions used and their absorption maxima (λ_{max}) in toluene and chloroform. Spectra of UV-Vis absorption of selected MEH-PPVs fractions in chloroform at a concentration 0.01 g/L are shown in Fig. 4.4. In these spectra we observe a systematic trend to larger values of λ_{max} with increasing M_w of polymers.

Table 4.4: Absorption maxima of MEH-PPVs fractions in chloroform and toluene, n is number of repetition unit, where n = M_n /260 (molecular mass of repeat unit), (-) not measured.

Polymer Fraction	M_n [kg/mol]	PDI [M_w/M_n]	n	λ_{max} in $CHCl_3$ [nm]	λ_{max} in toluene [nm]
P2mm	4.3	1.53	17	481	-
P1mm	5.8	2.33	22	485	-
P4b	11	2.23	42	491	-
P3j	17	2.69	65	494	496
P2i	18	2.55	70	494	497
P2g	30	2.54	113	496	498
P2h	33	2.52	127	497	499
P2f	55	3.34	212	499	500
P2j	78	2.34	299	498	501
P1h	115	4.15	441	500	503
P1j	140	2.66	526	499	503

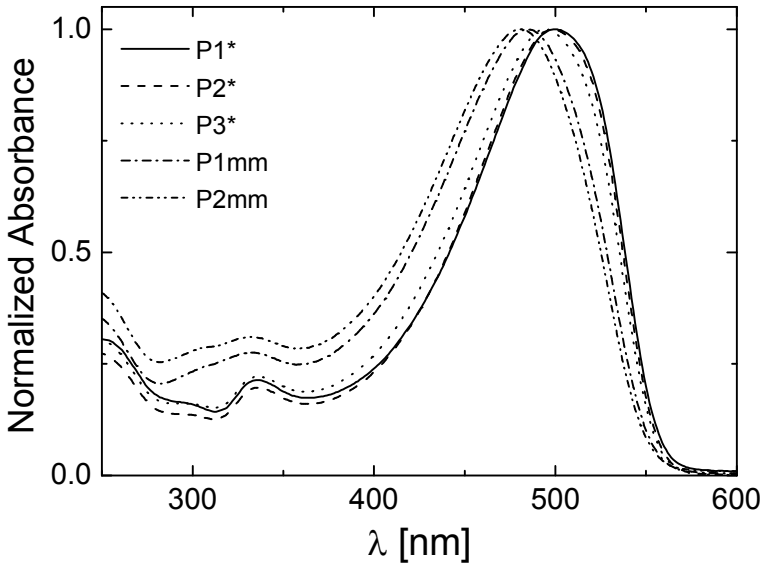

Fig. 4.4: UV-Vis Spectra of MEH-PPV fractions in chloroform

By using data listed in Table 4.4, we plot the absorption maxima of MEH-PPV fractions versus the number of repetition units. Fig. 4.5 shows data of MEH-PPV fractions in chloroform (circles) and oligomers data from Stalmach et al. (triangles) [Stalmach'96] that have well defined number of repetition unit as comparison. Because of uncertainty of chain length in our experiment, we put experimental error bars determined by ten percent of M_n value. Obviously, the data sets of Stalmach oligomers and MEH-PPVs fractions are different because of different substituents, but they were measured in the same solvent chloroform. However, they indicate a consistent trend.

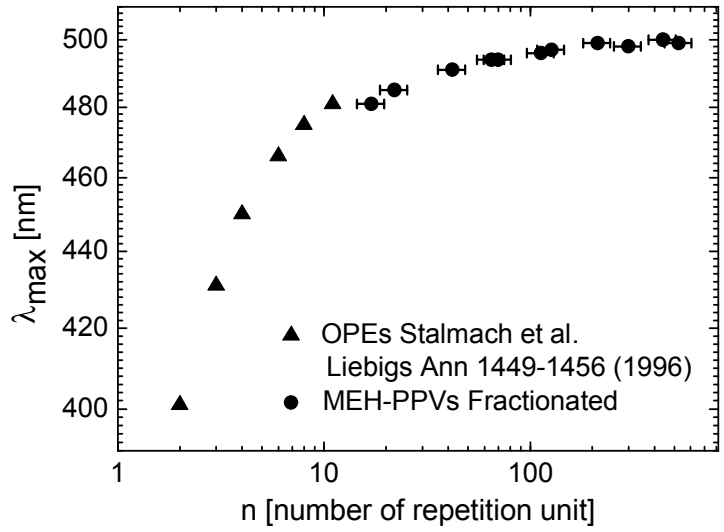

Fig. 4.5: Absorption maxima of MEH-PPV fractions (circles) and oligomers (triangles) in chloroform as function of number of repetition units.

The interesting point in Fig. 4.5 is that the absorption maxima still gradually increase from n = 17 until n ≈ 110. There are several different reports of the so-called saturation chain length, which means that λ_{max} does not increase anymore for longer chains. Meier et al. reported the saturated chain length at n = 11, Klaerner et al. at n = 10 and Oelkrug et al. at n = 8, respectively [Meier' 97, Klaerner'98, Oelkrug'01]. It means that we have the saturated chain length longer as compared to the ealier reports. Such long chain lengths of MEH-PPVs with narrow molecular weight distribution were not investigated earlier.

For polymeric materials, the absorption spectrum reflects the influence of a distribution of different actual conjugation lengths [Gierschner'07]. Therefore, the absorption maximum in polymers represents a mean value of the distribution [Rauscher'90, Mulazzi'99, Gierschner'07].

4.1.3 Summary and Conclusions

We succeed doing precipitation fractionation of MEH-PPV. In this work, there are two crucial parameters to obtain the desired fractions; proportions of the solvents and temperature when the precipitant is added. By combining these parameters, we have succeeded to obtain the desired P3 fraction with optimum amount. One of important steps in this fractionation is handling the first precipitation, because it predetermines the results of the next fractions. To inspect the cloud point visually, we used a halogen lamp equipped with an optical fiber and make an improved estimate of proportion of the solvents needed for the first precipitate. We also verified the cloudiness of solution mixtures by using UV-Vis spectroscopy, which indicated the onset of light-scattering by aggregated particles.

We used fractions of polymers to investigate the influence of molecular weight on solution properties of MEH-PPV. In this work, it is remarkable that wavelengths of the absorption maxima of MEH-PPVs fractions are still increasing with chain length until the number of repetition units approaches n ≈ 110.

4.2 Chain Scission by UV-Irradiation

Besides precipitation fractionation, we also performed UV-irradiation experiments to get low M_w of MEH-PPV. We have tried to cut the polymer chains in solution by using UV-light similar to earlier experiments performed with soluble polydiacetylene

[Müller'84, Rau'84]. For these experiments we used the shortest chain of MEH-PPV obtained by fractionation, the so-called P2mm fraction. We dissolved P2mm fraction in chloroform and irradiated the polymer solution by UV-light as described in Chapter 3.10 with different times. The solution was irradiated by using a high pressure 100 Watt mercury lamp filtered by water and UG-11 (50mm x 50mm x 2 mm). We irradiated the polymer solution at a distance of 7 cm from UG-11. After irradiation we evaporate chloroform because GPC does not work with this solvent.

4.2.1 Gel Permeation Chromatography

We have measured the molecular weight distribution of the irradiated samples by GPC using polystyrene as standards and THF as eluent. Fig. 4.6 displays GPC results of irradiated polymers with different irradiation time.

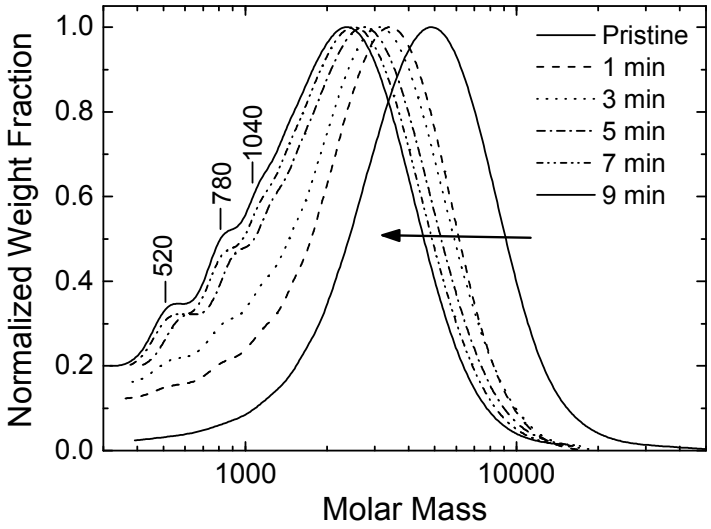

Fig. 4.6: GPC results of irradiated solutions of P2mm fraction. The arrow indicates the shift of GPC curves at increasing UV-irradiation times.

As UV-irradiation time increases, the molecular weight of the irradiated polymer solution is decreasing systematically, which means that the polymer chains were cut by UV-light. At an irradiation time of 9 minutes, there are three distinct shoulders in this curve around values of molecular weight at 520 g/mol, 780 g/mol and 1040 g/mol. The molecular mass of the repeat unit of MEH-PPV is 260 g/mol. Thus, these values reveal the appearance of dimers, trimers and tetramers of polymer as product of chain scission by UV-light.

4.2.2 UV-Vis Absorption Spectroscopy

After irradiating the polymer solution of P2mm fraction, we measure UV-Vis absorption for each sample by means of UV-Vis spectroscopy. Fig. 4.7 shows the UV-Vis spectra of irradiated solutions. The λ_{max} values of solutions shifted to smaller wavelengths (blue shifted) as the irradiation time increases. This blue shift is due to shorter conjugation lengths of the MEH-PPV chains.

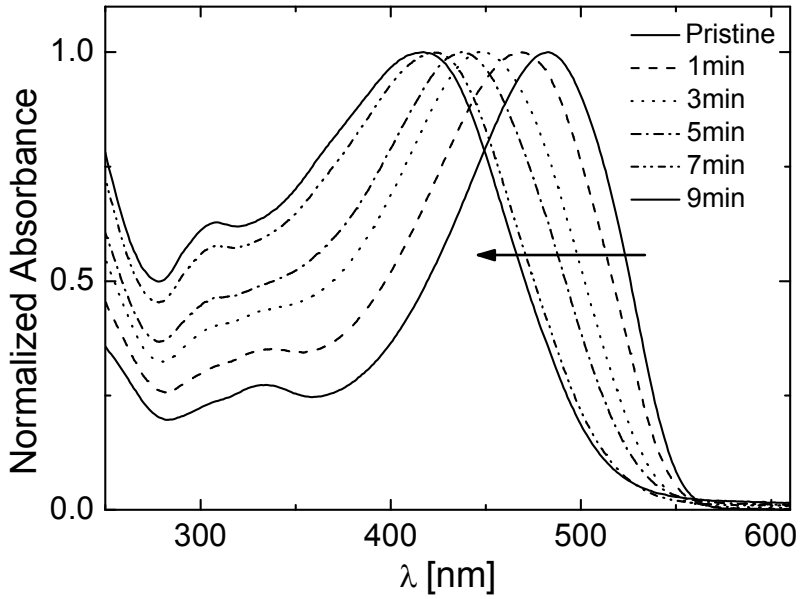

Fig.4.7: UV-Vis spectra of irradiated solutions of P2mm fraction in chloroform. The arrow indicates the shift of absorbance at increasing UV-irradiation time.

We make a plot of λ_{max} values as function of number of repetition unit of irradiated polymers by using data listed in Table 4.5. We put results from fractionation and UV-cleavage together in Fig. 4.8, where we also insert oligomer results from Stalmach et al. for comparison [Stalmach'96].

Table 4.5: Absorption maxima of MEH-PPVs irradiated in chloroform. Starting material is MEH-PPV P2mm fraction, n is number of repetition unit where $n = M_n /260$.

Irradiation Time [min]	Mn [g/mol]	PDI	n	λ_{max} in $CHCl_3$ [nm]
0	4300	1.53	17	481
1	2100	1.96	9	468
3	2000	2.0	8	446
5	1900	2.02	7	437
7	1600	1.95	6	422
9	1400	2.01	5	417

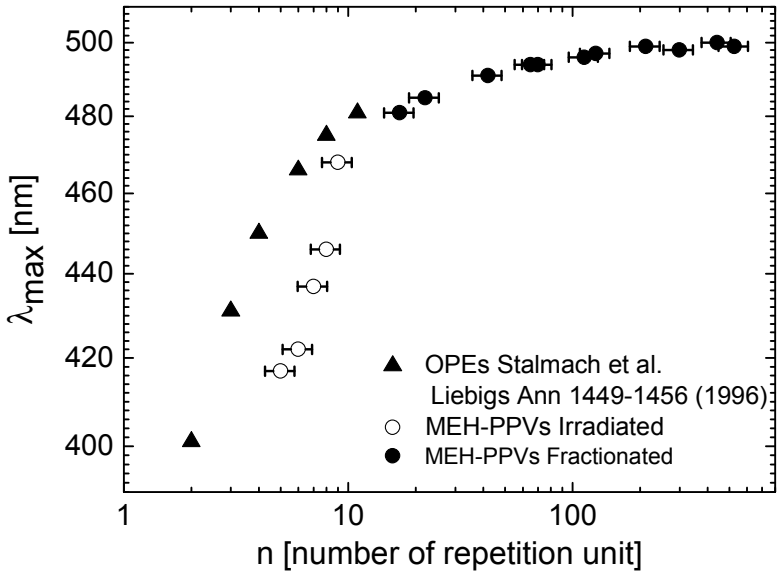

Fig. 4.8: Plot of λ_{max} of MEH-PPVs obtained from fractionation and irradiation as function of number of repetition unit n.The series data are compared with OPEs, which have a well defined number of repetition unit, from Stalmach et al. [Stalmach'96].

Fig. 4.8 shows that oligomers obtained by UV-cleavage are significantly different to the oligomers of Stalmach et al. At comparable n, the oligomers prepared by UV-cleavage have $\lambda_{max} < \lambda_{max}$ (Stalmach). This indicates significantly shorter conjugation length as compared to the physical length of the oligomers, which indicates defects of the conjugated chain. In order to confirm this defect, we have performed NMR and FTIR spectroscopy, which are described in the following.

4.2.3 NMR Spectroscopy

The presence of structural defects in MEH-PPV after irradiation was studied using ^{1}H NMR spectroscopy in $CDCl_3$. These experiments were carried out by Bhumika Saini under my supervision. Due to limited amount of MEH-PPV P2mm fraction, we used MEH-PPV (see Table 4.6) obtained from American Dye Source (ADS). We irradiated MEH-PPV in THF with a high pressure 100 Watt mercury lamp. At beginning we used UG-11 filter but after irradiated 200 minutes the change of UV spectra were not significant, so that we irradiated the polymer solution without UG-11 filter. Afterwards, we evaporated the solvent and measured the samples before and after irradiation by means of ^{1}H NMR, FTIR spectroscopy and GPC. Table 4.6 provides information about

GPC results measured by the polymer analytic group at MPI-P Mainz before and after irradiation. We present results of FTIR spectroscopy in chapter 4.2.4.

Table 4.6: GPC results of MEH-PPV before and after UV-irradiation.

ADS100RE Lot # 10E045A	Before irradiation	After irradiation
M_w [kg/mol]	1,675	18
PDI	5.7	2.9

Fig 4.9 shows the ^{1}H NMR spectra of solutions of MEH-PPV before and after irradiation. After irradiation, some new peaks appear and the intensity of some peaks is changed. Fig. 4.10 shows assignments of specific carbon positions of MEH-PPV.

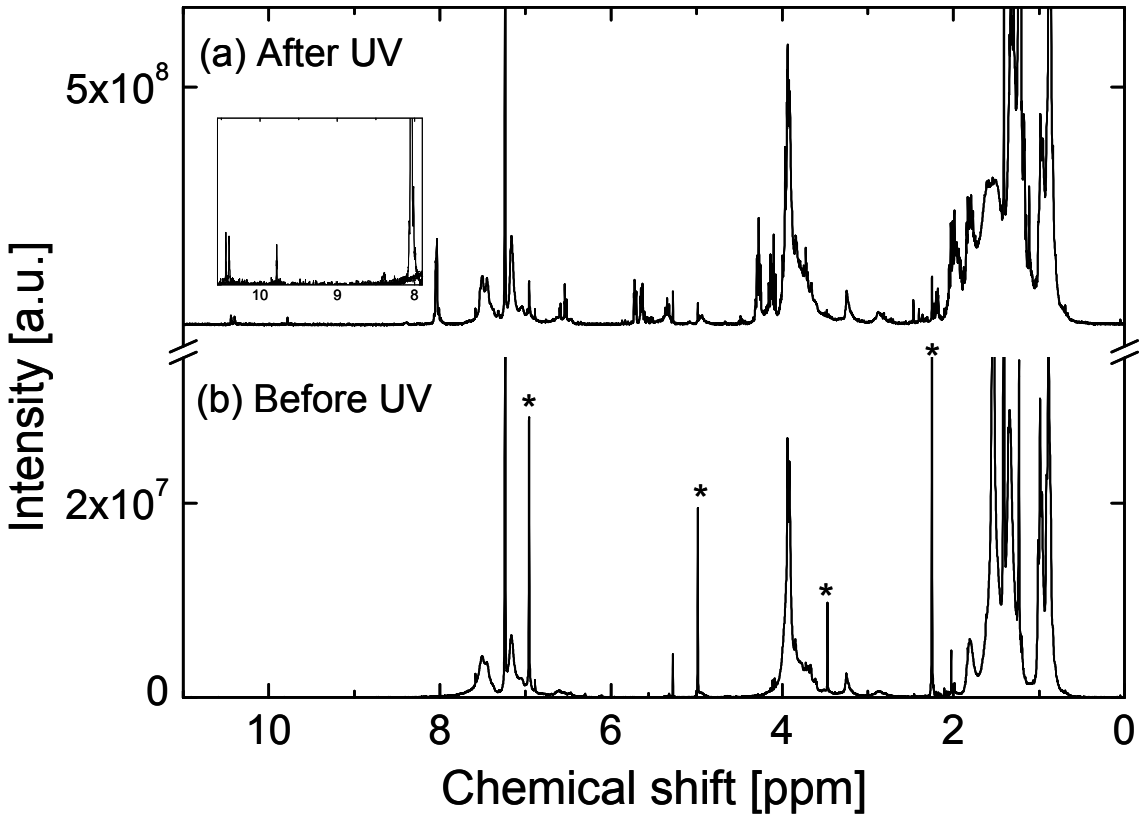

Fig. 4.9: Spectra of ^{1}H NMR of MEH-PPV before irradiation and after irradiation (asterisks are peaks from residual solvent, THF). Inset shows new peaks after irradiation in the range of 8 – 11 ppm.

The chemical shifts of the samples and their assignments are displayed in Table 4.7, where the intensity is normalized with respect to the peak at 7.5 ppm (assigned to aromatic a, a').

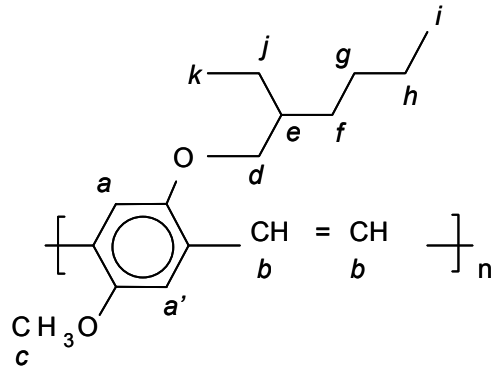

Fig. 4.10: Chemical structure of MEH-PPV.

Table 4.7: Chemical shifts of MEH-PPV. The observed chemical shifts before and after UV-irradiation are labeled δb and δa, respectively.

δb (ppm)	I	δa (ppm)	I	Lit.cited (ppm)	Assignment	Reference
0.89	0.23	0.89	0.19	1.0 – 0.9	CH_3: i,k	[Rahman'10, Fan'04]
0.98	0.18	0.98	0.11	1.0 – 0.9	CH_3: i,k	[Rahman'10]
-	-	1.21	0.34	1.21	CH_3	NMR database
1.23	0.20	1.23	0.59	1.3	Chain defect	[Holzer'04]
-	-	1.29	0.20	1.28	CH_2	NMR database
1.34	0.17	1.33	0.19	1.2-1.6	CH_2: j,h,	[Fan'04]
1.80	0.03	1.81	0.07	1.83	CH: e	[Rahman'10, Fan'04]
-	-	2.18	0.02	2.1 -2.3	CH3	NMR database
-	-	2.40	0.01	2.39	H from aldehyde	NMR database
-	-	2.47	0.01	2.2 – 2.6	CH_2 saturated	NMR database
2.87	0.003	2.87	0.006	2.9	Chain defect	[Becker'99,Holzer'04]
3.24	0.018	3.24	0.014	3.16	Chain defect	[Holzer'04]
-	-	3.73	0.04	3.7 – 3.9	CH3 ester	NMR database
3.85	0.03	3.84	0.05	4.25-3.25	OCH3 : c	[Holzer'04]
3.94	0.16	3.94	0.16	3.93	2H,OCH_2: d	[Becker'99]
-	-	4.1	0.05	4.1 – 4.7	CH2 ester	NMR database
-	-	4.27	0.06	4.4 - 4.5	Chain defect	[Holzer'04]
-	-	6.6	0.01	6.7	Chain defect	[Becker'99]
7.17	0.05	7.17	0.05	7.19	Vinylic bond:b	[Rahman'10]
7.51- 7.45	0.026	7.51- 7.45	0.026	7.54-7.47	Aromatic: a, a'	[Rahman'10]
-	-	8.03	0.05	8.03	H-heteroaromatic	NMRdatabase
-	-	9.78	0.004	9.57	Aliphatic aldehyde	NMR database
-	-	10.44-10.40	0.005	10.5	Aromatic aldehyde	[Pfeiffer'99]

The chemical shifts of irradiated sample demonstrate the presence of chain defects and formation of terminal aldehyde as shown in detail below.

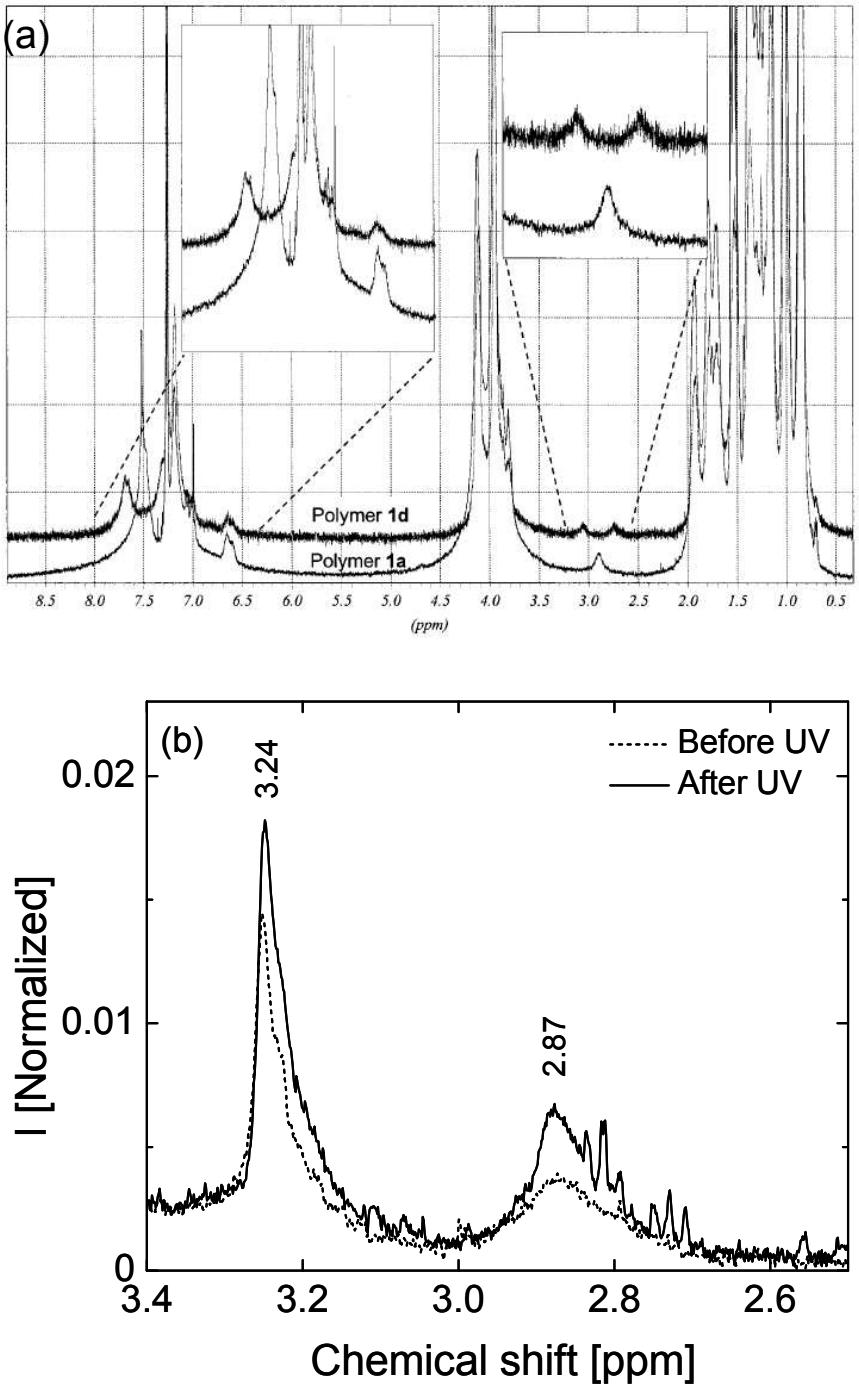

Fig. 4.11: Irradiated sample shows presence chain defect at 2.87 ppm [Becker'99].
(a) Figure taken from Becker et al. [Becker'99]. (b) Own data.

Fig. 4.11 displays one of the peaks at 2.87 ppm which shows a chain defect. We compare our peak with NMR spectra of Becker et al. [Becker'99]. The small peak at 2.9 ppm reflects an aliphatic, nonconjugated structure within the main chain of the polymer [Becker'99].

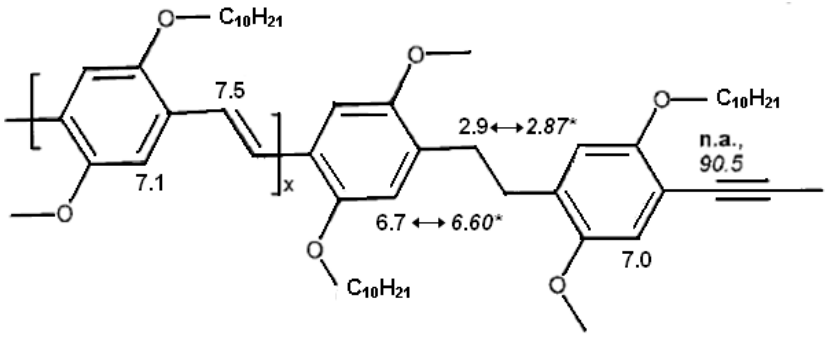

Scheme 4.1: NMR assignments of chain defects of MEH-PPV [Becker'99], italic letters with asterisk are from own work.

Scheme 4.1 represents positions of chain defects in the MEH-PPV backbone that interrupt the conjugated system. Furthermore, this chain defect also can be identified by some additional signal at 1.3, 1.5 and 4.4/4.5 ppm. Fig. 4.9 shows these peaks, which have been reported earlier [Holzer'04]. The strongest peak at 1.3 ppm in our work is shifted to 1.23 ppm and the peak at 4.4/4.5 ppm is shifted to 4.27 ppm.

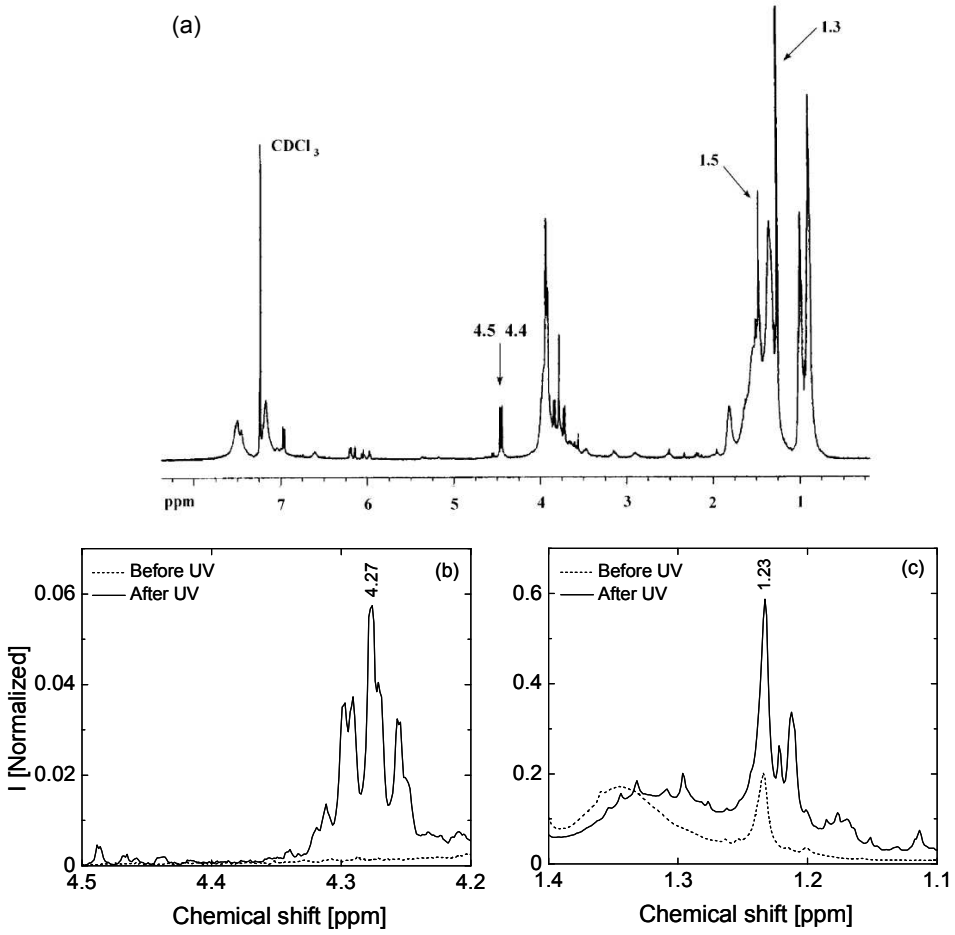

Fig. 4.12: Strong peak at 1.3 and 4.4/4.5 ppm related to chain defect in MEH-PPV [Holzer'04]. Figure (a) is taken from Holzer et al. [Holzer'04], (b) and (c) own work.

After irradiation some new peaks appeared in the range 8 – 11 ppm, see Fig. 4.13. These peaks evidence terminal aldehyde and were produced as degradation product. Fig. 4.14 shows the assignments of the peaks.

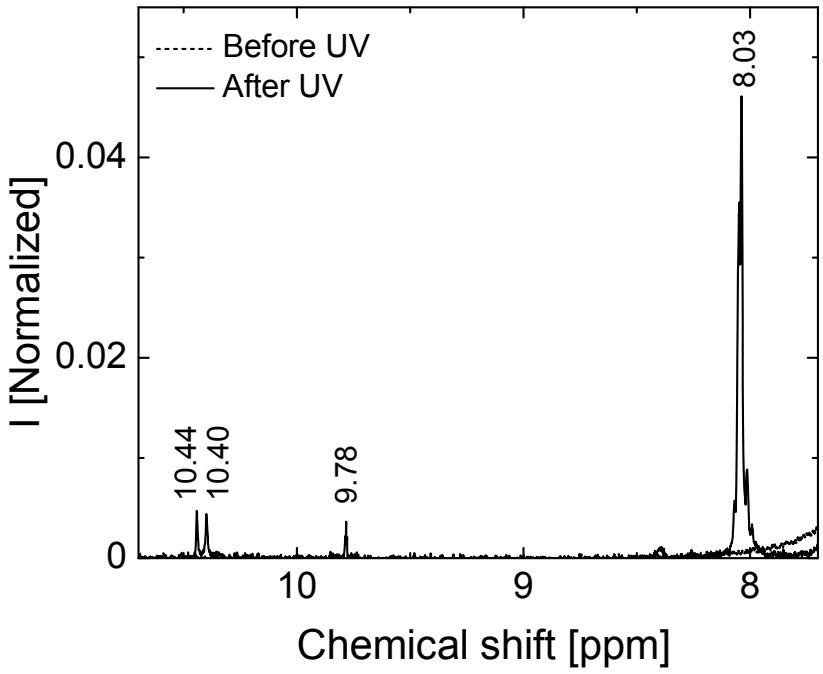

Fig. 4.13: New peaks after irradiation reflect aldehyde.

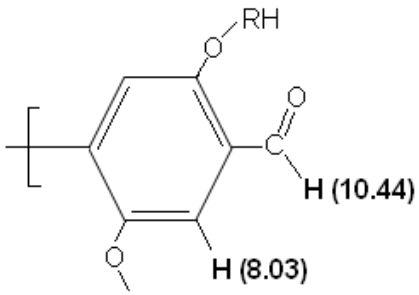

Fig. 4.14: Aromatic adehyde assignment

It is clearly observed that chain cleavage by UV-irradiation not only produces polymers with low M_w but also causes chain defects, which interrupt the π-electron conjugation along the MEH-PPV backbone. As reported by Müller et al. [Müller'84] and Rau et al. [Rau'84] they investigated chain-scission of polydiacetylenes (PDA) by UV-light and observed that M_w of PDA was decreased. Here we have observed that UV-irradiation also induces chain defects which shorten the conjugation length significantly.

4.2.4 Infrared Spectroscopy

We also characterized the presence of structural defects in MEH-PPV after irradiation by using FTIR spectroscopy. These experiments were carried out by Bhumika Saini under my supervision. We used MEH-PPV listed in Table 4.6 and irradiated MEH-PPV in THF with similar condition as described in Section 4.2.3. Afterwards, we made thin films of irradiated and pristine solutions on the wafer silicon substrates by drop casting and measured the samples before and after irradiation by means of FTIR spectroscopy. The IR spectra of MEH-PPV before and after UV irradiation are displayed in Fig. 4.15 for comparison.

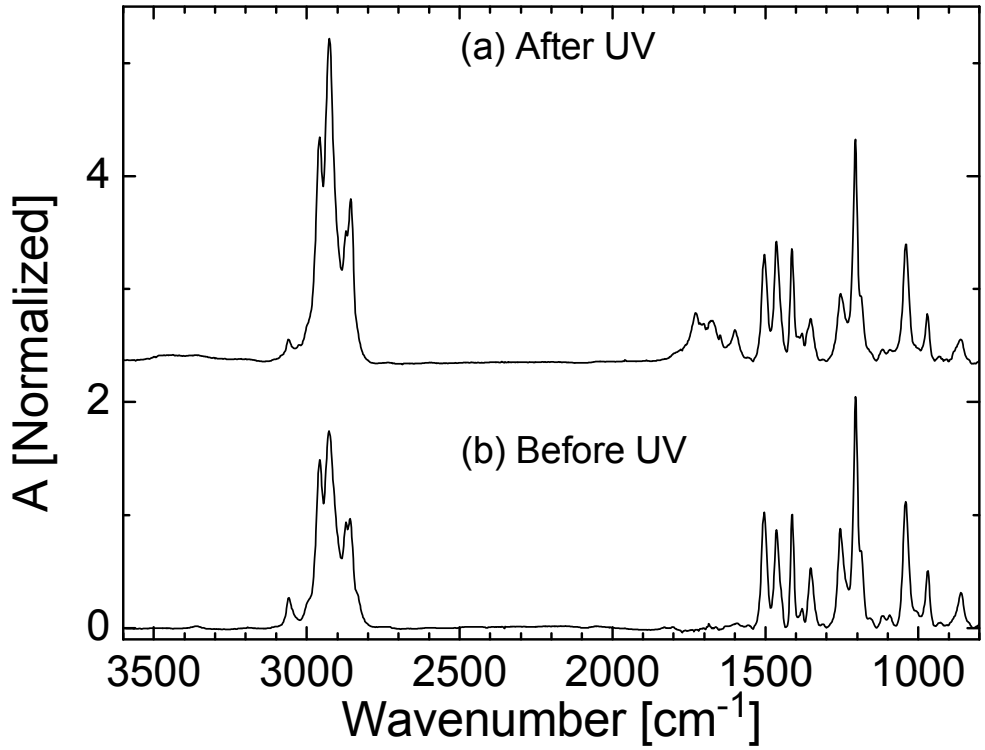

Fig. 4.15: FTIR spectra of MEH-PPV before and after irradiation. Absorbance A is normalized with respect to the band at 1415 cm^{-1}.

After irradiation the spectra changed and the detailed analyses of these changes are discussed as follows.

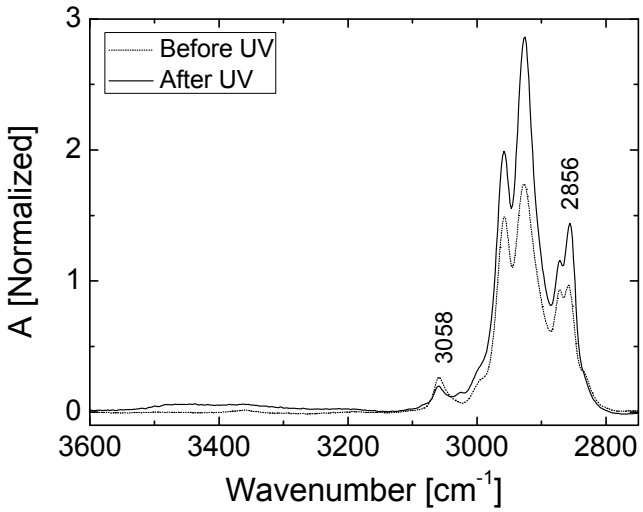

Fig. 4.16: FTIR spectra of MEH-PPV in the range 3600 – 2700 cm^{-1}.

Table 4.8: Assignment of IR bands of MEH-PPV before and after irradiation in the range 3600 – 2700 cm^{-1}. The measured wavenumbers of the bonds before and after UV irradiation are labeled υb and υa, respectively.

υb [cm^{-1}]	I	υa [cm^{-1}]	I	Lit.Cited [cm^{-1}]	Band Assignment	Reference
3058	0.215	3058	0.119	3058	Trans-vinylene C-H stretch	[Bradley'86]
2958	1.436	2958	1.86	2958	CH3 asymmetric stretching	[Atreya'99]
2925	1.707	2925	2.78	2928	C-H stretching	[Atreya'99]
2856	0.941	2856	1.39	2860	CH_2 stretch	[Atreya'99]

After irradiation the absorbance of the bands between 2700 – 3600 cm^{-1} are mostly increasing except the band at 3058 cm^{-1}. Attenuation of this band can be due to a chain defect at the vinylene bond after irradiation as explained in NMR section. Chain defects are indicated by decreasing of trans-vinylene C-H stretching at band 3058 cm^{-1} and meanwhile, the C-H stretching band at 2856 cm^{-1} increases. After irradiation, we also can observe a very weak, broad band centered around 3400 cm^{-1}. The broad bands in region of 3600 – 3200 cm^{-1} indicate hydrogen bonded hydroxyl groups. This band appears in very low concentration due to formation of hydroxyl groups and may further react to form an aromatic aldehyde.

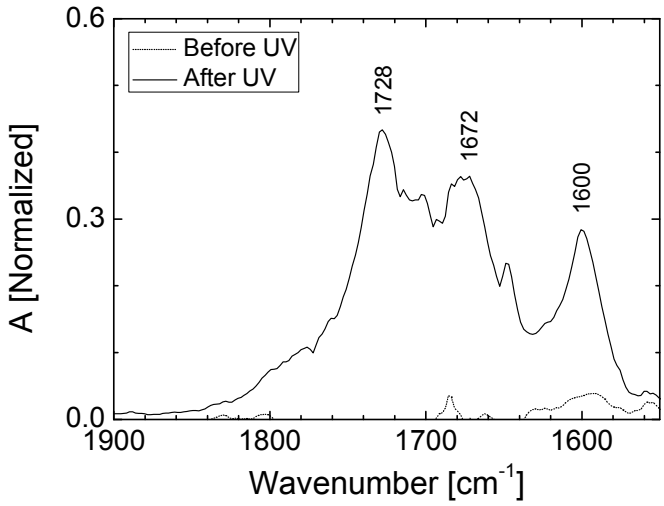

Fig. 4.17: FTIR spectra of MEH-PPV in the range 1900 – 1550 cm^{-1}.

Table 4.9: Assignment of IR bands of MEH-PPV before and after irradiation in the range 1900 –1550 cm^{-1}. The measured wavenumbers of the bonds before and after UV irradiation are labeled υb and υa, respectively.

υb [cm^{-1}]	I	υa [cm^{-1}]	I	Lit.Cited [cm^{-1}]	Band Assignment	Reference
-	-	1728	0.434	1740	Ester or carboxylic acid	[Cumpston'97,Atreya'99]
1672	-	1672	0.364	1685 1690	Aromatic Aldehyde	[Cumpston'97, Rothberg'96]
1600	-	1600	0.284	1600 1598	Phenyl quadrant ring stretch.	[Rothberg'96, Atreya'99]

After irradiation some new bands between 1900 – 1550 cm^{-1} appear and absorbances of some bands are increasing. The new bands are shown in Fig. 4.17 and the assignments of the bands are listed in the Table 4.9. The assignments show terminal aldehydes (1672 cm^{-1}) and esters or carboxylic acid (1728 cm^{-1}), which were produced by irradiation. The band at 1600 cm^{-1} indicates phenyl quadrant ring stretching. After UV irradiation, the band increases and provides evidence for chain scission at the vinyl double bond and formation of carbonyls [Rothberg'96, Cumpston'98 and Atreya'99]. These products reveal that UV light does not only cut the polymer chains but also causes degradation of the polymers. According to these new bands, Cumpston et al. proposed the mechanism of photo-degradation of MEH-PPV, which is depicted in Scheme 4.2.

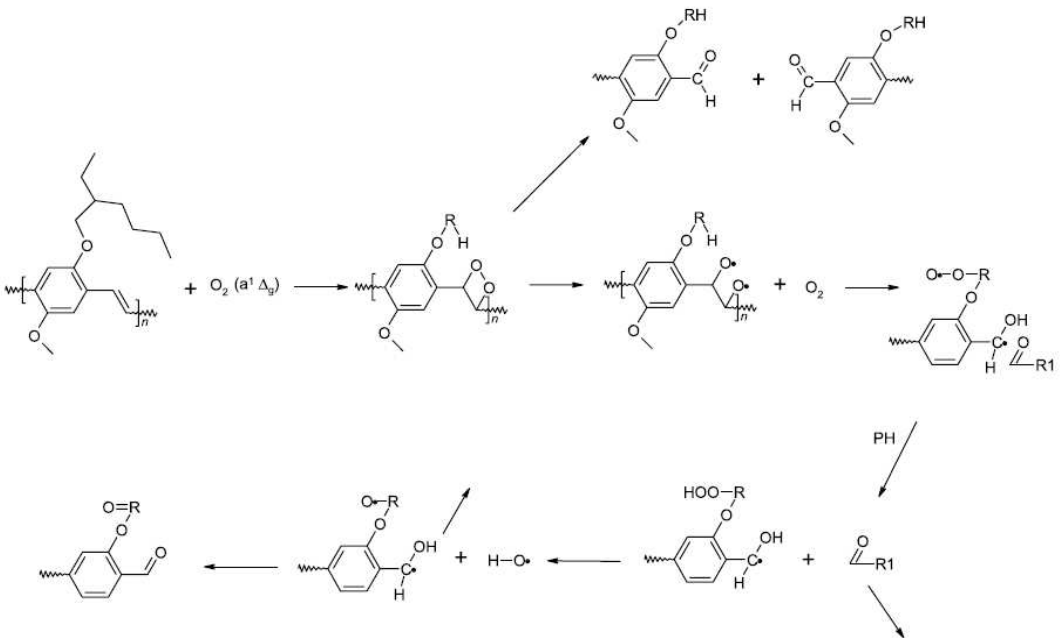

Scheme 4.2: Mechanism of photo degradation of MEH-PPV proposed by Cumpson et al. [Gardette'10].

The polymer absorbs the light followed by an energy transfer from the triplet state of PPV to oxygen. The result is the formation of singlet oxygen, which can react with the double bonds of PPV. This reaction gives an unstable endoperoxide that decomposes to give two aromatic aldehydes accompanied by chain scission [Gardette'10].

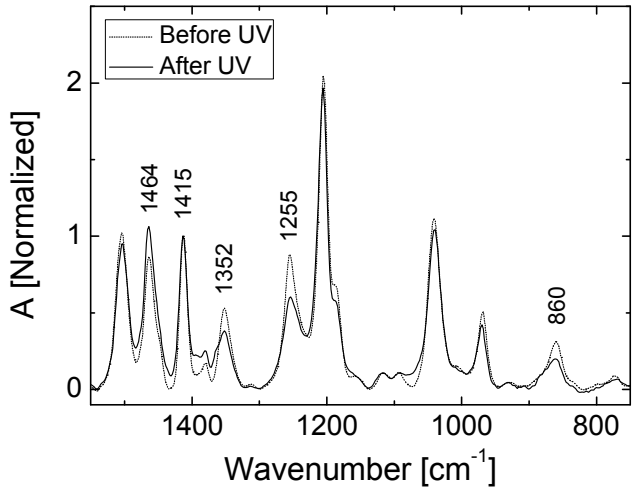

Fig. 4.18: FTIR spectra of MEH-PPV in the range 1550 cm^{-1}- 750 cm^{-1}, before irradiation (dotted line) and after irradiation (solid line).

Table 4.10: Assignment of IR band of MEH-PPV before and after irradiation in the range 1550 - 750 cm^{-1}. The measured wavenumbers of the bonds before and after UV irradiation are labeled υb and υa, respectively.

υb [cm^{-1}]	I	υa [cm^{-1}]	I	Lit.Cited [cm^{-1}]	Band Assignment	Reference
1502	1.023	1502	0.948	1506	Semicircular phenyl stretch(C-C aromatic)	[Atreya'99]
1464	0.868	1464	1.064	1464	Anti-symmetric alkyl CH2	[Atreya'99]
1414	1	1414	1	1415 1412	Semicircular phenyl stretch	[Bradley'86] [Atreya'99]
1352	0.532	1352	0.383	1350	C-O-C stretching	[Cumpson'98]
1255	0.881	1255	0.599	1255	C-O-C stretching	[Cumpson'98]
1205	2.047	1205	1.966	1204	Phenyl-Oxygen stretch	[Atreya'99]
1039	1.117	1039	1.042	1040	Alkyl-Oxygen stretch	[Atreya'99]
970	0.505	970	0.422	969	Trans double bond CH wag	[Atreya'99]
860	0.314	860	0.199	858	Out-of-plane phenyl CH wag	[Atreya'99]

Fig. 4.18 shows spectra in the region 1550 – 750 cm^{-1}. In this region, the absorbance increases at the band 1464 cm^{-1} and decreases for the 1352, 1255, 1205, 1039, 970 and 860 cm^{-1} bands, respectively. Attenuation of the trans-double bond CH wagging band at 970 cm^{-1} indicates that the conjugation length of polymer is reduced by scission of the vinyl double bond in the PPV backbone. The bands at 1352, 1255, 1205 and 1039 cm^{-1} represent ether C-O-C stretching [Cumpson'98] and after irradiation these bands decrease. We assume that long alkyl side chains of MEH-PPV are broken, the change of conformation may cause aggregate formation. Therefore, the bands at 1464 cm^{-1} and 2860 - 2960 cm^{-1}, which indicate CH2, CH, and CH3 stretching, are increasing. The possible reaction mechanism is depicted in Scheme 4.3.

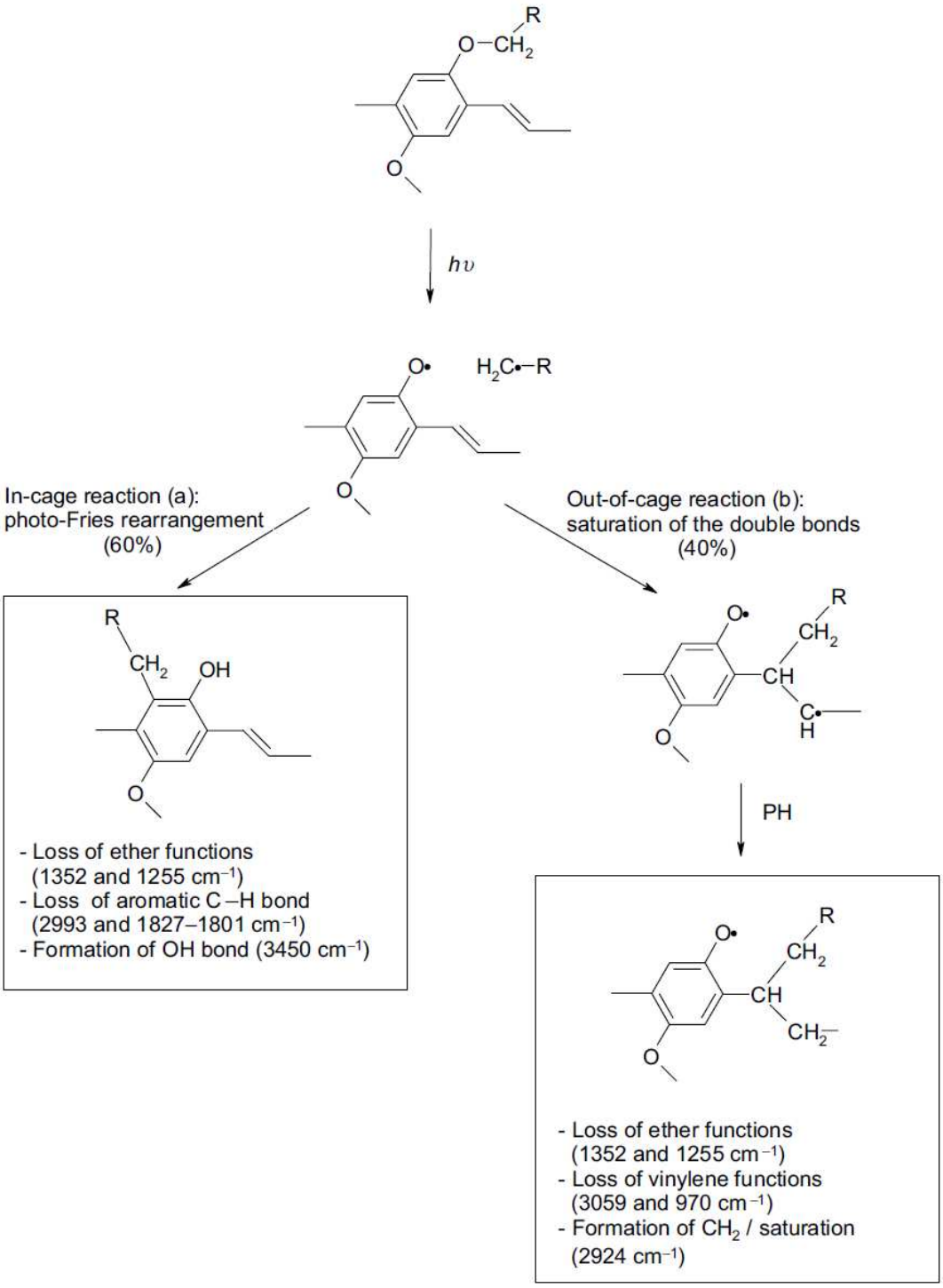

Scheme 4.3: Mechanism of disappearance of ether function [Gardette'10].

Our FTIR results reveal that after UV-irradiation MEH-PPV contains chain defects at vinylene bonds. Furthermore, aromatic aldehydes are appearing as reaction product of chemical decomposition.

4.3 Summary and Conclusions

We have tailored the molecular weight of MEH-PPV by precipitation fractionation, and alternatively, by UV-induced chain scission. To obtain a polymer with low M_w and small PDI, it turned out that precipitation fractionation is better suited as compared to chain scission by UV-irradiation. Investigations by using ^{1}H NMR and FTIR spectroscopy have demonstrated that UV-light induces chain defects at the polymer backbone, which shortens the conjugation length.

We have studied optical properties of solutions of different chain lengths of MEH-PPV fractions obtained by fractionation and UV-irradiation in chloroform. The λ_{max} values of MEH-PPVs obtained by fractionation still increase until the number of repetition units approaches 110 approximately. Meanwhile, oligomers obtained by UV-irradiation are compared to oligomers from Stalmach et al. [Stalmach'96] and have $\lambda_{max} < \lambda_{max}$ (Stalmach). This indicates significantly shorter conjugation length of UV-irradiated samples as compared to the physical length of the oligomers, which is explained by defects of the conjugated chains.

5 Thin Films Prepared by Spin Coating

In this chapter, we present influences of spin coating processing conditions (boiling temperature of solvent and casting temperature) on the morphology of MEH-PPV and its effect on the optical properties such as refractive index, birefringence and waveguide propagation loss. All experiments were performed with MEH-PPVs obtained by fractionation.

5.1 Influence of Molecular Weight

We used MEH-PPVs obtained by fractionation with various molecular weights. We prepared thin films by spin coating at room temperature and used toluene as solvent. Aim of this part is to show that the molecular weight has crucial impact on optical constants as reported by Koynov et al. [Koynov'06] and that it does not depend on the chemical route of synthesis. Also, we want to demonstrate the reproducibility of optical constants of thin film of polymers obtained by fractionation.

5.1.1 Film Preparation

All polymers were dissolved in toluene and filtered by using 0.45 - 2 µm syringe filters before the thin films were spin coated. Subsequently, the films were annealed in a vacuum oven for about 12 hours at 50 °C to remove residual solvent. The film thickness d was measured with a Tencor Model P 10 step-profiler. We used films with thickness $d \approx$ 50 – 70 nm for spectroscopic studies and thick films (400 - 800 nm) for optical waveguide experiments. The film thickness can be controlled by variation of concentration by weight C_w of the polymer solution and spinning speed ω using the spin coating parameters as defined by eq. (5.1) [Ziegler'00, Fitrilawati'02].

$$d_1 = d_0 \left(\frac{\omega_1}{\omega_0} \right)^{\alpha} \left(\frac{Cw_1}{Cw_0} \right)^{\beta} \qquad (5.1)$$

The coefficients d_0, α and β were obtained experimentally. The exponent α was -0.5, which is typical for the spin coating process. The thickness d_0 refers to the spin coating parameters ω_0 and Cw_0.

Parameters for the thin film preparations studied in this part are shown in Table 5.1. We also show the maximum concentration C_w, which yields good solutions without

gelation problems. Highly concentrated solutions were often treated by an ultrasonic bath to make homogenous solution and to avoid aggregates. As shown in Table 5.1, the parameters β and d_0 depend on molecular weight.

Table 5.1: Spin coating parameters for fractions P1*, P2* and P3* and toluene as solvent. (-) were not determined. The thickness d_0 was calculated at concentration of 1% by weight and spinning speed 1800 rpm.The exponents α and β refer to Eq. 5.1.

Materials	M_w [g/mol]	PDI	C_w [Max] for spincoating	d_0 [nm]	α	β
P1*	4.2×10^5	4.26	5.6 %	85 ± 2	-0.5	1.88 ± 0.02
P2*	1.8×10^5	2.08	-	81 ± 3	-0.5	1.35 ± 0.03
P3*	5×10^4	2.86	6.3 %	39 ± 2	-0.5	2.05 ± 0.02

5.1.2 Reflectometry

Transmission and reflection spectra of thin films ($d \approx 50 – 70$ nm) were measured by using a UV-Vis-NIR spectrophotometer (Perkin Elmer Model Lamda 900) with TE-polarization. All measurements were performed using a bare fused silica substrate as reference. Fig. 5.1 shows transmission and reflection spectra of fraction P2* with film thickness 55 nm. From these spectra we can derive the dispersion of intrinsic absorption coefficient $\alpha(\lambda)$ and the refractive index $n(\lambda)$ of thin films by means of the available computer program (Bitrab Version 2.0, 2007 [Scholdei´07]) based on the Fresnel equations and Lavenberg-Marquardt Algorithm.

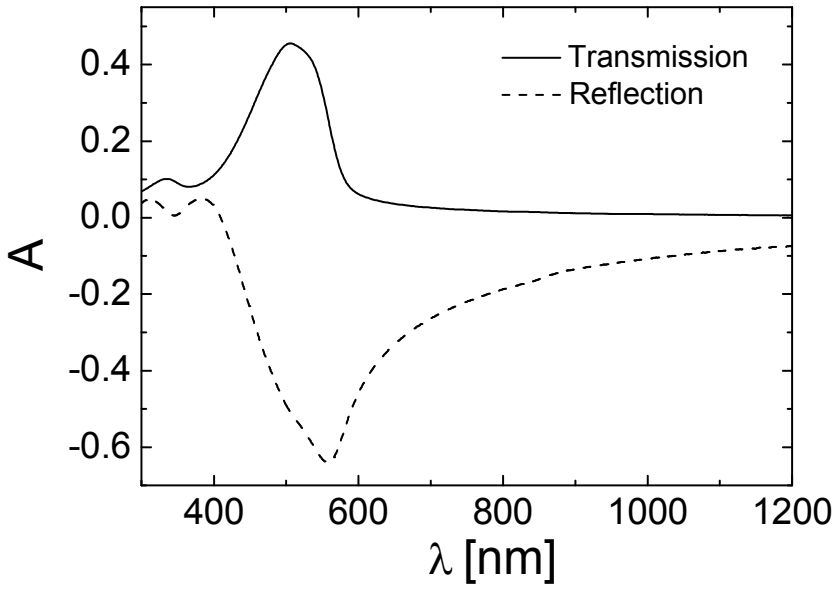

Fig. 5.1: Transmission and reflection spectra of a thin film (d = 55 nm) of fraction P2* on a fused silica substrate expressed in absorbance unit (A).

The absorption spectra and the dispersions of linear refractive index of thin films of MEH-PPVs are displayed in Fig. 5.2. A systematic trend to larger values of α_{max} and n_{TE} with increasing molecular weight is observed in the spectra. Fraction P1* has the strongest absorption maximum α_{max} and refractive index as compared to other fractions because it has the highest molecular weight and the longest conjugated chains. In consequence, P1* has the highest number of π-electron and polarizability which produce large values of α_{max} and refractive index. Additionally, the orientation of chain segments depends on molecular weight, which causes increasing birefringence at larger M_w [Koynov´06].

We also measured refractive index of fraction P1*, P2*, and P3* by means of prism coupling. We could not measure P2mm fraction by prism coupling due to the small available amount of this polymer. Refractive indices measured by prism coupling at 633 nm in TE-polarization are in good agreement with the results from reflectometry.

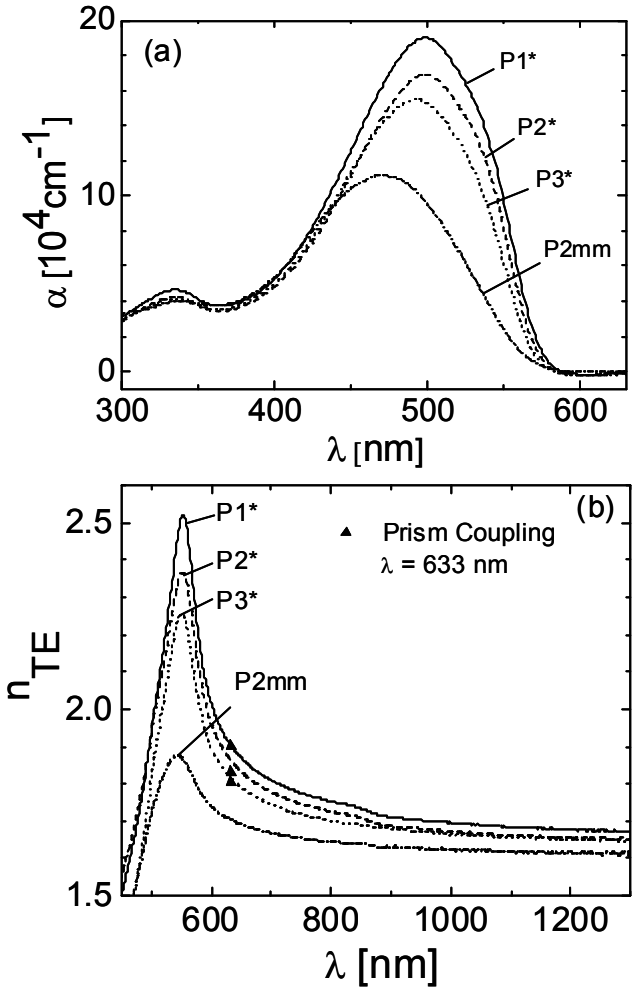

Fig. 5.2: Spectra of linear absorption coefficient $\alpha(\lambda)$ of thin films (a) and dispersion of refractive indices n at transverse electric (TE) polarization of MEH-PPVs (b). Triangle data points are measured by prism coupling at λ = 633 nm.

5.1.3 Prism Coupling

Refractive index of thin films were measured by means of prism coupling (m-line technique) at laser wavelength 633 nm at both transverse electric polarization, n_{TE}, and transverse magnetic polarization, n_{TM}, by changing the polarization of the incident beam. We measured MEH-PPV waveguides with typical thicknesses in the range 400 – 1000 nm. Fig. 5.3 shows refractive index of MEH-PPVs with different molecular weights in TE and TM polarization measured by prism coupling at 633 nm. We plot results from this work together with results from Koynov et al. [Koynov'06]. Fig. 5.3 (a) presents refractive index as a function of M_w and Fig. 5.3 (b) refractive index as a function of M_n.

Results from this work lie in the same line of the results reported by Koynov et al. It evidences excellent reproducibility of n for different sources of MEH-PPV.

As shown in Fig. 5.3 (a), refractive index increases gradually as M_w is increasing. Surprisingly, the plot of n as function of M_n shows that the birefringence (n_{TE}-n_{TM}) is increasing abruptly at M_n = 100 kg/mol. Fig. 5.4 (a) and (b) evidence the same trend of waveguide loss as a function of M_w and M_n.

From the plot of n and α_{gw} with respect to M_n, we assume that there are three regions of morphology of thin films of MEH-PPV. The first is an amorphous structure, where M_n < 8 kg/mol, which has a very low waveguide loss value. The second is an intermediate range, 8 < M_n < 100 kg/mol, where the birefringence and waveguide loss are increasing only gradually. The third is a structure which contains aggregates, M_n > 100 kg/mol, where the birefringence and waveguide loss are large and increasing abruptly. However, these interpretations need further experiments. In order to confirm structure that contains aggregates, we investigate the crystalline content of MEH-PPV by using wide angle X-Ray scattering.

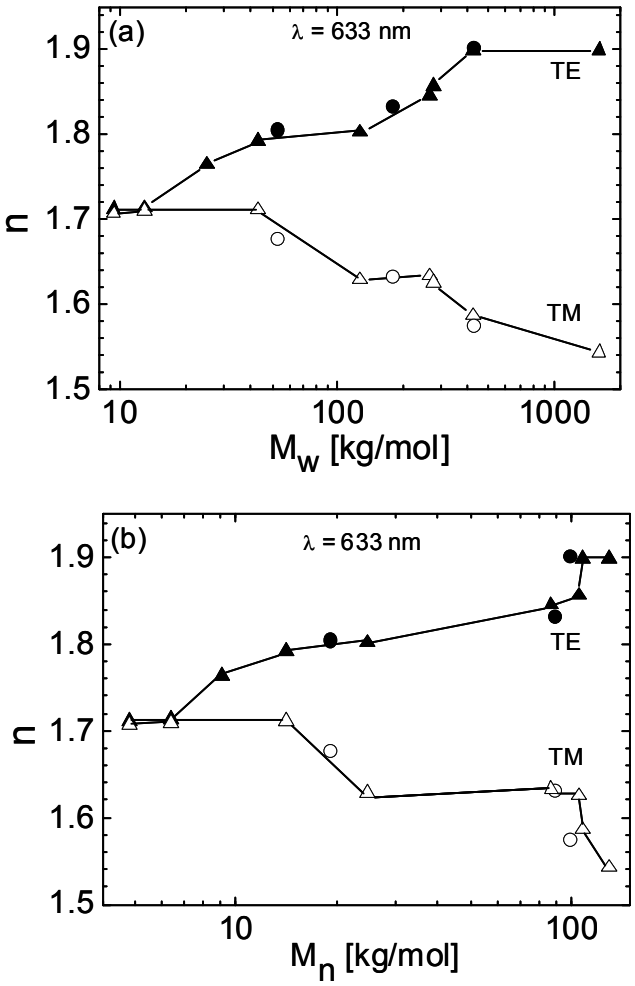

Fig. 5.3: Refractive index of MEH-PPVs measured by prism coupling at 633 nm. The circle data points are from this work (fractions P1*, P2* and P3*) and triangle data points are from Koynov et al. [Koynov'06].

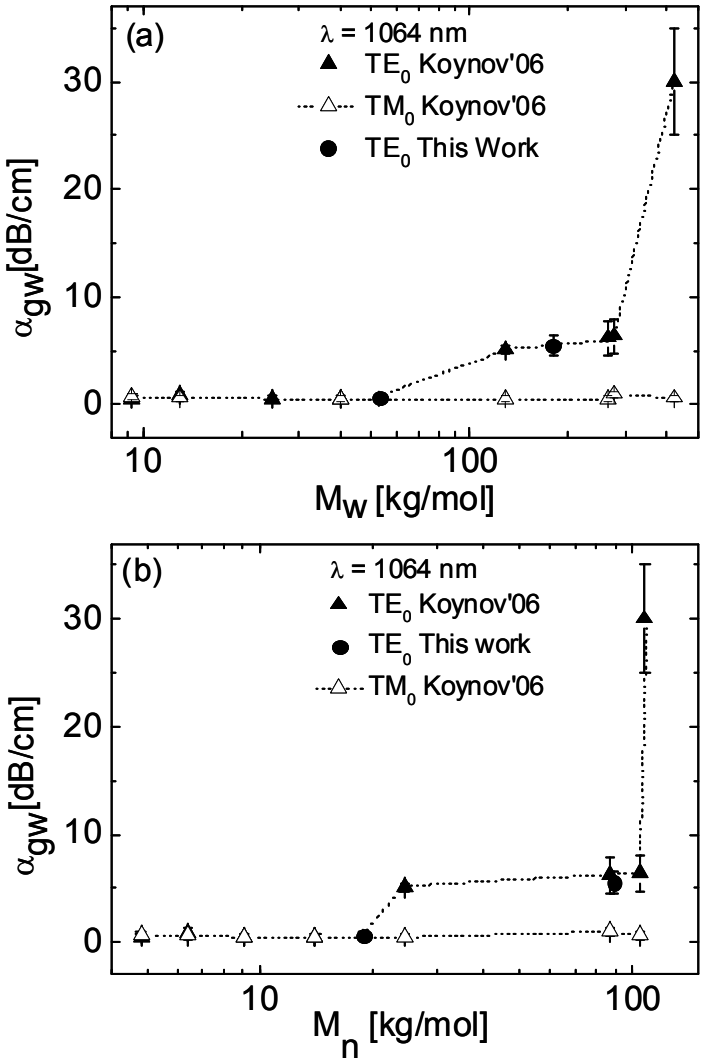

Fig. 5.4: Waveguide loss of MEH-PPVs measured at 1064 nm. Circle data points are from this work (fraction P1*, P2* and P3*) and triangle data points are from Koynov et al. [Koynov'06].

5.1.4 Wide Angle X-Ray Scattering

We characterized the extent of crystallinity of polymer films by using wide angle X-ray scattering (WAXS). This technique gives information about amorphous and crystalline form of polymers. We prepared MEH-PPV films of fraction P1* and P3* by spin coating and used toluene as solvent ($d \approx 1.5$ - 2 μm). Subsequently, they were annealed in a vacuum oven for about 12 hours at 50 °C. The measurements were conducted using Philips goniometer PW 1820 system with beam 1.541 Å at room temperature under step-scan rate of 0.05 in scattering angle range of $2\theta = 1^{o} – 45^{o}$. The WAXS profiles are depicted in Figure 5.5.

The profile of fraction P3* indicates an amorphous structure. However, the higher M_w sample (P1*) shows a peak at the diffraction angle 24°. This peak indicates an additional crystalline region.

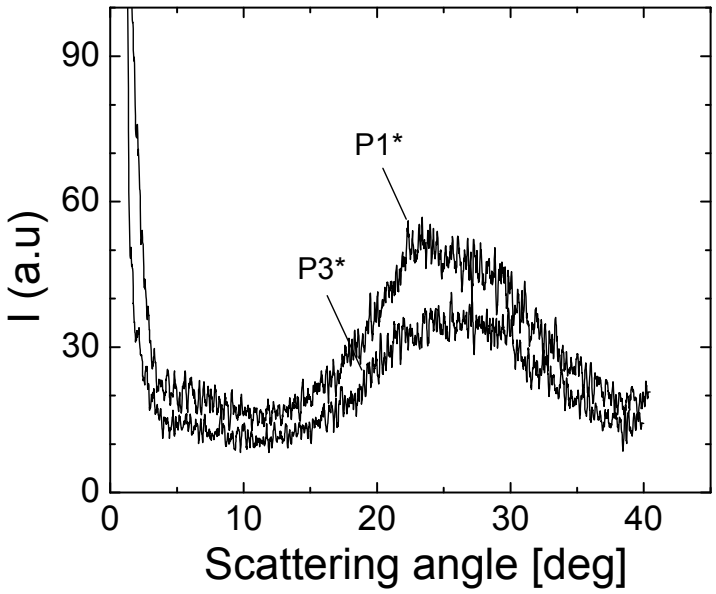

Fig. 5.5: WAXS profile of thin films of fractions P1* and P3*

By using Bragg's law shown in equation 5.2 the peak appearing in the vicinity of 2θ = 24° has a *d*-spacing value of 3.7 Å. This value is related to the typical stacking distance of aromatic π–electron systems, which is in the order of 3.3 – 3.8 Å as described in Fig. 5.6 [Yang'98].

$$2d \sin \theta = n \lambda. \qquad (5.2)$$

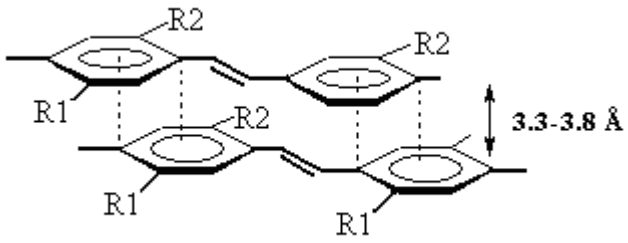

Fig. 5.6: Aromatic π – π interplanar distance in MEH-PPV. R1: OCH_3 , R2: OC_8H_{17}.

The small peak at 24° in Fig 5.5 leads us to conclude that there are some parts in films of MEH-PPV with high M_w (in this case fraction P1*), which contain crystalline regions or

aggregates which are caused by short-range interchain attraction forces. Therefore, MEH-PPV with high M_w has different morphology and optical properties as compared to low M_w.

5.1.5 Summary and Conclusions

We have investigated optical constants of thin films of MEH-PPVs prepared by spin coating, measured by reflectometry and prism coupling technique. The results show an excellent reproducibility of n for different sources of MEH-PPV. We also characterized crystallinity of thin films of MEH-PPVs by using wide angle X-ray scattering (WAXS). For M_n > 100 kg/mol, the result shows some part of MEH-PPV containing crystalline structure. The results are compatible with results from prism coupling and waveguide loss measurements. We assume that for M_n > 100 kg/mol the aggregates appear and increase the waveguide propagation loss of the films.

5.2 Influence of Film Casting Conditions

In this section we study the influence of film casting conditions on the optical properties of thin films. All experiments for this investigation were performed with the fraction P2*.

5.2.1 Solvent Effects

In this part we study effects of solvents on the properties of thin films of MEH-PPV such as film thickness, average surface roughness, refractive index, birefringence and waveguide propagation loss. We also investigate influences of solvents on polymer chain packing by using Fourier Transform Infrared (FTIR) spectroscopy in two measuring configurations: transmission and grazing incidence reflection.

Film Thickness and Average Surface Roughness

We performed these experiments by using various good solvents with different boiling temperature. In order to select good solvents for MEH-PPV we used Hansen solubility parameter, δ ($cal^{1/2}cm^{-3/2}$). We also calculated δ for MEH-PPV by using the method of group contribution of Hoftzyer and Van Krevelen [Krevelen'08]. The

obtained value by using this method is 9.4 $cal^{1/2}cm^{-3/2}$ (see Appendix D for the complete calculation). The solvents, boiling temperatures T_b, spin coating parameters, boiling temperatures of solvents increase from 61 °C to 131 °C.

Table 5.2: Parameters of solvents, spin coating processing conditions of fraction P2*, and resulting film parameters. Solubility parameter (δ) is taken from Barton [Barton'75]. R_a/d is normalized surface roughness.

Solvent	T_b [°C]	δ [$cal^{1/2}cm^{-3/2}$]	C_w [%]	ω [rpm]	d [nm]	R_a [nm]	R_a/d [%]
$CHCl_3$	61	9.3	2.6	800	1888 ± 116	99.3 ± 20.7	5.3
Me-THF	80	8.9	2.6	800	742.5 ± 55	29.6 ± 11	4.0
Toluene	111	8.9	2.3	600	518.6 ± 6	2.8 ± 0.8	0.5
Chlorobenzene	131	9.5	2.3	760	462.8 ± 9.5	1 ± 0.5	0.2

We measured the thickness and surface roughness of the films by using Tencor Model P10 step-profiler. Thickness and roughness as function of boiling temperature of solvent are displayed in Figure 5.7. We observe a general trend in these graphs: As the boiling point of solvents is increasing, the thickness and roughness of the films is decreasing.

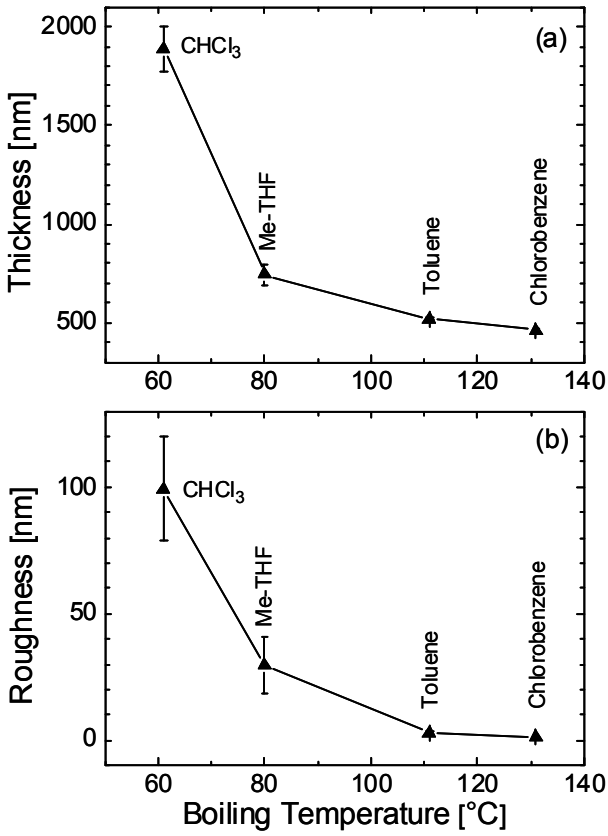

Fig. 5.7: The thickness (a) and the roughness (b) of thin films of fraction P2* in different solvents.

The trend seen in Figure 5.7 can be interpreted in the following way. Chloroform has the lowest boiling point and the fastest evaporation rate as compared to the other solvents. As reported by Meyerhofer [Meyerhofer'78], the solvent evaporation rate is a critical parameter for the thickness of thin films prepared by spin coating. Thickness is proportional to spinning speed, viscosity and evaporation rate. The solvent evaporation process influences the flow of the solution. Solvents with fast evaporation will flow slower because of the higher viscosity of the solution. Solvents with faster evaporation rate produces thicker film because the polymer looses the solvent and freezes faster without having enough time to become thin and spread uniformly, while solvents with slower evaporation rate have more time for fluid out-flow and produce thinner films.

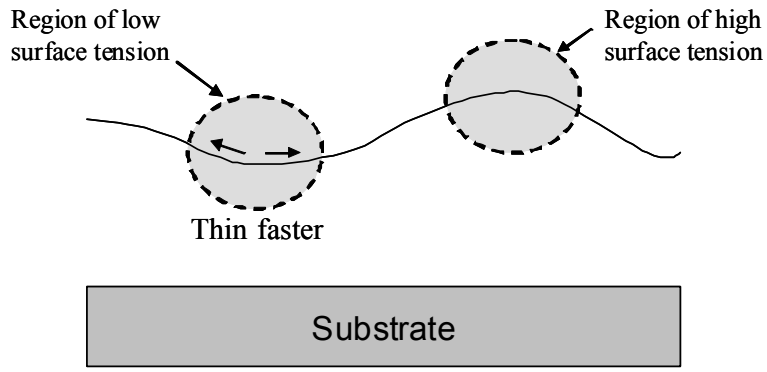

Fig. 5.8: Marangoni instabilities.

Surface roughness of thin film has strong impact to the optical properties and its application. Strawhecker et al. reported the roughness of the coating films is primarily induced by the solvent evaporation rate [Strawhecker'01]. The solvent with rapid evaporation creates so-called Marangoni instabilities. As shown in Fig. 5.8, rapid evaporation rate gives a non-uniform evaporation. Thus, surface tension at the peak will be higher than surface tension at the valley. The valley will get thin faster than the peak. After the film is solidified, the surface roughness is fixed.

Refractive Index and Birefringence

We measured refractive index and optical anisotropy (birefringence) of the films by using prism coupling at 633 nm at both polarizations, n_{TE} and n_{TM}. Figure 5.9 shows refractive index (a) and birefringence (b) of thin films of fraction P2* in different solvents. The refractive index at TE and TM polarization increases as boiling temperature of solvent is increasing. However, n_{TE} is increasing more than n_{TM}. Consequently, the birefringence is also increasing.

We interpret the observation that the refractive index at TE polarization is higher than at TM polarization because the polymer backbone becomes more oriented parallel to the substrate and light propagates slower along polymer chain due to higher electron density of the backbone bonds and produce high refractive index.

Thin films prepared from chloroform solutions have the smallest birefringence. Obviously, the use of chloroform causes more randomly oriented chains as compared to other solvents with higher T_b. It can be understood because chloroform has low boiling point and fast evaporation rate. As the solvent evaporates the chains are frozen faster and do not have time to align parallel to the substrate surface. On the other hand,

chlorobenzene has high boiling point and evaporates slowly. Thus, the chains have enough time to align parallel to the substrate and get aggregated with neighbouring chain segments. Therefore, films prepared from chlorobenzene solutions have a large degree of ordering and more oriented chains parallel to the substrate plane. Consequently, these films have high birefringence.

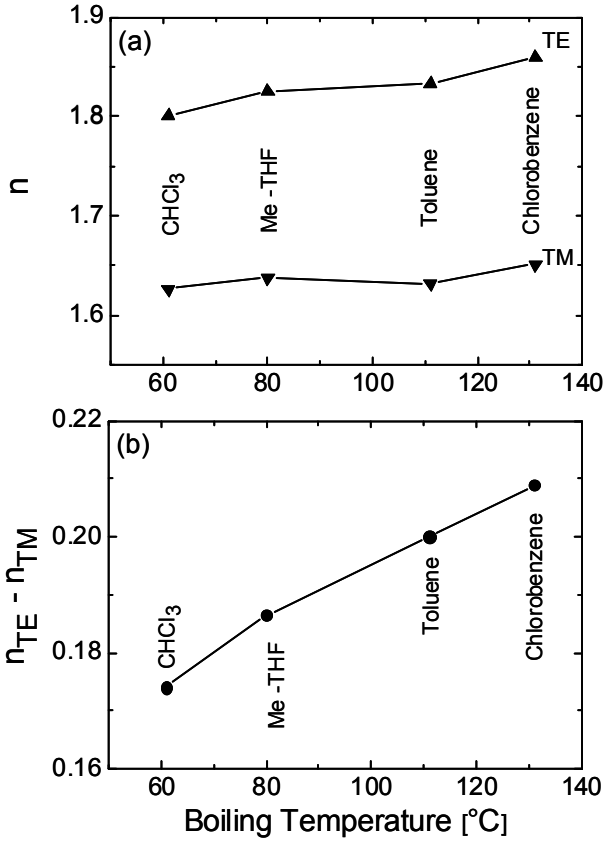

Fig. 5.9: Refractive index (a) and birefringence (b) of thin films of fraction P2* at $\lambda = 633$ nm cast from different solvents.

Waveguide Propagation Loss

We measured waveguide propagation loss at 1064 nm in TE polarization by means of cw-Nd:YAG laser as described in Chapter 3. The waveguide propagation loss was determined by measuring the stray light of TE_0 modes as a function of distance from the prism coupling point. Fig. 5.10 displays the decay of the scattered light at the diode array for fraction P2*.

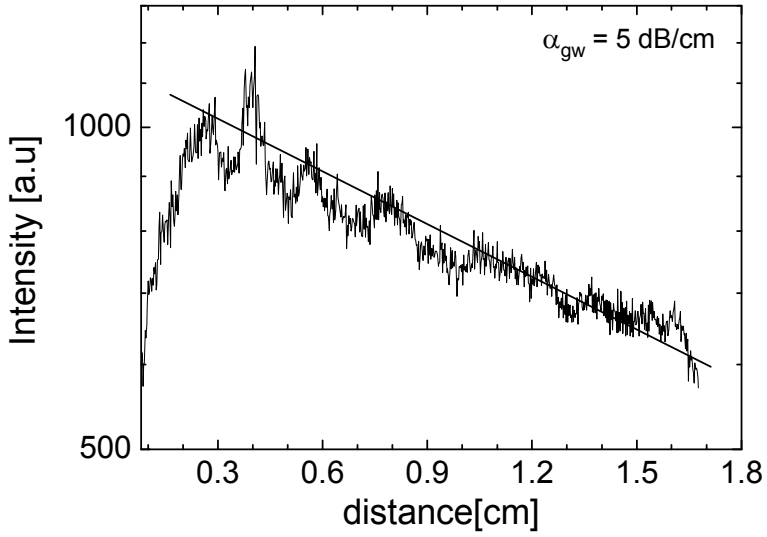

Fig.5.10: Stray light of TE_0 mode of fraction P2* in toluene waveguide versus distance from prism coupling at laser wavelength λ = 1064 nm. The solid line represents the waveguide propagation loss coefficient α_{gw}.

The obtained waveguide propagation loss coefficients α_{gw} and solvents are listed in Table 5.3 and shown in Figure 5.11 The films prepared from chloroform and Me-THF have large experimental errors because of the large surface roughness and inhomogeneities of these films.

Table 5.3: Waveguide propagation loss coefficient α_{gw} of MEH-PPV fraction P2*. The films were prepared from different solvents.

Solvent	Boiling Point [°C]	α_{gw} [dB/cm]
$CHCl_3$	61	4 ± 2
Me-THF	80	3 ± 2.5
Toluene	111	5.5 ± 1
Chlorobenzene	131	10 ± 1

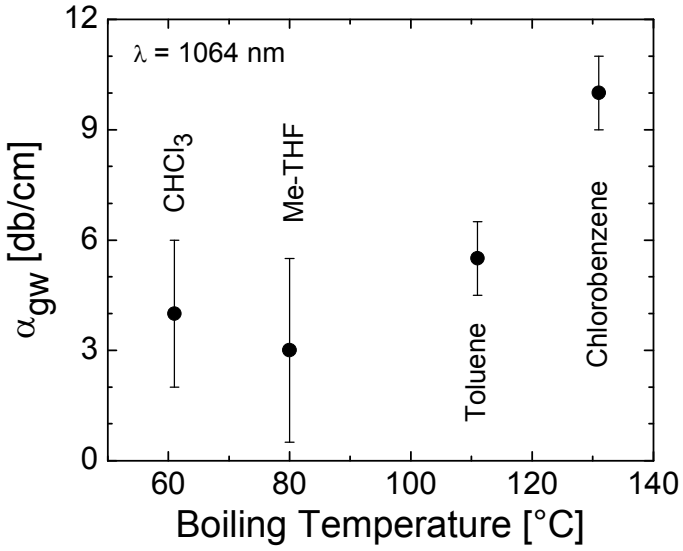

Fig. 5.11: Attenuation loss coefficients of thin films of MEH-PPV (P2*) spin cast from different solvents for TE_0 mode at the laser wavelength λ = 1064 nm.

As shown in Fig. 5.11, solvents influence the waveguide propagation loss. The attenuation loss tends to increase as boiling point is increasing. But the film prepared from chloroform has higher value of attenuation loss compared to films from Me-THF.

There are several factors, which influence the attenuation loss such as absorption loss, scattering losses arising from surface roughness and intrinsic scattering centers such as aggregates, and polarization-dependent loss [Ma'02, Noorwood'01]. It is difficult to distinguish which source gives contribution to attenuation loss, whether from absorption loss or scattering loss [Ma'02]. In our experiments we used the same material with the same molecular weight to create the same condition of absorption loss, which is negligibly small at 1064 nm because MEH-PPV does not absorb at this wavelength.

There are two kind of scattering losses: extrinsic and intrinsic scattering loss. In general, extrinsic scattering losses come from thin films preparation that produces voids, cracks bubbles and surface roughness, which result from unfiltered particles, dust, dissolved air bubbles, and inappropriate solvents. Meanwhile, intrinsic scattering loss comes from density fluctuations and compositional inhomogeneities. The film using higher boiling point has longer evaporation time and facilitates the growth of a highly crystalline film or gives more time to polymer chain entanglement and formation of aggregates [Koynov'06]. Meanwhile when using solvent with lower boiling point, the solvent evaporates faster and has limited time to crystallize during the spin coating process.

As shown in Table 5.2, the film cast from chlorobenzene has surface roughness smaller than film cast from toluene; however, the attenuation loss coefficient is higher than the film cast from toluene. Chlorobenzene has longer evaporation time as compared to toluene, so that the film cast from chlorobenzene has aggregation domains more than films cast from toluene. The aggregation domains create the local change of refractive index in the boundary between amorphous regions and crystalline region or aggregates as described in Fig. 5.12. They will cause light scattering and intrinsic scattering loss and affect the attenuation loss coefficient significantly.

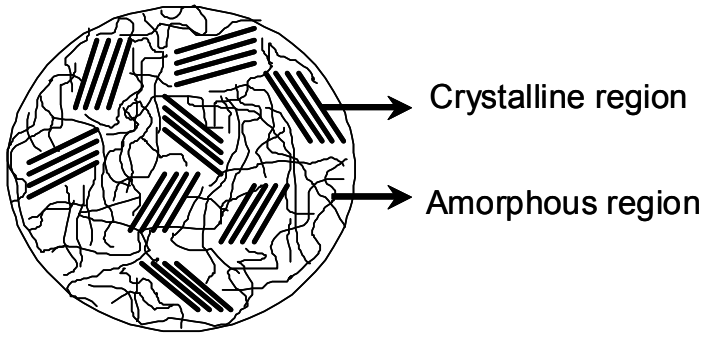

Fig. 5.12: Visualization of crystalline and amorphous regions in thin polymer films.

Even though the film prepared from chloroform solution has nearly amorphous structure, it has higher waveguide loss coefficient as compared to the film cast from Me-THF. We interpret this by the larger surface roughness of films cast from chloroform shown in Table 5.2 and Fig. 5.5, respectively.

Fourier Transform Infrared Spectroscopy

We investigate the molecular orientation of MEH-PPV (fraction P2*) in thin polymer films with respect to the substrate by means of Fourier Transform Infrared (FTIR) spectroscopy in two configurations: transmission and grazing incidence reflection, which are shown in Fig. 3.3. In the transmission at perpendicular incidence, the electrical field vector is oriented parallel to the plane of film, denoted $E_{\|}$. The angle between the transition dipole moment of the vibrational mode and the chain direction is called φ. Therefore, if the polymer chains are oriented parallel to the film plane, it will lead to strong absorption for the vibration bands with angle $\varphi \approx 0$ ($\vec{M}$ parallel to $\vec{E}$) and a small absorption for $\varphi \approx 90^0$ ($\vec{M}$ perpendicular to $\vec{E}$). We also measured the IR spectra of thin films, which were spin-cast on evaporated gold layers on glass microscope slides, at

grazing incidence reflection condition. In this case, the electrical field vector of the incident light is perpendicular to the film plane and we denote it $E_{\perp}$. Then, the vibration bands with angle $\varphi \approx 90^0$ will have strong absorption and the absorption will be small for $\varphi \approx 0$

The IR bands shown in the Table 5.4 give information on the chain orientation because their assignment to molecular vibrations and angles φ are known from earlier work [Bradley'86, Tian'91, Scott'96, Bahtiar´04, Koynov´06]. As the spectra were measured at films with slightly different thicknesses, we used the band at 1415 cm^{-1} for normalization of the spectra. The transition dipole moment vector of the vibration mode of this band is oriented at the angle φ = 64°, which makes this band particularly suitable for normalization.

Table 5.4: Assignment of IR bands of unsubstituted PPV

Wavenumber [cm^{-1}]	assignment	Angle,φ [°]
861	Out of plane phenyl CH wag	83
968	Trans-vinylene CH wag	84
1415	Semicircular phenyl stretch	64
3058	Trans-vinylene C-H stretch	30

Figure 5.13 shows FTIR spectra of thin films MEH-PPV (P2*), cast from different solvents in two configurations, transmission ($E_{\parallel}$) and reflection ($E_{\perp}$) spectroscopy, respectively.

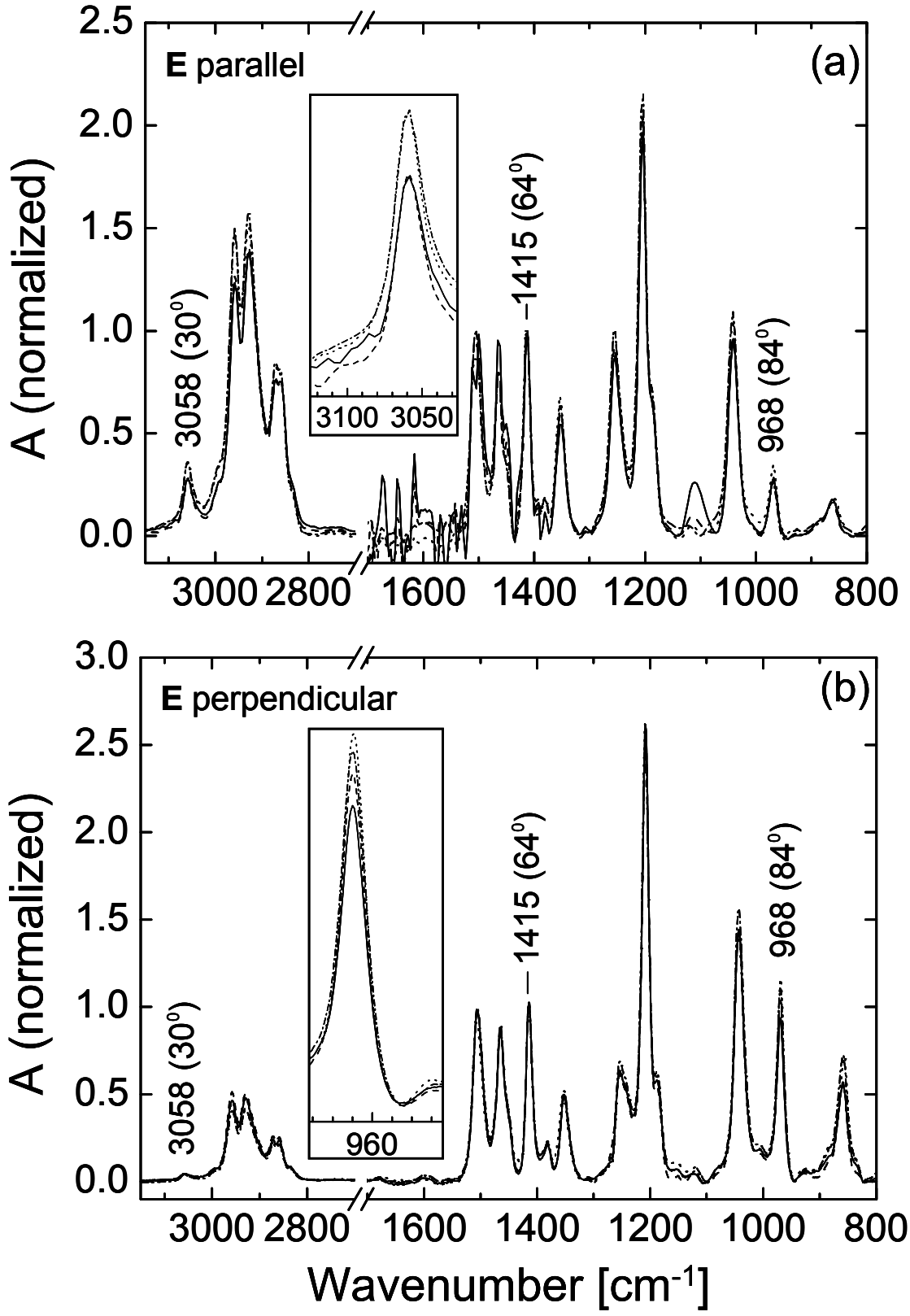

Fig. 5.13: FTIR spectra of thin films of MEH-PPV cast from different solvents. Chlorobenzene (solid line), Toluene (dashed line), Me-THF (dotted line), $CHCl_3$ (dashed dot line). (a) Transmission spectroscopy. (b) Reflection spectroscopy. Inset shows the different absorbance of the band at 3058 cm^{-1} (a) and 968 cm^{-1} (b) of each solvent.

The spectra of P2* films prepared from different solvents are rather similar. The main differences are the relative band intensities at $E_{\|}$ and $E_{\perp}$. The intensities of bands with φ = 83°, φ = 84° are higher at $E_{\perp}$ than $E_{\|}$ but for the band with φ = 30° the intensities at $E_{\|}$ are higher as compared to $E_{\perp}$. These intensity ratios provide evidence that most polymer chains are oriented parallel to the substrate.

We compare the intensities of the bands with φ = 83°, φ = 84° and φ = 30° with respect to φ = 64°. Table 5.5 displays relative intensities of these bands in different solvents for E parallel (5.5a) and E perpendicular (5.5b). We also compare the absorbances *A* of the bands at 968 cm^{-1} (φ = 84°) and 3058 cm^{-1} (φ = 30°) as ratio R A_{968} / A_{3058}.

Table 5.5a: Absorbance data of thin films cast from different solvents measured at E parallel, i.e., as evaluated from transmission spectrum of Fig. 5.13a.

Film casting solvent	$CHCl_3$	Me-THF	Toluene	Chlorobenzene
A_{3058}	0.244	0.248	0.220	0.186
A_{1415}	1.0	1.0	1.0	1.0
A_{968}	0.310	0.322	0.286	0.286
A_{861}	0.178	0.168	0.156	0.161
A_{968}/A_{3058}	1.27	1.29	1.30	1.54

Table 5.5b: Absorbance data of thin films cast from different solvents measured at E perpendicular, i.e., as evaluated from grazing incidence spectrum of Fig. 5.13b.

Film casting solvent	$CHCl_3$	Me-THF	Toluene	Chlorobenzene
A_{3058}	0.0260	0.0250	0.0296	0.0267
A_{1415}	1.0	1.0	1.0	1.0
A_{968}	1.15	1.23	1.06	0.936
A_{861}	0.725	0.781	0.577	0.565
A_{968}/A_{3058}	44.2	49.2	35.8	35.0

As shown in Table 5.5, R = A_{968}/A_{3058} at $E_{\|}$ increases as boiling temperature of solvent is increasing and vice versa for R at $E_{\perp}$. From relative intensities of bands listed in Table 5.5

and R = A_{968}/A_{3058}, we conclude that average orientation of vinylene and phenyl ring tend to be oriented more parallel to the substrate for lower boiling point of solvents (chloroform and Me-THF) and perpendicular for higher boiling point (toluene and chlorobenzene). Results in this work are in agreement with the results of Shi et al. [Shi'00]. They reported two possible orientations of aromatic ring of thin films of MEH-PPV measured by contact angles as shown in Fig. 5.14. Films spun with chloroform and THF may have more aromatic rings lying parallel to the surface and films spun with toluene and chlorobenzene have more aromatic rings perpendicular to the surface [Shi'00]. According to Shi et al. this is related to the chemical nature of the solvents and their polarity.

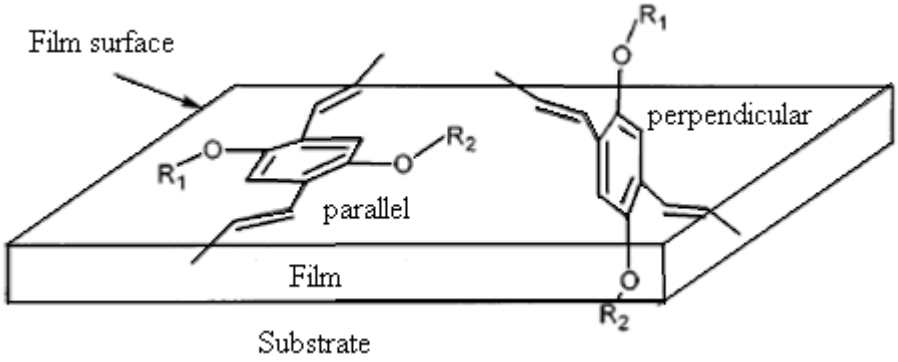

Fig. 5.14: Molecular orientation of MEH-PPV films in $CHCl_3$ and Me-THF (parallel to the substrate) and films in toluene and chlorobenzene (perpendicular to the substrate) [Shi'00].

Thus, by combining measurement by using FTIR and prism coupling we found that films using solvent with high boiling point have large birefringence because the polymer backbones are more oriented parallel to the substrate and have a large degree of ordering but the molecular orientation of phenyl ring and vinylene groups tends to perpendicular orientation relative to the substrate. Meanwhile, the films cast from lower boiling point have nearly amorphous structure and have molecular orientations of phenyl ring and vinylene groups, which tend to be more parallel to the substrate.

5.2.2 Influences of Film Casting Temperature

We made thin polymer films at different casting temperatures to study their influence on optical properties of thin films such refractive index and birefringence. We carried out these experiments with fraction P2* and used toluene as solvent at the concentration C_w = 3%. We performed the spin coating experiments at 25 °C, 40 °C and

50 °C by heating the substrate (fused silica) in a special sample holder, which can transfer the heat uniformly to the entire substrate surface. At the same time we also heat the solution at desired temperature and flooding the solution on the substrate after the temperature achieved. Subsequently, we annealed the films at 55 °C for about 12 hours.

Film Thickness and Average Surface Roughness

The spinning speed, thickness and roughness obtained of fraction P2* are listed in Table 5.6 As shown in this table, for the same parameters of film preparations such as solvent, concentration and spinning speed, the thickness and surface roughness obtained at different casting temperature increase as casting temperature is increasing.

Table 5.6: Influence of casting temperature on film thickness and roughness at constant spin coating parameters (fraction P2*, ω = 1000 rpm, C_w = 3 %).

Casting Temperature	d [nm]	R_a [nm]
25 °C	759	8.9 ± 4.5
40 °C	794	13.9 ± 3.3
50 °C	889	18.5 ± 5

At increasing casting temperature, we see a trend to larger film thickness and roughness, respectively. This trend is similar to the trend that we discussed previously in the part of solvent effects on optical properties. Polymer films produced with solvents of lower boiling temperature evaporate faster and yield thicker and rougher films. At elevated temperature of casting, the solvent evaporates faster than at lower casting temperature. This causes faster solvent evaporation and produces thicker and rougher films.

Refractive Index and Birefringence

We measured refractive index of the films by means of prism coupling at 633 nm in both polarizations: n_{TE} and n_{TM}. Figure 5.15 displays refractive index and birefringence of polymer P2* at different casting temperature.

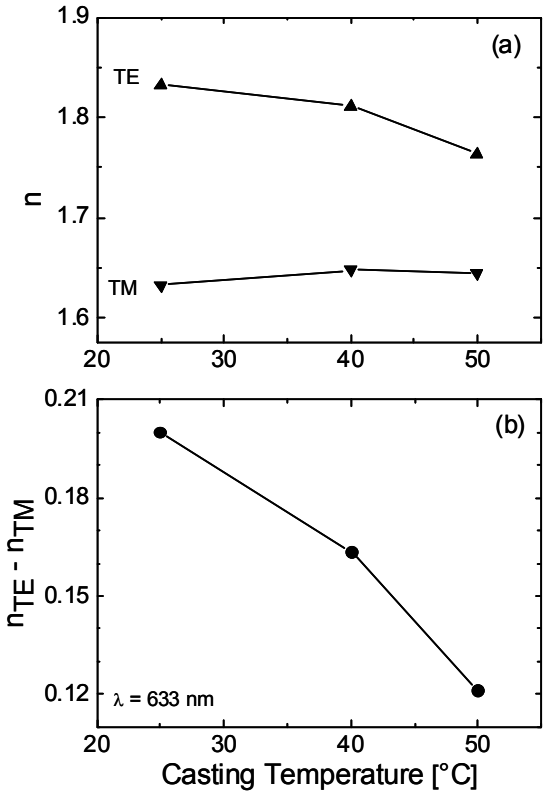

Fig. 5.15: Refractive index and birefringence of thin film of MEH-PPV (P2*) in different casting temperature used toluene as solvent.

As shown in Fig 5.15, the refractive index n_{TE} is decreasing by increasing of casting temperature, but n_{TM} tends to increase slightly. The birefringence systematically decreases by increasing the casting temperature. This result indicates that the films spun at lower temperature have the backbone of chains mainly parallel to the substrate and more oriented than films spun at elevated temperature. Meanwhile, films spun at elevated temperature tend to form more amorphous structure. At elevated casting temperature the solvent evaporates faster than at lower casting temperature. Consequently, the polymer chains do not have enough time to align parallel to the substrate surface and get a more randomly oriented structure. This result agrees with results reported by Prest et al. who reported that the birefringence of polystyrene films decreases as the casting temperature is increased [Prest'80].

5.3 Summary and Conclusions

We investigated the factors that influence the morphology of thin polymer films prepared by spin coating such as molecular weight, boiling temperature of solvent and casting temperature. The morphology of thin polymer films prepared by spin casting can

be controlled by choosing appropriate processing conditions. As an example, we are able to control the thickness and surface roughness of thin films by choosing appropriate boiling temperature of solvent or casting temperature.

The optical properties such as refractive index, birefringence and waveguide propagation loss depend on molecular weight, boiling point of solvent and casting temperature. Higher molecular weight and boiling point of solvent will produce thin films with higher birefringence and higher attenuation loss. High molecular weight has long polymer chains which allow polymer chain entanglement and formation of aggregation domains; meanwhile, high boiling point of solvent causes longer evaporation time and facilitates the growth of a highly crystalline film. It also causes the polymer backbone to align more parallel to the substrate and have a large degree of ordering. These conditions favor aggregation and yield large birefringence and high value of attenuation loss.

Thin films prepared at elevated temperature will produce films with more amorphous structure. At elevated casting temperature the solvent evaporates very fast and as a consequence the polymer chains do not have enough time to align parallel to the substrate surface and get a more randomly oriented structure.

We are able to produce good quality of waveguides which has low attenuation loss by using MEH-PPV with low M_w and M_n ($M_w \approx 4.03 \times 10^4$ g/mol), choosing solvent with intermediate boiling point, for instance toluene and casting in the room temperature [Koynov´06, Bahtiar'09].

We also observed that the molecular orientation of thin films is influenced by the kind of solvents, their polarity and different boiling temperature. We found that as boiling temperature of solvents increase the planes of phenyl ring and vinylene groups show a small trend to align more perpendicular to the substrate.

6 Dip Coating Experiments

We have collaboration with Applied Quantum Physics group at Department of Physics, Mainz University. They made bottle microresonators which are often used for nonlinear optics applications and have potential for switches in optical communications [Pöllinger'09]. For the realization of optical switching applications, they need an appropriate nonlinear material as cladding of bottle microresonators. As reported recently, MEH-PPV with M_w = 40 kg/mol is a very suitable material for optical switching devices [Koynov'02, Koynov'06, Bahtiar'06, Bahtiar'08]. We have obtained this type of MEH-PPV by fractionation as described in Chapter 4. We prepared thin films on the resonators by using the dip coating technique. First, we performed dip coating experiments by using planar substrates to determine some parameters such as withdrawal velocity, concentration and immersion time to produce homogeneous films and then we made thin films on fibers. Aim of these experiments is to prepare dip-coated films on fibers with controlled thickness.

6.1 Planar Substrates

We prepared dip-coated films on planar substrates using the MEH-PPV fraction P1* and toluene as solvent with a concentration of 1% by weight. The substrate was cleaned and then was immersed vertically into the coating solution with constant velocity as described in Chapter 3. After certain storage times in solution, the substrates were removed. Subsequently, the film was annealed under vacuum at T ≈ 50 °C for at least 12 hours. The film thickness h is predicted by Landau, Levich and Derjaguin which is known as LLD theory [Landau'42, Deryaguin'43, Quèrè'99]

$$h = 0.94\left(\frac{\gamma}{\rho g}\right)^{1/2} Ca^{2/3}, \tag{6.1}$$

where γ is surface tension, ρ is density, g is the gravity acceleration, and Ca is the capillary number given by

$$Ca = \frac{\eta V}{\gamma}, \tag{6.2}$$

where η is the viscosity and V is the withdrawal velocity. According to Eq. 6.1, the film thickness is a function of withdrawal velocity. In order to get thick films, we have performed experiments with the highest withdrawal velocity of our equipment which is 10 mm/s. Pontin et al. reported that increasing the immersion time produced significantly thicker films [Pontin'05]. Thus, we prepared dip-coated films with a withdrawal velocity of 10 mm/s at different immersion times. Table 6.1 shows the obtained thicknesses of these experiments.

Table 6.1: Thickness of dip-coated films of fraction P1* in toluene (C_w = 1%) on planar substrates at different immersion times, obtained at constant withdrawal velocity of 10 mm/s.

Immersion time (minutes)	Thickness (nm)
0.5	230 ± 4
1	237 ± 5
1.5	246 ± 3
2	256 ± 2
2.5	258 ± 3

As shown in Table 6.1, the thickness of the films increases as immersion time is increasing. However, the increase is not very significant. We also observed that the film thickness was not constant over the size of the substrate, which is 12 mm x 25 mm. In order to investigate the thickness distribution of the film on the substrate, we measured the film thickness at the *x*- and *y*-axis of the substrate as shown in Fig. 6.1.

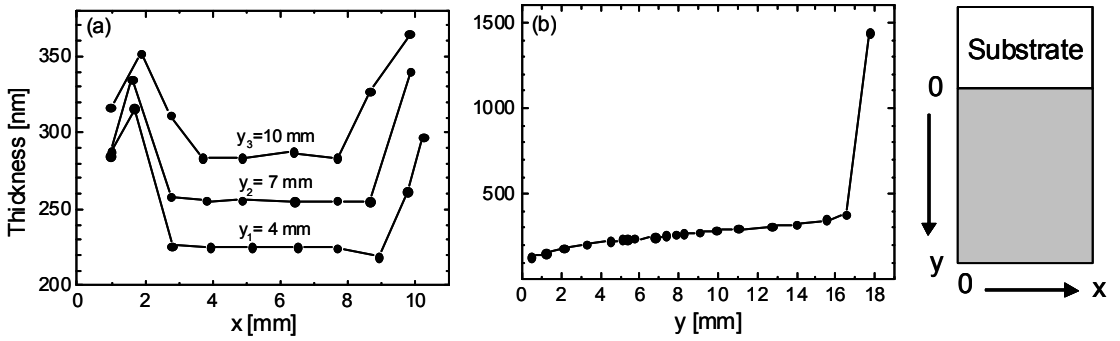

Fig. 6.1: Thickness distribution of a dip-coated film of fraction P1* at different *x* and *y* positions of the substrate. Parameters: withdrawal velocity 10 mm/s, immersion time 2 minutes, *x*-position of graph (b) is x = 6.

The thickness distribution along the *y*-axis as depicted in Fig. 6.1 (b) is not constant because the solution at the top of the film drains down, resulting in an uneven distribution. The distribution of film thickness along the *y*-axis can be divided into three regions as shown in Fig. 6.2 [Krozel'00]. The first is the film thickness at the upper part in the so-called transient region that pertains to Jeffereys theory. The second is a constant film thickness region that pertains to Landau-Levich theory. The third, close to the bath, is the meniscus region. The critical plane separates regions I and II.

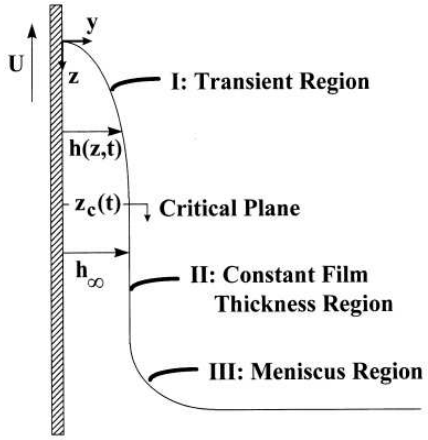

Fig. 6.2: Thickness profile of dip-coated films. Three major regions are labeled. The critical plane separates regions I and II, and moves downward over time [Krozel'00].

According to these specified regions, the film thickness shown in Fig. 6.1 (b) should show a constant region. But this is not really observed. May be, the substrate was not long enough to approach this constant film thickness region.

6.2 Fibers

We also prepared dip-coated films of MEH-PPV fraction P1* with concentration of 1% by weight in toluene on fused silica fibers. In order to realize optical switching, a bottle microresonator is required with a diameter around 40 μm [Poellinger`10]. Thus, we prepared dip-coated films on fibers, which had a diameter of 35 μm at a withdrawal velocity 10 mm/s and immersion time 2 minutes. To verify the thickness distribution of the coated film on the fiber, we measured the film thickness along *y*-axis as shown in Fig. 6.3.

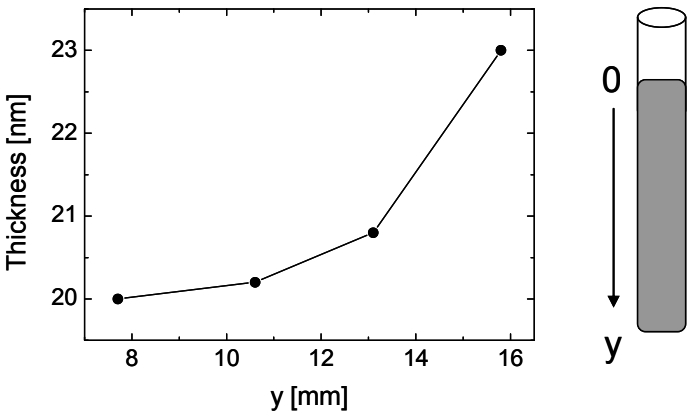

Fig. 6.3: Thickness of dip-coated film of fraction P1* (C_w = 1%) in toluene at different *y*-positions of the fiber. The withdrawal velocity is 10 mm/s and immersion time 2 minutes.

The thickness distribution of film on the fiber along *y*-axis is almost similar to the thickness distribution on planar substrate. According to calculations of bottle resonator designs, we need a film with thickness 800 nm for optimum results of optical switching for wavelengths around 1080 nm [Poellinger`10]. In order to get thicker films, we prepared solutions of MEH-PPV fraction P3* in higher concentrations and made films again on fibers with diameter 35 µm. Table 6.3 shows the obtained thicknesses for different concentrations of solutions.

Table 6.3: Thickness of dip-coated films of MEH-PPV fraction P3* with different concentrations on fibers with diameter 35 µm. Parameters: withdrawal velocity 10 mm/s, immersion time 2 minutes, *y*-axis position 9 mm. (-) not measured because of viscosity problem.

C_w (%)	Thickness (nm)
3.6	30 ± 5
5.6	85 ± 5
6	95 ± 5
9.2	-
14.6	-

Due to the viscosity problem, we were not able to make films using higher concentrations of 9.2% and 14.6%. The maximum concentration to get a thicker film was C_w = 6 %.

6.3 Summary of Fiber Resonator Studies

Coating the bottle microresonators with a nonlinear polymer is a promising approach for realization of all-optical switching with a bandwith of up to several GHz and at the same time only moderate power requirements in the sub-Watt range. This application relys on the spatial and temporal confinement of light by the microresonator, characterized by the resonator's mode volume V and its quality factor Q. The ratio of Q/V defines a key figure relating the coupling strength between light and matter in the resonator to the dissipation rates of the coupled system. For a given input power, the nonlinear shift of the resonance frequency in units of the resonators linewidth is proportional to n_2Q^2/V, where n_2 is the nonlinear refractive index. Therefore the power at which switching occurs is proportional to $V/(n_2Q^2)$ [Pöllinger'10].

We have prepared thin films of MEH-PPV on the bottle microresonators by means of dip coating. We used MEH-PPV fraction P3* in toluene with concentration 6 % by weight and used bottle microresonators with diameter 35 μm. Unfortunately, we were not able to measure the coated resonators with laser at wavelength 1080 nm where the n_2 of MEH-PPV is the highest [Koynov´02, Bahtiar´06], because this laser wavelength was not available for the fiber resonator studies. The spectral properties of the coated resonators with thickness 95 nm are investigated with a distributed feedback (DFB) laser at 850 nm. Quality factors of 3×10^5 to 5×10^5 are observed at TM polarization [Pöllinger`10]. The resonator device performance is based on nonlinearity properties, which are strongly wavelength dependent. Therefore, they have to be optimized for operation at a particular wavelength. We have shown that coating the bottle microresonators with a nonlinear polymer presents a promising route towards high-bandwidth all-optical signal processing.

7 Influence of Side-Chain Substitution on Film Morphology Investigated by FTIR Spectroscopy

7.1 Materials

The aim of this chapter is to reveal the systematic trends in the structure-property relations of the impact of side-chain substitution of PPV derivatives on the morphology of the films. Scheme 7.1 shows the chemical structures of several alkoxy-subsituted PPVs. We have prepared thin film of PPV-derivatives; M3EH-PPV and MEH-M3EH-PPV by spin coating and comparing the results with MEH-PPV from previous studies. These materials are alkoxy-substituted PPVs, which have different degree of long alkyl side-chains and all of them have a similar molecular weight (for their full chemical names and M_w see appendix B). These polymers were provided by H.-H. Hörhold and their synthesis was reported earlier [see our refs. 32-34 in [Bahtiar´09]]. The results of this Chapter were published already [Bahtiar´09].

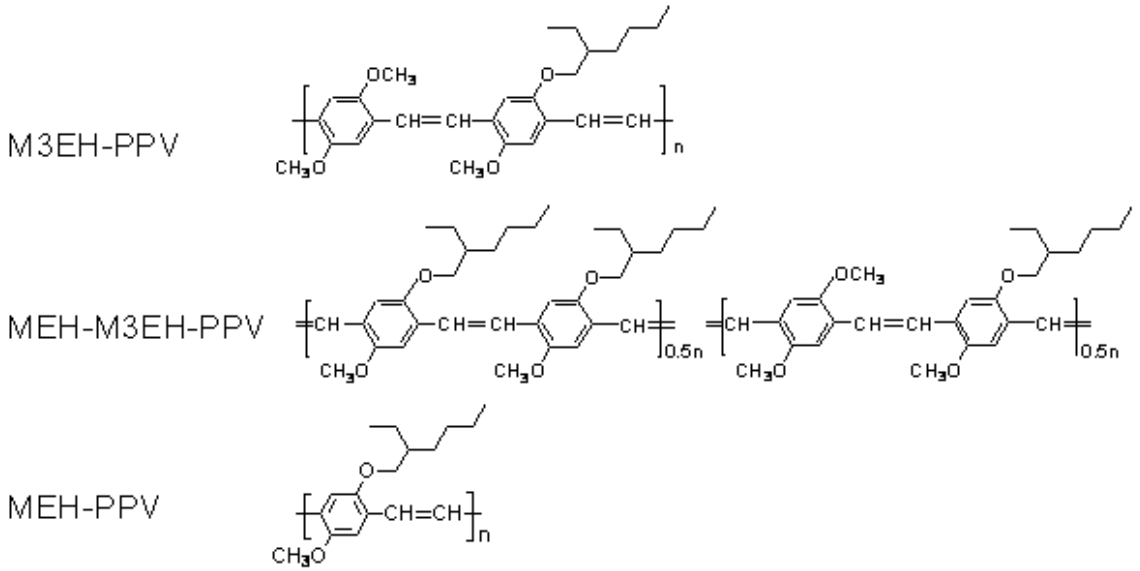

Scheme 7.1**:** Chemical structures of poly-(*p*-phenylenevinylene) (PPV) derivatives. Their full chemical names are given in Appendix B [Bahtiar'04].

7.2 FTIR Spectroscopy

7.2.1 Results

We used Fourier Transform Infrared (FTIR) spectroscopy with polarized light to study the average chain orientation in thin films of PPVs with typical thickness of 70 nm. As the transition dipole moment vector of a vibration mode $\vec{M}$ is oriented at a specific

angle φ relative to the chain axis, polarized IR spectra can be used to obtain information on the chain orientation by comparing the relative strength of vibration bands with different φ [Bubeck'91 and Michl'95]. We have measured M3EH-PPV and MEH-M3EH-PPV in two configurations: transmission and grazing incidence reflection. The FTIR spectra of thin films of M3EH-PPV and MEH-M3EH-PPV are shown in Fig. 7.2.

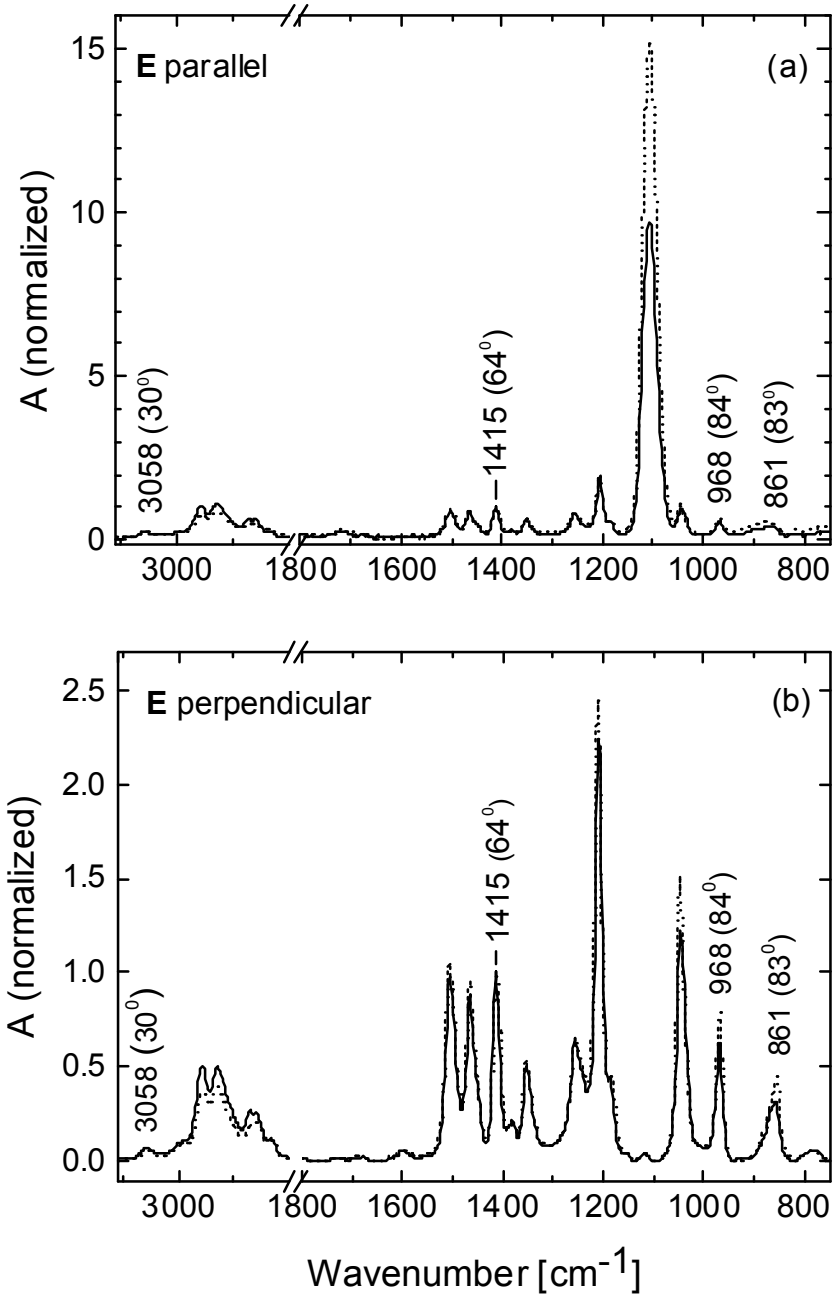

Fig. 7.2: FTIR spectra of MEH-M3EH-PPV (solid line) and M3EH-PPV (dashed line). (a) Transmission spectroscopy. (b) Reflection spectroscopy. Absorbance A is normalized with respect to the band at 1415 cm^{-1}. Wavenumbers and angles φ are shown for selected bands only.

7.2.2 Discussion

As described in Chapter 5, we used IR bands with specific φ listed in Table 5.4 to determine chain orientations. We also used the band at 1415 cm^{-1} for normalization of the spectra. The spectra of M3EH-PPV and MEH-M3EH-PPV are rather similar to the spectra of MEH-PPV reported by Koynov et al. [Koynov'06]. Their main differences are the relative band intensities. This gives further evidence that the average chain orientations of the PPV derivatives are different. For quantitative evaluation, we define the ratio of the absorbances A of the bands at 968 cm^{-1} ($\varphi = 84°$) and 3058 cm^{-1} ($\varphi = 30°$) measured at grazing incidence condition with the electric field vector perpendicular to the substrate plane as $R_\perp = A_{968} / A_{3058}$. The results are displayed in Table 7.2. The ratio $R_\perp$ depends on the average angle between polymer chain axis and substrate normal. But it also depends on the tilt angle of the phenyl rings with respect to the layer plane because the transition dipole moment vector of the 968 cm^{-1} mode is mainly oriented perpendicular to the phenyl ring plane [Fukurawa'07]. Therefore, $R_\perp$ will be largest for parallel alignment of the chain axis and for the orientation of the phenyl rings parallel to the substrate plane. Inspection of Table 7.2 shows, that the data of $R_\perp$ are largest for M3EH-PPV and decrease with increasing amount of alkyl substitution. We conclude that the degree of alkyl substitution has strong impact on the average chain orientation of the PPV derivatives.

Table 7.2: Comparison of the ratio R of the IR absorbance of the bands at 968 cm^{-1} ($\varphi = 84°$) and 3058 cm^{-1} ($\varphi = 30°$) measured for incident electric field perpendicular and parallel to the film plane, respectively. Data of MEH-PPV are taken from [Bahtiar`04].

Polymer	M_w[kg/mol]	R at $E_\perp$	R at $E_\parallel$
M3EH-PPV	44.0	18	2.3
MEH-M3EH-PPV	32.3	10.5	2.4
MEH-PPV	40.3	8	1.8

8 Summary

We have investigated the conjugated model polymer MEH-PPV to gain deeper insights to structure-property relations. We have carried out precipitation fractionation to get MEH-PPV with different molecular weight (M_w), in particular MEH-PPV with low M_w as this is optimally suited for optical waveguide devices. We found that the choice of of solvents and temperature when the precipitant is added is crucial to obtain MEH-PPV with low M_w with sufficient amount and narrow molecular weight distribution. Alternatively, we studied UV-induced chain scission effects. We conclude that precipitation fractionation is more suitable to get MEH-PPV with specific M_w as compared to chain scission by UV-irradiation, because UV-light causes chain defects along the polymer backbone which we characterized by means of ^{1}H NMR and FTIR spectroscopy. We observe that the wavelengths of absorption maxima of MEH-PPV fractions are still increasing with chain length until the number of repetition units approaches n ≈ 110, which is significantly larger as reported earlier.

We have measured optical properties of MEH-PPV waveguides and demonstrated excellent reproducibility of their optical constants. We have studied the influences of casting solvents and spin casting temperature of thin films on film thickness, surface roughness, refractive index, birefringence and waveguide propagation loss. We found that as boiling point of solvents increases, thickness and roughness are decreasing but the refractive index, birefringence and waveguide attenuation loss are increasing. We conclude that high boiling points of solvents cause slow evaporation rate, which facilitates the formation of aggregates during the spin coating process. On the other hand, increasing casting temperature causes increasing thickness and roughness, but refractive index and birefringence are decreasing.

We have investigated the film preparation by means of dip coating on planar glass slides and thin fibers of fused silica. The thickness of dip-coated films depends on concentration of solution, withdrawal velocity and immersion time. We have prepared dip-coated films of MEH-PPV on bottle microresonators for studies of all-optical switching. Coating the bottle microresonators with MEH-PPV with low M_w is a promising route towards high-bandwidth all-optical signal processing.

We have also studied the morphology of thin films of other PPV-derivatives related to MEH-PPV by using FTIR spectroscopy. We found that the degree of alkyl substitution has strong impact on the average orientation of the polymer backbones in thin films.

9 Zusammenfassung

In der vorliegenden Arbeit wurden Struktur-Eigenschaftsbeziehungen des konjugierten Modell-Polymers MEH-PPV untersucht. Dazu wurde Fällungs-fraktionierung eingesetzt, um MEH-PPV mit unterschiedlichem Molekulargewicht (M_w) zu erhalten, insbesondere MEH-PPV mit niedrigem M_w, da dieses für optische Wellenleiterbauelemente optimal geeignet ist Wir konnten feststellen, dass die Präparation einer ausreichenden Menge von MEH-PPV mit niedrigem M_w und geringer M_w-Verteilung wesentlich von der geeigneten Wahl des Lösungsmittels und der Temperatur während der Zugabe des Fällungsmittels abhängt. Alternativ dazu wurden UV-induzierte Kettenspaltungseffekte untersucht. Wir folgern aus dem Vergleich beider Vorgehensweisen, dass die Fällungsfraktionierung verglichen mit der UV-Behandlung besser geeignet ist zur Herstellung von MEH-PPV mit spezifischem M_w, da das UV-Licht Kettendefekte längs des Polymerrückgrats erzeugt. ^{1}H NMR and FTIR Spektroskopie wurden zur Untersuchung dieser Kettendefekte herangezogen. Wir konnten außerdem beobachten, dass die Wellenlängen der Absorptionsmaxima der MEH-PPV Fraktionen mit der Kettenlänge zunehmen bis die Zahl der Wiederholeinheiten n ≈ 110 erreicht ist. Dieser Wert ist signifikant größer als früher berichtet.

Optische Eigenschaften von MEH-PPV Wellenleitern wurden untersucht und es konnte gezeigt werden, dass sich die optischen Konstanten ausgezeichnet reproduzieren lassen. Wir haben die Einflüsse der Lösungsmittel und Temperatur beim Spincoaten auf Schichtdicke, Oberflächenrauigkeit, Brechungsindex, Doppelbrechung und Wellenleiter-Dämpfungsverlust untersucht. Wir fanden, dass mit der Erhöhung der Siedetemperatur der Lösungsmittel die Schichtdicke und die Rauigkeit kleiner werden, während Brechungsindex, Doppelbrechung sowie Wellenleiter-Dämpfungsverluste zunahmen. Wir schließen daraus, dass hohe Siedetemperaturen der Lösungsmittel niedrige Verdampfungsraten erzeugen, was die Aggregatbildung während des Spincoatings begünstigt. Hingegen bewirkt eine erhöhte Temperatur während der Schichtpräparation eine Erhöhung von Schichtdicke und Rauhigkeit. Jedoch nehmen Brechungsindex und der Doppelbrechung dabei ab.

Für die Schichtpräparation auf Glassubstraten und Quarzglas-Fasern kam das Dip-Coating Verfahren zum Einsatz. Die Schichtdicke der Filme hängt ab von Konzentration der Lösung, Transfergeschwindigkeit und Immersionszeit. Mit Tauchbeschichtung haben

wir Schichten von MEH-PPV auf Flaschen-Mikroresonatoren aufgebracht zur Untersuchung von rein-optischen Schaltprozessen. Dieses Verfahren erweist sich insbesondere für MEH-PPV mit niedrigem M_w als vielversprechend für die rein-optische Signalverarbeitung mit großer Bandbreite.

Zusätzlich wurde auch die Morphologie dünner Schichten aus anderen PPV-Derivaten mit Hilfe von FTIR Spektroskopie untersucht. Wir konnten herausfinden, dass der Alkyl-Substitutionsgrad einen starken Einfluss auf die mittlere Orientierung der Polymerrückgrate in dünnen Filmen hat.

10 References

[Atreya'99] M. Atrey, S. Li, E.T. Kang, K. G. Neoh, Z. H. Ma, K. L. Tan, W. Huang. *Polymer Degrsgation And Stability*, **1999**, *65*, 287 -296.

[Bahtiar'04] A. Bahtiar,"Optical Waveguides of Conjugated Polymers for All-Optical Switching Devices", *Ph.D Dissertation*, University of Mainz, **2004**.

[Bahtiar'08] A. Bahtiar, K. Koynov, T. Ahn and C. Bubeck, *J. Phys. Chem. B*, **2008**, *112*, 3605.

[Bahtiar'09] A. Bahtiar, K. Koynov, Y. Mardiyati, H.-H. Hörhold and C. Bubeck, *J. Mater. Chem.* **2009**, *19*, 7490 – 7497.

[Barbosa'09] H. M. C. Barbosa, M. M. D. Ramos, *J. Mater Sci : Mater Electron*. **2009**, *20*, S336-S340.

[Bader'02] M.A. Bader, G. Marowsky, A. Bahtiar, K. Koynov, C. Bubeck, H. Tillmann, H.-H. Hörhold, P S. ereira, *J. Opt. Soc. Am. B* **2002**, *19*, 2250-2262.

[Barton'75] Allan F. M. Barton, *Chem. Rev*.**1975**, *75*, 6.

[Becker'99] H. Becker, H. Spreitzer, K. Ibrom, W. Kreuder, *Macromolecules*, **1999**, *32*, 4925 – 4932.

[Bell'73] R. J. Bell, B. Fisher, *I. L. Tyler, Appl. Opt*. **1973**, *12*, 832.

[Boudrioua'00] A. Boudrioua, P. A. Hobson, B. Matterson, I. D. W. Samuel, W. L. Barnes, *Synth. Met*. **2000**, *111-112*, 545.

[Bradley'86] D. D. C. Bradley, R. H. Friend, H. Lindenberger and S. Roth, *Polymer*. **1986**, *27*, 1709.

[Braun'91] D. Braun and A. J. Heeger, *Appl. Phys. Lett*. **1991**, *58*, 1982.

[Bubeck'91] C. Bubeck and D. Holtkamp, *Adv. Mater.***1991**, *3*, 32.

[Campoy'05] M. Campoy-Quiles, P.G. Etchegoin, D.D.C. Bradley, *Phys. Rev. B* **2005**, *72*, 045209.

[Cantow'67] Manfred J. R. Cantow, *Polymer Fractionation*, Academic Press, New York, London, **1967**.

[Cragg'46] L. H. Cragg and H. Hammerslag, *Chem. Rev*. **1946**, *39*, 79.

[Cumpston'97] B. H. Cumpston, I. D. Parker, K. F. Jensen, *J. Appl. Phys*. **1997**. *81*, 8.

[Deryaguin'43] B. V. Deryaguin, *Acta Phys. Chim. URSS*. **1943**, *20*, 349.

[Desreux'52] V. Desreux and A. Oth, *Chem Weekblad* **1952**, *48*, 247.

[Fitrilawati'02] F. Fitrilawati, M.O. Tjia, S. Pfeiffer, H.-H. Hörhold, A. Deutesfeld, H. Eichner and C. Bubeck, *Opt. Mater.* **2002**, *21*, 511.

[Francuskiewicz'94] F.Francuskiewicz, *Polymer Fractionation*, Springer Lab Manual, Springer-Verlag, Berlin, Heidelberg, New York, London, Tokyo, **1994**.

[Fukurawa'07] Y. Furukawa, *Vibrational Spectroscopy of Conducting Polymers: Fundamentals and Applications*, in *Handbook of Vibrational Spectroscopy*, Vol. *4*: *Vibrational Spectroscopy of Polymers: Principles and Practice*, N. J. Everall, J. M.Chalmers and P. R.Griffiths (Eds.), J. Wiley & Sons, **2007**.

[Friend'99] R. H. Friend, R. W. Gymer, A.B. Holmes, J. H. Burroughes, R. N. Marks, C. Taliani, D. D. C. Bradley, D. A. Dos Santos, J. L. Bredas, M. Lögdlund, W. R. Salaneck, *Nature* **1999**, *397*, 121.

[Gaal'03] M. Gaal, C. Gadermeier, H. Plank, E. Moderegger, A. Pogantsch, G. Leising, E. J. W. List, *Adv. Mater*. **2003**, *15*, 1165.

[Gardette'10] J-L Gardette, A. Rivaton, S. Therias in *Photochemistry and Photophysics of Polymer Materials*. Edited by Norman S. Allen, Chap. 15, J.Willey & Sons, Inc., Hoboken, New Jersey, **2010**.

[Gierschner'07] J. Gierschner, J. Cornil, H-J. Egelhaaf, *Adv. Mater*. **2007**, *19*, 173 - 191.

[Grulke'99] E. A Grulke, *Solubility Parameter Values* in: *Polymer Handbook*, Vol. *7*, J. Brandrup, E. H. Immergut, E. A. Grulke, editors, 4th ed, New York, NY: Wiley; **1999**. p 675 – 714.

[Guzmán'61] G. M. Guzmán, in *Progress in high polymers,*Vol. I, p.113, J. C. Robb and F. W. Peaker (Eds), London, Heywood, **1961**.

[Hansen'00] C. M. Hansen, *Hansen Solubility Parameters: a user's Handbook*, F. L. Boka Raton, CRC Press, **2000**.

[Harris'69] J. H. Harris and R. Shubert, *Beam Coupling to Film*, Conf. Abstracts, URSI (Int. Sci. Radio Union) Spring Meeting, Washington, D. C. **1969**, p.71.

[Harris'70] J. H. Harris, R. Shubert and J. N. Polky, *J. Opt. Soc. Am*. **1970**, *60*, 1007.

[Hecht'87] E. Hecht,"Optics", 2nd edition, Addison Wesley Inc. USA, **1987**.

[Hildebrand'49] J. Hildebrand and R. Scott, *The Solubility of Nonelectrolytes*, 3rd ed., Reinhold, New York, **1949**.

[Holzer'04] W. Holzer, A. Penzkofer, H. Tilmann, H-H. Hörhold, *Synth. Metals*, **2004**, *140*, 155 – 170.

[Hornak'92] L. A. Hornak, *Polymers for Lightwave and Integrated Optics: Technology and Applications*, Marcel Dekker, New York, **1992**.

[Huggins'67] Maurice L. Huggins and Hiroshi Okamato in: *Polymer Fractionation*, M. J. R. Cantow, Ed., Chap. A., Academic Press, New York, N. Y. **1967**.

[Hunsperger'84] R. G. Hunsperger, *Integrated Optics: Theory and Technology*, 2nd ed., Springer Series in Optical Sciences, Vol. 33, Chap. 2,3,6 (Springer-Verlag, Berlin, Heidelberg, New York, Tokyo), **1984**.

[Ickenroth'02] Dirk Ickenroth, Silke Weissmann, Norbert Rumpf and Herbert Meier, *Eur. J. Org. Chem.* **2002**, 2808-2814.

[Iogansen'62] L. V. Iogansen, *Sov. Phys.-Tech. Phys*. **1962**, *8*, 295.

[Jaczewska'08] J. Jaczewska, A. Budkowski, A. bernasik, E. Moons and J. Rysz, *Macromolecules*. **2008**, *41*, 4802-4810.

[Jeffereys'30] H. Jeffereys, The draining of a vertical plate, *Proceeding of the Cambrige Philosophical Society Magazine* **1930**, *26*, 204 – 205.

[Jeng'05] U. Jeng, C. H. Hsu, H. S. Sheu, H. Y. Lee, A. R. Inigo, H. C. Chiu, W. S. Fann, S. H. Chen, A. C. Su. T. L. Lin, K. Y. Peng and S. A. Chen, *Macromolecules*. **2005**, *38*, 6566-6574.

[Kim'07] Y-H. Kim, Y. U. Lee, J-I Han, S-M Han and M-K Han, *J. The Elec. Chem Society*. **2007**, *154*, 12.

[Kogelnik'79] H. Kogelnik, *Theory of Dielectric Waveguides* in *Integrated Optics*, 2nd. ed., ed by T. Tamir, Topics Appl. Phys., Vol.**7**, Chap. 2, Springer, Berlin, Heidelberg, New York, **1979**.

[Koningsveld'70] R. Koningsveld, *Adv. Polymer Sci*. **1970**, *7*, 1-69.

[Kranzelbinder'02] G. Kranzelbinder, E. Toussaere, J. Zyss, A. Pogantsch, E.W.J.List, H. Tillmann, H.-H. Hörhold, *Appl. Phys. Lett.* **2002**, *80*, 716-718.

[Krevelen'08] D.W. Van Krevelen, K.te Nijenhuis, *Properties of Polymers - Their Correlation with Chemical Structure; Their Numerical Estimation and Prediction from Additive Group Contributions*, chap.7. fourth edition. Elvesier. **2008**.

[Kotera'67] A. Kotera, in: *Polymer Fractionation*, M. J. R. Cantow, Ed., Chap. B. 1, Academic Press, New York, N. Y. **1967**.

[Koynov'02] K. Koynov, N. Goutev, F. Fitrilawati, A. Bahtiar, A. Best, C. Bubeck, H.-H. Hörhold, *J. Opt. Soc. Am. B* **2002**, *19*, 895-901.

[Koynov'04] K. Koynov, A. Bahtiar, T. Ahn, C. Bubeck, H.-H. Hörhold, *Appl. Phys. Lett.* **2004**, *84*, 3792-3794.

[Koynov'06] K. Koynov, A. Bahtiar, T. Ahn, R. M. Cordeiro, H.-H. Hörhold and C. Bubeck, *Macromolecules.* **2006**, *39*, 8692.

[Krozel'00] J. W. Krozel, A. N. Palazoglu, R. L. Powell, *Chem. Eng. Sci*. **2000**, *55*, 3639 – 3650.

[Landau'42] L. D. Landau and V. G. Levich, *Acta Phys. Chim. URSS*. **1942**, *17*, 42-54.

[Liu'01] J. Liu, Y. Shi and Y. Yang, *Adv. Funct. Mater.* **2001**, *11*, 6.

[Ma'02] H. Ma, Alex K.-Y. Jen and L. R. Dalton, *Adv. Mater.* **2002**, *19*, 14.

[Marcuse'74] D. Marcuse, *Theory of Dielectric Waveguides*, Academic, New York, **1974**.

[Mathy'96] A. Mathy, K. Ueberhofen, R. Schenk, H. Gregorius, R. Garay, K. Müllen, C. Bubeck, *Phys. Rev. B*. **1996**, *53*, 4367.

[Matsumoto'54] S. Matsumoto and Y. Ohyanagi, *Kobunshi Kagaku*. **1954**,*11*.7.

[McGehee'00] M. D. McGehee, A. J. Heeger, *Adv. Mater*. **2000**, *12*, 1655.

[McKenna'67] J. McKenna: *Bell Syst. Techn.J*. **1967**, *46*, 1491.

[McWhorter'63] A. McWhorter, *Solid-State Electr* **1963**, *6*, 417.

[Meier'97] H. Meier, U. Stalmach and H. Kolshorn, *ActaPolymer* **1997**, *48*, 379-384.

[Mencer'88] H. J. Mencer, *Pol. Eng. and Sci*. **1988**, *8*, 28.

[Meyerhofer'78] D. Meyerhofer, *J. Appl. Phys*. **1978**, *49*, 3993.

[Michl'95] J. Michl and E. W. Thulstrup, *Spectroscopy with Polarized Light*, VCH Publishers, **1995**.

[Midwinter'70] J. E. Midwinter, F. Zernike, *App. Phys. Lett*. **1970**, *16*, 198.

[Miller-Chou'03] B. A. Miller-Chou and Jack L. Koenig, *Prog. Polym. Sci*. **2003**, *28*, 1223 - 1270.

[Möller'88] K. D. Möller,"Optics", University Science Books, USA, **1988**.

[Mulazzi'99] E. Mulazzi, A. Ripamonti, J. Wery, B. Dulieu, S. Lefrant, *Phys. Rev. B: Condens. Matter Mater. Phys*. **1999**, *60*, 16519.

[Müllen'98] K. Müllen, G. Wegner, *Electronic Materials: The Oligomer Approach*, Wiley-VCH, Weinheim, Germany, **1998**.

[Müller'84] M. A. Müller and G. Wegner, *Macromol. Chem*. **1984**, *185*, 1727 – 1737.

[Nguyen'99] T-Q. Nguyen, V. Doan, B. J. Schwartz, *J. Chem. Phys*. **1999**, *110*, 4068.

[Nguyen'00] T-Q. Nguyen, I. B. Martini, J. Liu, B. J. Schwartz, *J. Phys. Chem. B*. **2000**, *104*, 237.

[Nguyen'01] T-Q. Nguyen, R. Y. Yee, B. J. Schwartz, *J. Photochem and Photobio A: Chem*. **2001**, *144*, 21-30.

[Nguyen'02] T-Q. Nguyen and B. J. Schwartz, *J. Chem. Phys*. **2002**, *18*, 116.

[Oelkrug'01] D. Oelkrug, J. Gierschner, H.-J. Egelhaaf, L. Lüer. A. Tompert, K. Müllen, U. Stalmach, H. Meier, *Synth. Met*. **2001**, *121*, 1693.

[Osterberg'64] H. Osterberg, L. W. Smith, *J. Opt. Soc. Am*. **1964**, *54*, 1078.

[Penzkofer'98] A. Penzkofer, E. Drotleff, W. Holzer, *Opt. Commun*. **1998**, *158*, 221.

[Petrisch'99] K. Petrisch, R. H. Friend, *Synth. Met*. **1999**, *102*, 976.

[Poellinger`09] M. Pöllinger, D. O'Shea, F. Warken and A. Rauschenbeutel, *Physc. Rev. Lett*. **2009**, *103*, 053901.

[Poellinger`10] M. Pöllinger. *PhD Dissertation*, University of Mainz, Germany, **2010**.

[Pontin'05] M. G. pontin, F. F. Lange, A. J. Sánchez-Herencia and R. Moreno, *J. Am. Cerm. Soc*. **2005**, *88*, 2945 – 2948.

[Quèrè'99] D. Quèrè, Ann. Rev. Fluid Mech. **1999**, *31*, 347 – 84.

[Rauscher'90] U. Rauscher, H. Bässler, D. D. C. Bradley, M. Hennecke, *Phys. Rev. B: Condens. Matter Mater. Phys*. **1990**, *42*, 9830.

[Rau'84] N. O. Rau, R. C. Schilz, *Macromol. Chem*. *Rapid Commun*. **1984**, *5*, 725 – 729.

[Rothberg'96] L.J. Rothberg, M. Yan, F. papadimitrakopoulos, M. E. Galvin, E. W. Kwock, T. M. Miler, *Synthetic Metals*, **1996**, *80*, 41 – 58.

[Ruini'04] A. Ruini, A. Ferretti, G. Bussi, E. Molinari and M. J. Caldas, *Semicond. Sci. Technol*. **2004**, *19*, S362-S364.

[Sariciftci'93] N. S. Sariciftci, D. Braun, C. Zhang, V. I. Srdanov, A. J. Heeger, G. Stucky, F. Wudl, *Appl. Phys. Lett*. **1993**, *62*, 585.

[Scatchard'49] G. Scatchard, *Equilibrium in nonelectrolyte mixtures*, Chem. Rev. **1949**, *44*(1): 7-35.

[Scholdei'07] Computer program is developed by W. Scholdei, Max Planck Institute for Polymer Research, **2007**, unpublished.

[Schwartz'03] B. J. Schwartz, *Annu. Rev. Phys. Chem*. **2003**, *54*, 141-72.

[Scott'53] R. L. Scott, *Ind. Eng. Chem*. **1953**, *45*, 2532.

[Scott'96] J. C. Scott, J. H. Kaufman, P. J. Brock, R. DiPietro, J. Salem and J. A. Goitia, *J. Appl. Phys.* **1996**, *79*, 2745.

[Shi'00] Y. Shi, J. Liu and Y. Yang, *J. Appl. Phys*. **2000**, *87*, 9.

[Small'53] P. A. Small, J. Appl. Chem. **1953**, *3*, 71 – 80.

[Snyder'83] A. W. Snyder and J. D. Love, *Optical Waveguide theory*, Chapman and Hall, New York, **1983**.

[Sperling'01] L. H. Sperling, *Introduction to Physical Polymer Science*, 3rd ed. Chap.3, J. Wiley & Sons, **2001**.

[Stalmach'96] Ulf Stalmach, Heinz Kolshorn, Isabella Brehm and Herbert Meier, *Liebigs Ann.* **1996**, 1449-1456.

[Stegeman'89] G.I. Stegeman, R.H. Stolen, *J. Opt. Soc. Am. B* **1989**, *6*, 652-662.

[Strawhecker'01] K. E. Strawhecker and S. K. Kumar, *Macromolecules*. **2001**, *34*, 4669-4672.

[Tammer'02] Tammer, M.; Monkman, A.P. *Adv. Mater*. **2002**, *14*, 210- 212.

[Tamir'71] T. Tamir, H. L. Betoni, *J. Opt. Soc. Am*. **1971**, *61*, 1397.

[Taylor'74] H. F. Taylor and A. Yariv, *Proc. IEEE* **1974**, *62*, 1044.

[Teraoka'02] I. Teraoka, *Polymer Solutions an Introduction to Physical Properties*, J. Wiley & Sons, New York, **2002**.

[Tian'91] B. Tian, G. Zerbi and K. Müllen, *J. Chem. Phys.* **1991**, *95*, 3198.

[Tien'69] P. K. Tien, R. Ulrich, and R. J. Martin, *Appl. Phys. Lett*. **1969**, *14*, 29.

[Tien'71] P. K. Tien, *Appl. Opt*. **1971**, *10*, 2395.

[Tien'77] P. K. Tien, *Rev. Mod. Phys*. **1997**, *49*, 361 – 387.

[Tsao'10] H. N. Tsao and K. Müllen, *Chem. Soc. Rev*. **2010**, *39*, 2372- 2386.

[Turnbull'03] G. A. Turnbull, P. Andrew and W. L. Barnes, I. D. W. Samuel, *Appl. Phys. Lett.* **2003**, *82*, 313.

[Ueberhofen'96] K. Ueberhofen, *PhD Dissertation*, University Mainz, Germany, **1996**.

[Ulrich'70] R. Ulrich, *J. Opt. Soc. Am*. **1970**, *60*, 1337.

[Ulrich'73] R. Ulrich, R. Torge, *Appl. Opt*. **1973**, *12*, 2901.

[Ulrich'74] R. Ulrich, D. Chen, *App. Opt*. **1974**, *13*, 1850.

[Ward'75] I. M. Ward, *Structure and Properties of Oriented polymers*, chap.3, Applied Science Publishers LTD, London, **1975**.

[Wasey'01] J. A. E. Wasey, A. Safonov, I. D. W. Samuel, W. L. Barnes, *Phys. Rev. B*. **2001**, 64, 205201.

[Weil'88] A. Weil, E. Dechenaux, *Polymer Eng. And Sci*. **1988**, *28*, 15.

[Yang'98] C. Y. Yang, F. Hide, M. A. D. Gracia, A. J. Heeger, Y. Cao, *Polymer* **1998**, *39*, 2299-2304.

[Yariv'76] A. Yariv, *Introduction to optical Electronics*, 2nd ed. Chap.13, Holt, Rinehart and Winston, New York, **1976**.

[Yeh'88] P. Yeh, "*Optical Waves in Layered Media*", John Wiley & Sons Inc., USA, **1988**.

[Yu'95] G. Yu, J. Gao, J. C. Hummelen, F. Wudl and A. J. Heeger, *Science* **1995**, *270*, 1789.

[Ziegler'00] J.Ziegler, *PhD Dissertation*, University of Mainz, Germany, **2001**.

APPENDIX A

GPC Results of Fractionations

Fractionation A

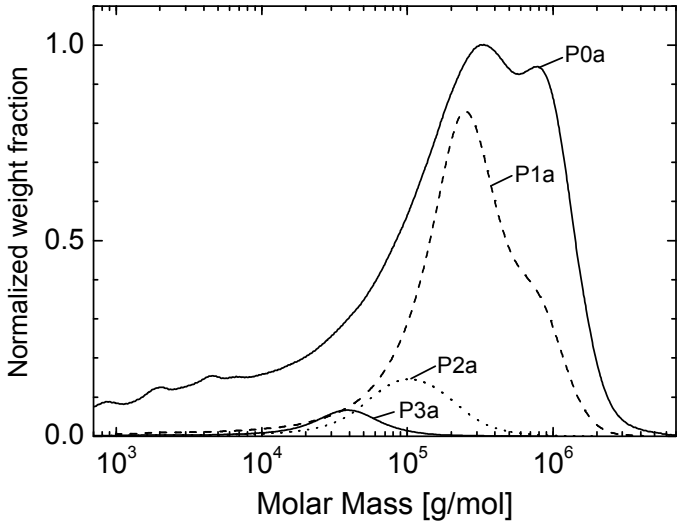

Polymer	M_w (g/mol)	M_n (g/mol)	D (M_w/M_n)	Amount (mg)
P0a	4.7×10^5	9.7×10^4	4.85	200
P1a	3.7×10^5	9.1×10^4	4.09	106
P2a	1.3×10^5	4.5×10^4	2.85	15
P3a	4.7×10^4	2.9×10^4	1.63	5

Fractionation B

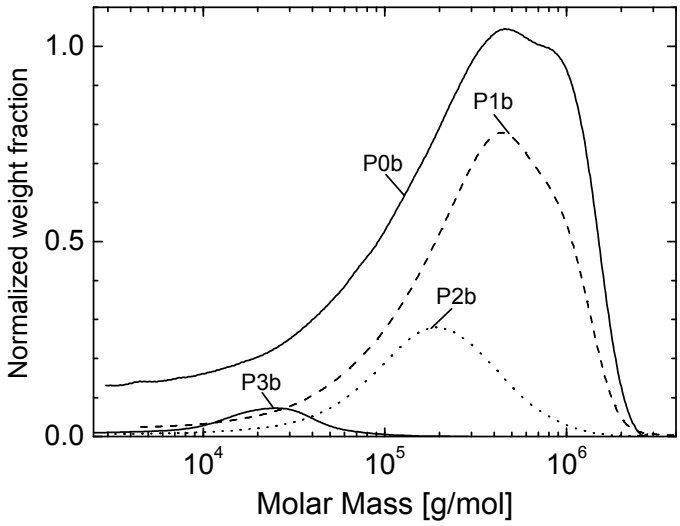

Polymer	M_w (g/mol)	M_n (g/mol)	D (M_w/M_n)	Amount (mg)
P0b	4.4×10^5	5.2×10^4	8.31	1000
P1b	4.7×10^5	1.3×10^5	3.68	566
P2b	2.4×10^5	8.6×10^4	2.83	375
P3b	2.6×10^4	1.4×10^4	1.84	36

Fractionation C

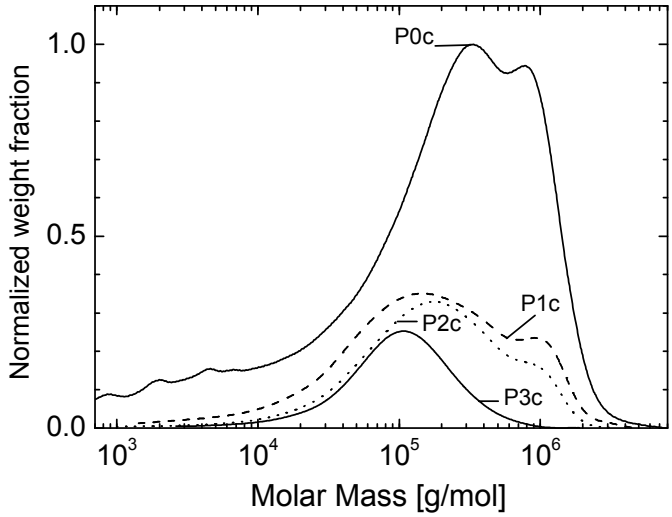

Polymer	M_w (g/mol)	M_n (g/mol)	D (M_w/M_n)	Amount (mg)
P0c	4.65 x 10^5	6.1 x 10^4	7.62	200
P1c	3.6 x 10^5	5.0 x 10^4	7.45	71
P2c	3.0 x 10^5	8.5 x 10^4	3.70	66
P3c	2.0 x 10^5	5.0 x 10^4	3.25	51

Fractionation D

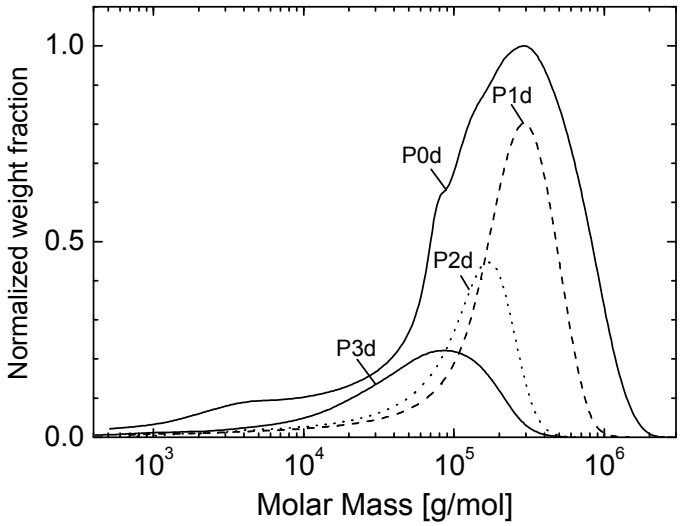

Polymer	M_w (g/mol)	M_n (g/mol)	D (M_w/M_n)	Amount (mg)
P0d	2.9 x 10^5	2.6 x 10^4	10.97	1000
P1d	2.7 x 10^5	5.5 x 10^4	4.93	439
P2d	1.4 x 10^5	3.4 x 10^4	3.95	235
P3d	7.8 x 10^4	1.4 x 10^4	5.44	252

Fractionation E

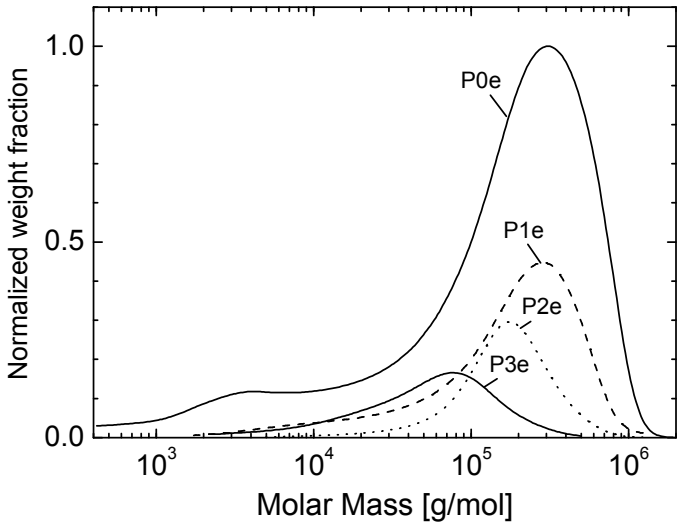

Polymer	M_w (g/mol)	M_n (g/mol)	D (M_w/M_n)	Amount (mg)
P0e	2.6 x 10^5	2.1 x 10^4	12.46	970
P1e	2.4 x 10^5	5.5 x 10^4	4.42	362
P2e	1.9 x 10^5	1.0 x 10^5	1.8	180
P3e	7.7 x 10^4	2.7 x 10^4	2.79	146

Fractionation F

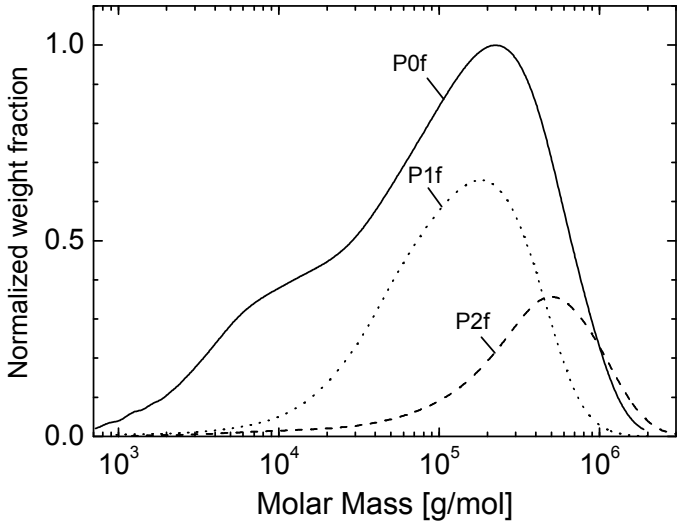

Polymer	M_w (g/mol)	M_n (g/mol)	D (M_w/M_n)	Amount (mg)
P0f	2.8 x 10^5	2.3 x 10^4	12.2	317
P1f	5.2 x 10^5	9.1 x 10^4	5.67	66
P2f	1.8 x 10^5	5.5 x 10^4	3.34	147

Fractionation G

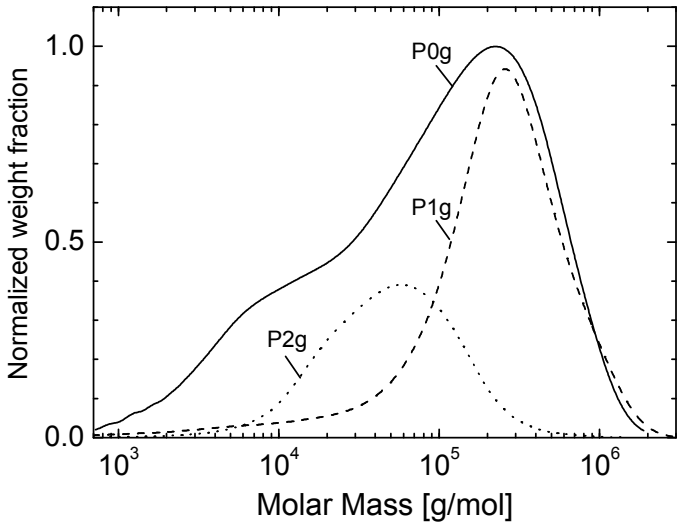

Polymer	M_w (g/mol)	M_n (g/mol)	D (M_w/M_n)	Amount (mg)
P0g	2.0 x 10^5	2.0 x 10^4	10.01	321
P1g	3.3 x 10^5	5.4 x 10^4	6.11	168
P2g	7.5 x 10^4	3.0 x 10^4	2.54	84

Fractionation H

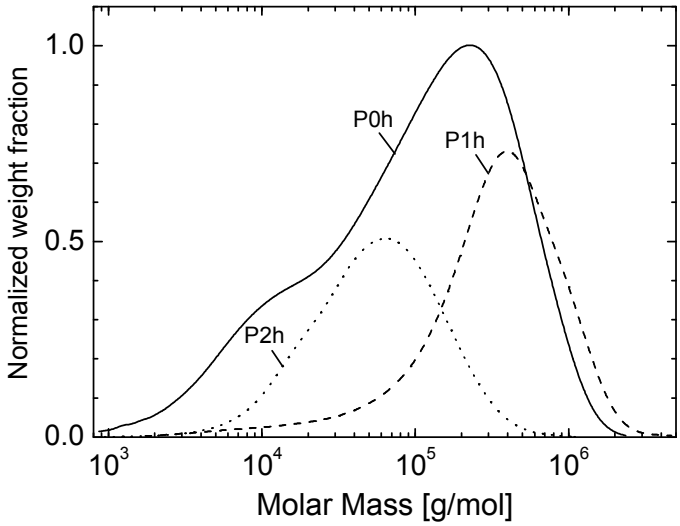

Polymer	M_w (g/mol)	M_n (g/mol)	D (M_w/M_n)	Amount (mg)
P0h	2.14 x 10^5	2.7 x 10^4	7.88	470
P1h	4.8 x 10^5	1.2 x 10^5	4.15	212
P2h	8.3 x 10^4	3.3 x 10^4	2.52	168

Fractionation I

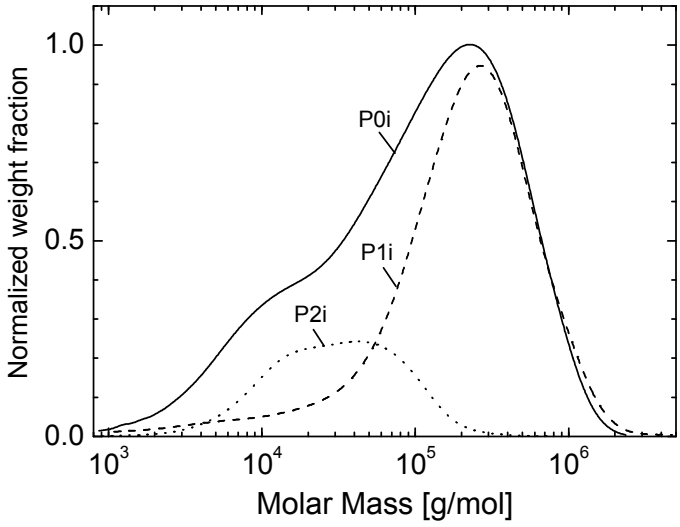

Polymer	M_w (g/mol)	M_n (g/mol)	D (M_w/M_n)	Amount (mg)
P0i	1.86 x 10^5	2.3 x 10^4	7.98	307
P1i	3.2 x 10^5	6 x 10^4	5.36	195
P2i	4.7 x 10^4	1.8 x 10^4	2.55	60

Fractionation J

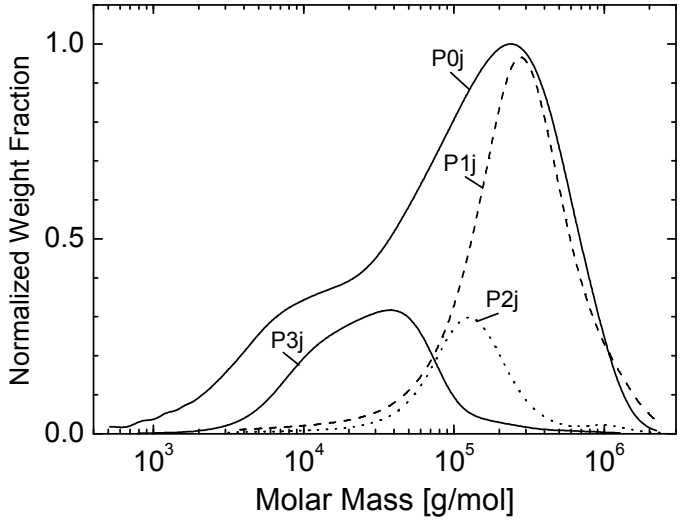

Polymer	M_w (g/mol)	M_n (g/mol)	D (M_w/M_n)	Amount (mg)
P0j	2.2 x 10^5	2.0 x 10^4	10.67	978
P1j	3.6 x 10^5	1.4 x 10^5	2.66	503
P2j	1.8 x 10^5	7.8 x 10^4	2.34	130
P3j	4.5 x 10^4	1.7 x 10^4	2.69	211

Fractionation K

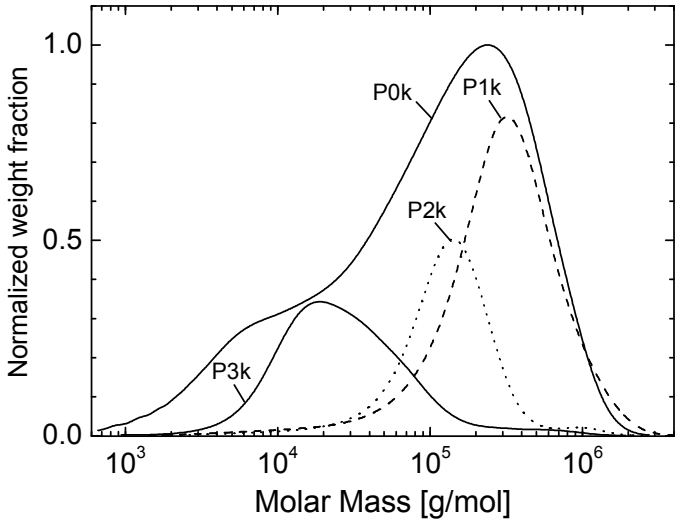

Polymer	M_w (g/mol)	M_n (g/mol)	D (M_w/M_n)	Amount (mg)
P0k	2.2 x 10^5	2.2 x 10^4	9.93	1066
P1k	4.0 x 10^5	1.4 x 10^5	2.96	468
P2k	1.7 x 10^5	7.9 x 10^4	2.13	230
P3k	5.2 x 10^4	1.7 x 10^4	2.95	242

Fractionation L

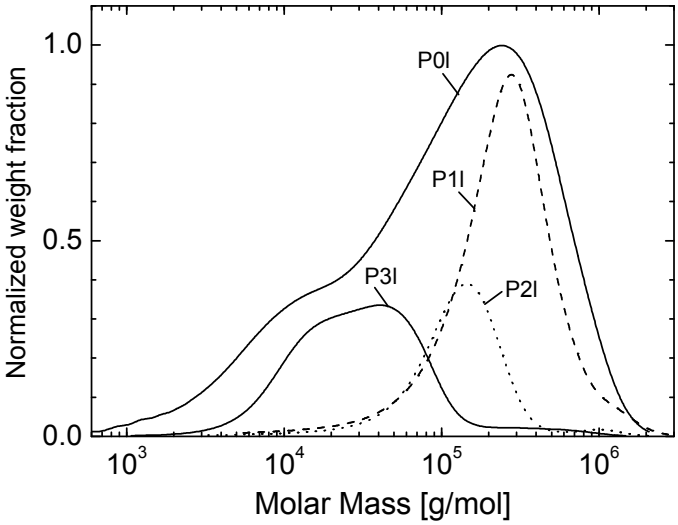

Polymer	M_w (g/mol)	M_n (g/mol)	D (M_w/M_n)	Amount (mg)
P0l	2.2 x 10^5	2.4 x 10^4	9.18	2072
P1l	3.2 x 10^5	1.5 x 10^5	2.16	897
P2l	1.7 x 10^5	8.4 x 10^4	2.00	339
P3l	5.5 x 10^4	1.9 x 10^4	2.84	497

Fractionation M

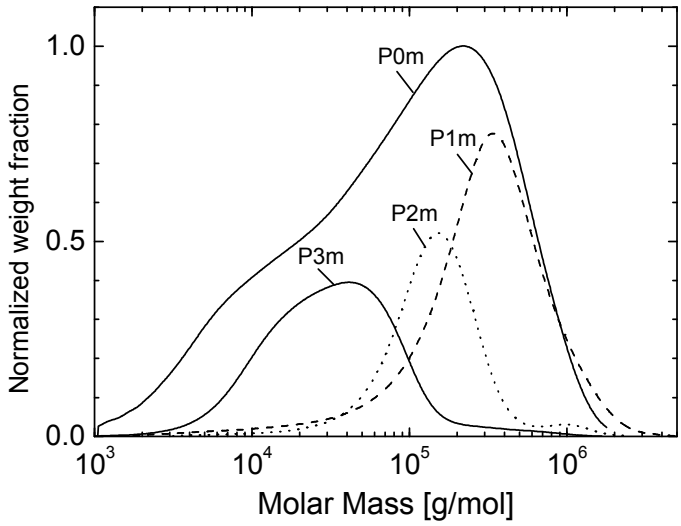

Polymer	M_w (g/mol)	M_n (g/mol)	D (M_w/M_n)	Amount (mg)
P0m	1.9 x 10^5	2.3 x 10^4	8.45	2318
P1m	4.2 x 10^5	1.2 x 10^5	3.53	910
P2m	1.9 x 10^5	9.6 x 10^4	1.97	488
P3m	5.4 x 10^4	2.0 x 10^4	2.68	600

Appendix B

Full Chemical Names and Properties of PPV Derivatives

MEH-PPV: Poly[2-methoxy-5-(2-ethylhexyloxy)-1,4-phenylene-vinylene].

M3EH-PPV: Poly[2,5-dimethoxy-1,4-phenylene-1,2-ethenylene, 2-methoxy-5-(2-ethylhexyloxy)-1,4-phenylene-vinylene].

MEH-M3EH-PPV: Poly[2-methoxy-5-(2-ethylhexyloxy)-1,4-phenylene-vinylene-2,5-dimethoxy-1,4-phenylene-vinylene-2-methoxy-5-(2-ethylhexyloxy)-1,4-phenylene-vinylene]

Properties of PPV-derivatives

Polymer	M_w [g/mol]	M_n [g/mol]	PDI
MEH-PPV	4.03×10^4	1.41×10^4	2.86
M3EH-PPV	4.40×10^4	1.20×10^4	3.67
MEH-M3EH-PPV	3.23×10^4	1.14×10^4	2.83

Appendix C

UV- Vis Spectra of MEH-PPV in Mixed Solutions

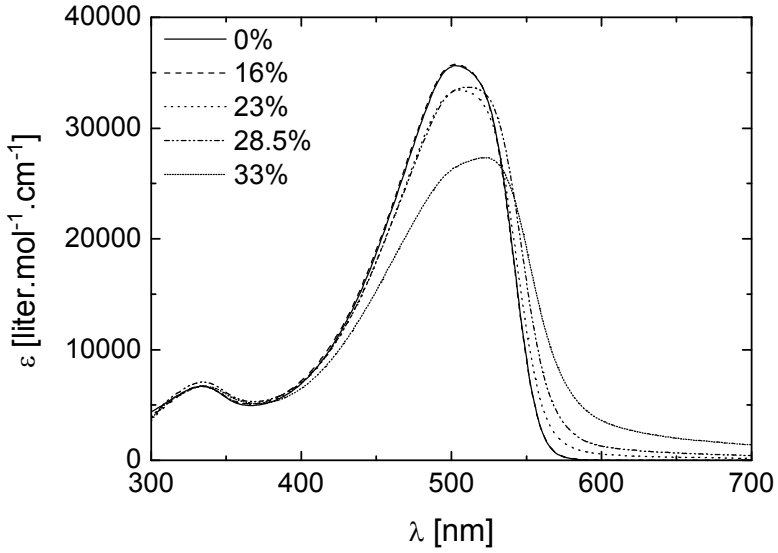

Fig. C.1: UV-Vis spectra of P1* fraction in mixed solutions of methanol and toluene. The inset shows the relative volume content of methanol.

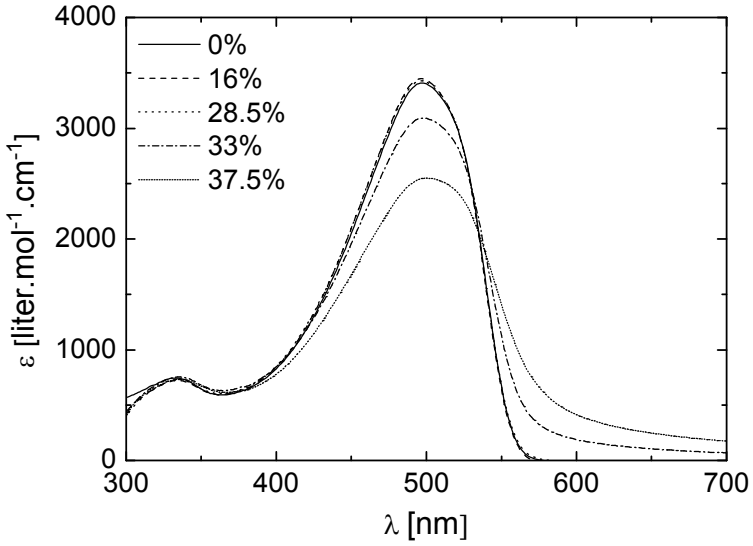

Fig. C.2: UV-Vis spectra of P3* fraction in mixed solutions of methanol and toluene. The inset shows the relative volume content of methanol.

Appendix D

Calculation of Solubility Parameter δ of MEH-PPV by Using Method of Group Contribution of Hoftzyer and Van Krevelen.

Structural Group	F_{di} ($J^{1/2}.cm^{3/2}.mol^{-1}$)	F^2_{pi} ($J^{1/2}.cm^{3/2}.mol^{-1}$)	E_{hi} (J/mol)
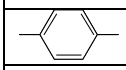	1 x 1270 = 1270	1 x (110^2) = 12100	0
$-CH_3$	3 x 420 = 1260	0	0
-O-	2 x 100 = 200	2 x (400^2) = 320000	2 x 3000 = 6000
$-CH_2$	5 x 270 = 1350	0	0
>CH	1 x 80 = 80	0	0
=CH-	2 x 200 = 400	0	0
	$\sum F_{di}$ = 4560	$\sum F^2_{pi}$ = 332100	$\sum E_{hi}$ = 6000

$$\delta_d = \frac{\sum F_{di}}{V} \qquad \delta_d = 4560 / 245 = 18.6\ J^{1/2}.cm^{-3/2}$$

$$\delta_p = \frac{\sqrt{\sum F^2{}_{pi}}}{V} \qquad \delta_p = (332100) / 245 = 2.35\ J^{1/2}.cm^{-3/2}$$

$$\delta_h = \sqrt{\frac{\sum E_{hi}}{V}} \qquad \delta_h = (6000 / 245)^{1/2} = 4.95\ J^{1/2}.cm^{-3/2}$$

$\delta^2 = \delta_d^2 + \delta_p^2 + \delta_h^2 = 19.4\ J^{1/2}.cm^{-3/2}$

$\delta = 9.4\ cal^{1/2}cm^{-3/2}$

Appendix E

^{1}H NMR of MEH-PPV

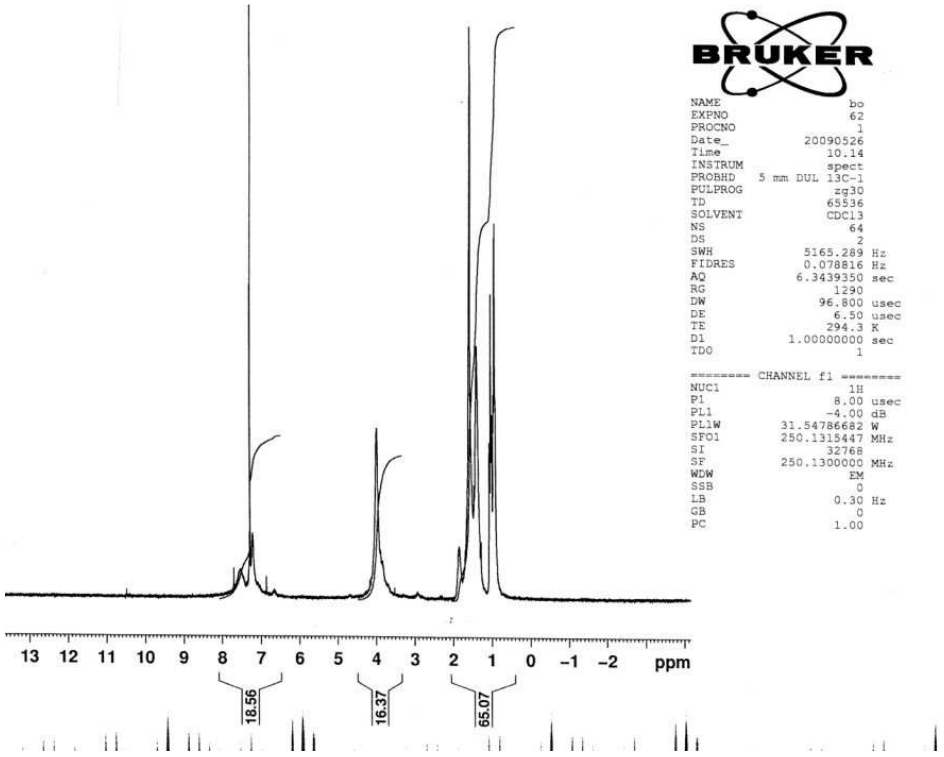

Fig. E.1: ^{1}H NMR spectra of P0J

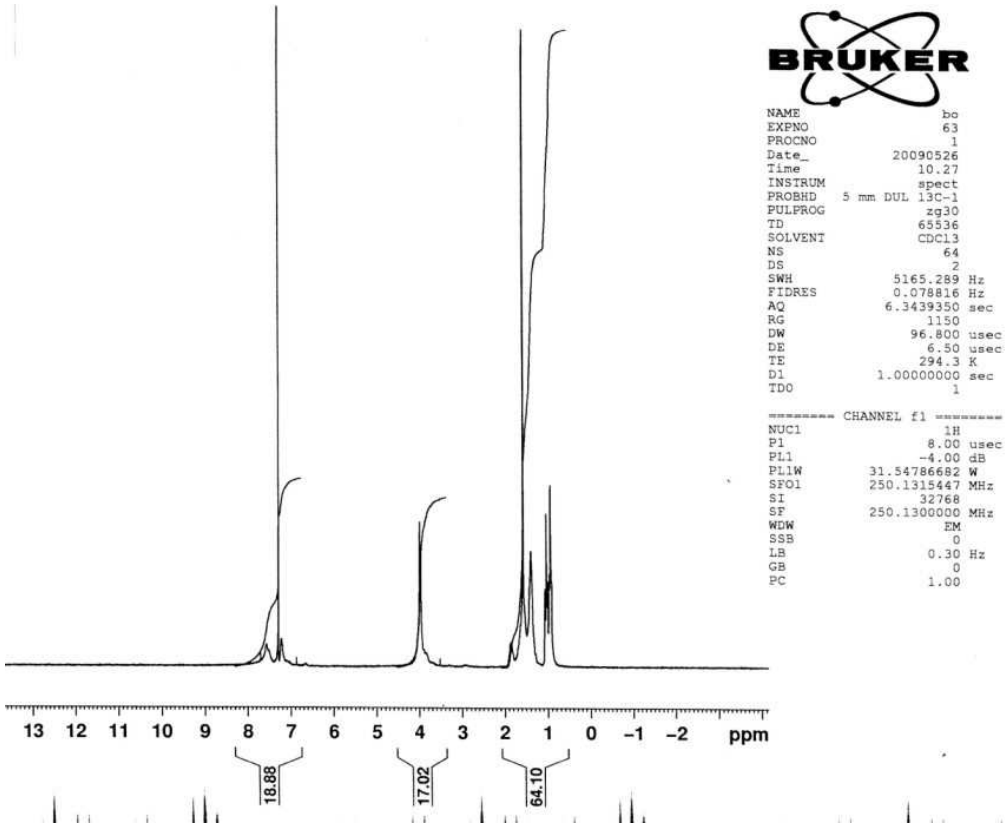

Fig. E.2: ^{1}H NMR spectra of P2*

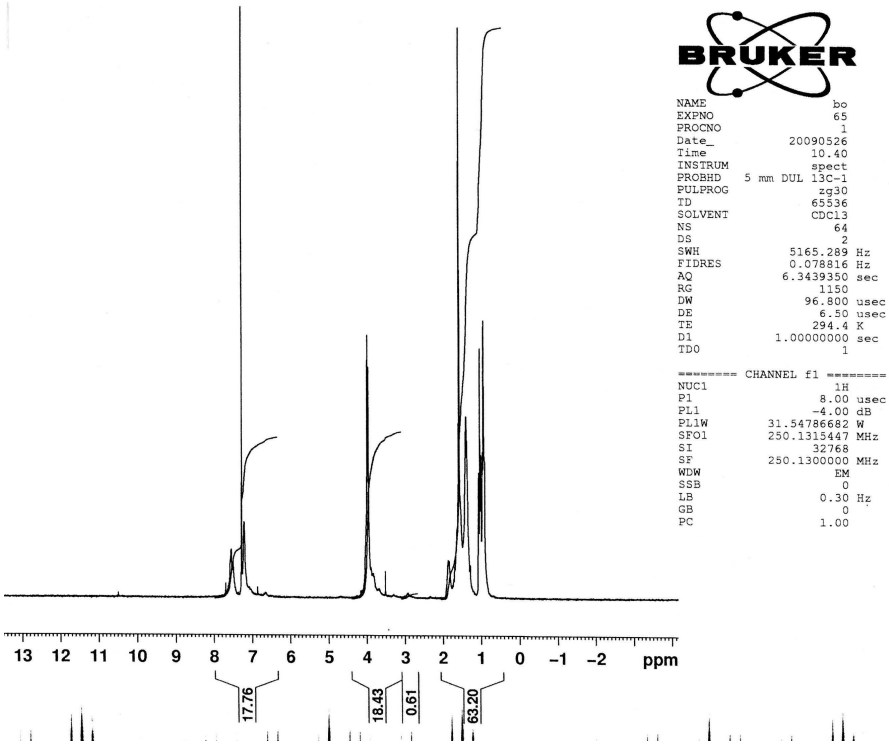

Fig. E.3: ^{1}H NMR spectra of P3*

Appendix F

Studies of Dip Coating on Fibers

We prepared dip-coated films of MEH-PPV fraction P3* on fibers with different diameters and using toluene as solvent with concentration 3.2% by weight. Table F.1 shows the obtained thicknesses for different diameters of fibers at similar withdrawal velocity and immersion time.

Table F.1: Thickness of dip-coated films of MEH-PPV fraction P3* on different diameters of fibers, withdrawal velocity 10 mm/s, immersion time 2 minutes.

Diameter of fiber (μm)	Thickness (nm)
45	68.5 ± 1.3
72	96.3 ± 2.3
200	122.3 ± 19

Thickness of dip-coated film increase as diameter of fiber is increasing. The film thickness can be expressed as [Quèrè'99]

$$h = 1.34 r Ca^{2/3}$$

where r is radius of fiber.

List of Publications

1. A. Bahtiar, K. Koynov, **Y. Mardiyati**, H-H. Hörhold, and C. Bubeck, "Slab waveguides of poly-para-phenylenevinylenes for all-optical switching: impact of side-chain substitution"*, Journal of Materials Chemistry*, 2009, 19, 7490 – 7497.

2. A. Bahtiar, K. Koynov, **Y. Mardiyati**, H-H. Hörhold, and C. Bubeck, "Polymer Slab Waveguides for all-Optical Switching", *ACS Polymer Preprints*, 2008, 49, 1003.

3. D. Wang, **Y. Mardiyati**, J. Shu, C. Bubeck, H.-J. Butt, K. Koynov, "Single Chain and Agregate Evollution of Conjugated Polymer in Dilute Solution Investigated by Fluorecence Correlation Spectroscopy", *in preparation*.

4. **Y. Mardiyati**, C. Bubeck, "Fractionation studies and solution properties of the conjugated polymer MEH-PPV", *in preparation.*

5. **Y. Mardiyati**, C. Bubeck, "Influence of molecular weight and film preparation condition of the conjugated polymer MEH-PPV on morphology and optical properties", *in preparation.*